Numerical modelling of localised thinning processes for packaging steels.

Fieldhouse, Michael

NUMERICAL MODELLING OF LOCALISED THINNING PROCESSES FOR PACKAGING STEELS

MICHAEL FIELDHOUSE

SWANSEA UNIVERSITY
SCHOOL OF ENGINEERING
DEPARTMENT OF MATERIALS SCIENCE AND ENGINEERING
RESEARCH, DEVELOPMENT & TECHNOLOGY

Declaration

THESIS

This work has not previously been accepted in substance for any degree and is not being concurrently submitted in candidature for any degree.

Signed . ..... (candidate)

Date 17.07.12

STATEMENT 1

This thesis is the result of my own investigations, except where otherwise stated. Where correction services have been used, the extent and nature of the correction is clearly marked in a footnote(s).

Other sources are acknowledged by footnotes giving explicit references. A bibliography is appended.

Signed .... (candidate)

Date 17.07.12

STATEMENT 2

I hereby give consent for my thesis, if accepted, to be available for photocopying and for inter-library loan, and for the title and summary to be made available to outside organisations

Signed ..... (candidate)

Date 17.07.12

Abstract

THESIS

With the European Union putting pressure on companies within the packaging chain to recycle, cheap and readily available packaging materials are highly in demand. Steel is the most recycled packaging material and to keep it there research continues in this area.

More recently research has switch from developing and altering tooling to fit certain materials, to developing improved materials for a given manufacturing process, steel can production for example. This has lead to the desire to understand how materials behave under different forming conditions.

The solution which would best suit packaging manufacturing companies would be, knowing the material properties, to develop a numerical model which would be able to predict how the material would perform under different forming conditions. This model could be used as an aid to see which new materials should be further developed.

To measure these different forming conditions a forming limit diagram is used. A forming limit diagram shows how a material can perform under altering forming conditions, from uniaxial through plane to biaxial strain.

Before a model can be produced though, experimental results are needed to validate the model. The current International Standard 12004-2, which is used to produce a forming limit diagram, does not allow materials under a certain thickness. Almost all packaging steel grades are thinner and have proven difficult to obtain reliable results.

This thesis outlines the development of a simplified experimental test which is used to measure strain path dependant failure limits of several packaging steels. These results are then used then to generate a computer model in which the different strain conditions can be closely matched to the experiment test method.

Acknowledgements

THESIS

I would first like to thank both the industry sponsor, TATA and EPSRC, the Engineering and Physical Sciences Research Council, for giving me the opportunity to take part in the Engineering Doctorate Scheme and for their financial support over the four years.

Next I would like to thank both my academic and industrial supervisors for there input and support given to me over the course of the Engineering Doctorate Scheme, pointing me in the right direction when problems arose.

Special thanks go to all who helped me during my time in Ijmuiden Holland, all those in the packaging and automotive centre who helped and gave me support during my experimental testing. Another special thanks must go to Melanie from Rockfield Software for her support finding bugs and errors when the computer model was developed.

Contents

THESIS

Chapter 1

INTRODUCTION

Chapter 1

INTRODUCTION

1.1 Introduction to packaging steels

In 1994 the European Union (EU) introduced the directive 94/62/EC with regards to packaging and packaging waste (European Parliament Council, 1994). The directive was to encourage countries to reuse and recycle therefore avoiding the increasing problems associated with ever filling landfill sites. Figure 1.1 shows the overall increase in steel packaging recycling rates from 1993 to 2008. The recycling rate of steel has more than doubled since the introduction of the EU directive.

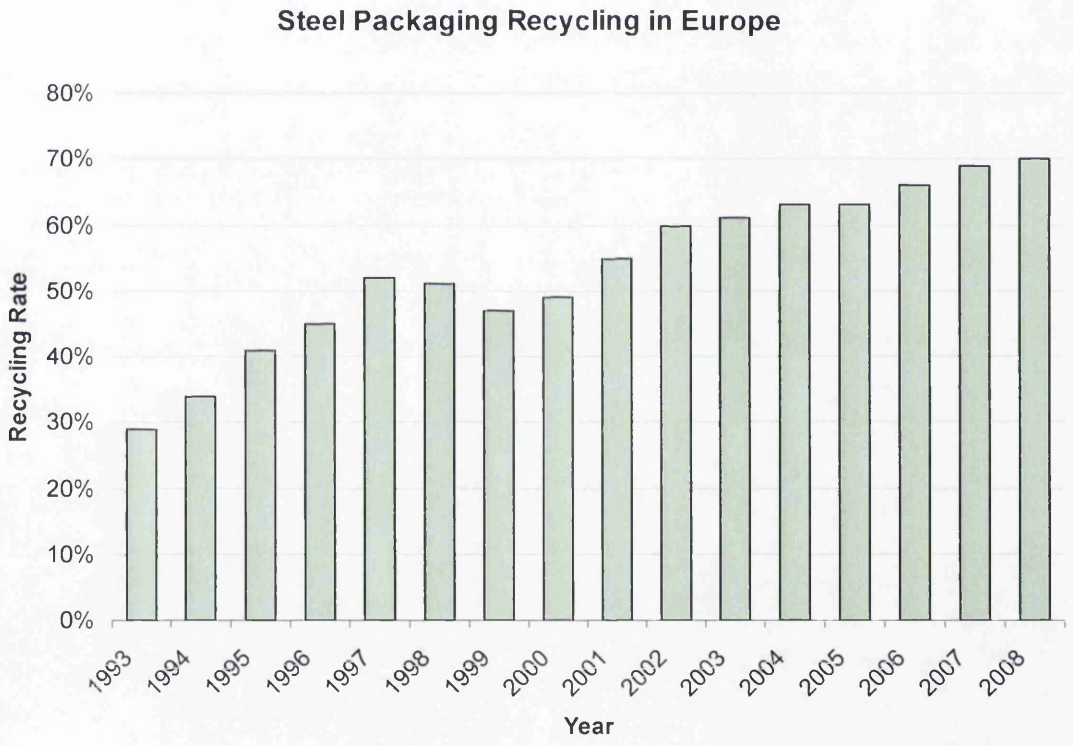

Figure 1.1. Steel packaging recycling rates from 1993 to 2008 (APEAL1, 2010).

The UK implemented this directive as the producer responsibility obligations regulations in 1997 (OPSI, 1997). The regulations have placed a commitment on companies within the packaging chain, to ensure the recovery and recycling of packaging waste that they produce. This has introduced accredited recycling plants of packaging waste that are able to issue Packaging

Waste Recovery Notes (PRNs). PRNs are bought by the companies who produce, manufacture and sell packaging for products. The PRNs provide evidence to the EU that recovery and recycling of packaging waste has taken place. The money raised from the sale of PRNs can be reinvested in recycling, for example in improving collection schemes or help suicides the recycling process (DEFRA, 2006).

There are many different materials used for packaging products. The most common types are glass, plastic, paper and metal. Because of the implementation of PRNs there has been an increase for the easily recyclable packaging like glass and metals that can be simply re-melted down, recast, or added to new virgin material during manufacture. Paper can be recycled but only a limited number of times before the paper fibres are to short and unable to form paper, however plastics have suffered the most. There are many different types of plastic, including HIPS, PET, PETE, which can not be recycled together. This makes it very difficult to collect and separate them, as the general public can not tell the different plastics apart (Ashby et al, 2006). The few types of plastics that are recyclable are hard and expensive too, making it very difficult for accredited recycling plants to recycle them. The ease of recycling is seen in figure 1.2, in 2008 steel recycling rates were about 70%, aluminium was 63%, glass 62%, paper 33% and plastics were 29%. This shows just how much of a problem plastics are to recycle.

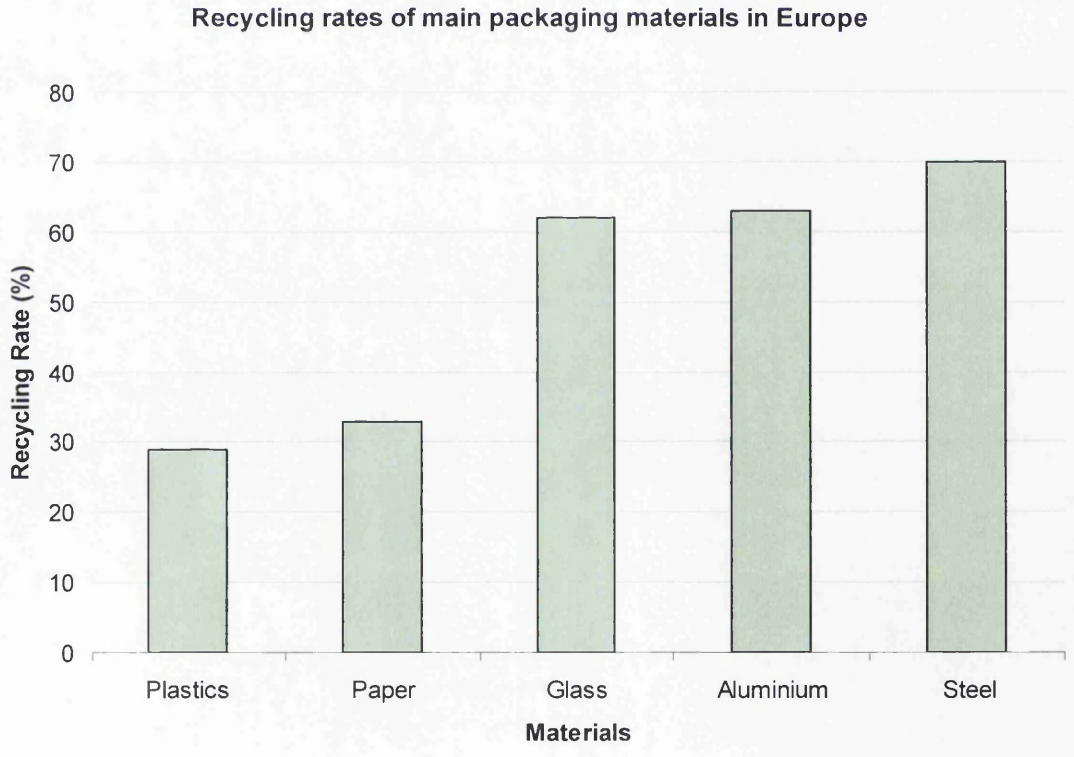

Figure 1.2. Recycling rates of main packaging materials in the EU in 2008 (APEAL2, 2010 and Labberton, 2009)

With fewer plants recycling plastics, the cost of plastic PRNs increases greatly which encourages companies to switch their packaging to materials that have low cost PRNs, like metals and glasses, to help keep their expenditure down.

The two most widely recycled materials are metals, steel and aluminium. They are recycled the most because they have a relatively large monetary value as scrap, compared to plastics, paper and glass. There is however problems associated with aluminium recycling. Aluminium is a non magnetic metal and therefore automatic separation processes in recycling plants are difficult compared to the benefit of steels magnetic properties. Aluminium also needs to be recycled by alloys, for example, you can not make an aluminium can from an aluminium car. Different alloys need to be separated at an early stage of recycling, which brings the same problems as plastics in regards to collection and separation of waste. Steel uses less energy to produce the packaging per unit volume of content then aluminium (Ashby et al, 2006). Steel covers a wide variety of packaging products, for example, food and drink cans, household product including aerosol and deodorant cans and industrial products such as paint packaging. Hence obtaining steel to be recycled is easier, which is shown in figure 1.2 which has steel with the largest recycling rate.

Both TATA, (2010) and Apeal, (2010) agree that using steel as a packaging product has many advantages over other packaging materials. These include:-

- Different finishes enables brand companies to have unique packaging.
- Steel is strong and durable compared to other packaging materials making them ideal for transportation. Paper is weak and can be pierced easily and glass is difficult to transport because if its brittleness.
- Steel protects the content against liquids, oxygen, light and other factors that could spoil it.
- Steel enables high speed process operations reducing factory operation times and increasing throughput.
- Heat processed foods packaged using steel do not require preservatives to extend the self live and also do not require antioxidants to keep, for example, the red colour in tomato soup.
- Steel is 100% recyclable, other packaging materials like plastics and paper are harder or unable to be recycled.
- The energy used to produce the packaging per unit volume of content is lowest with steel (Ashby et al, 2006)

It is from the EU directive of packaging waste and the UK regulations implemented that research into different and improved steel packaging continues.

1.2 Project introduction

TATA Steel is one of largest European companies that supply a complete range of high quality steel grades for packaging products. It supplies approximately 1.5 million tones of high quality light grade steels to the packing industry and produces material for delivery to over 50 counties world wide. TATA also continues research into development and improvement of steel packaging for packaging manufacturers to encourage them to continue buying TATA steel and to attract new companies to use steel as their packaging material of choice (TATA, 2011).

In more recent years with the advancement of computers, computer simulation programs based on finite element techniques have been introduced to develop metal forming processes and operations within the packaging industry. Using these programs reduces the time to market period and product costs. They also help to increase the understanding of how different grades of steel perform under processing techniques. The same programs will be used in this project. The finite element computer software for this project is being supplied by Rockfield Software Ltd (RSL) and is called ELFEN.

1.3 Project approach

Sheet metal forming process is an important technology in manufacturing, particularly in the packaging industry. During sheet metal forming where plastic deformation is present, thinning of the material may occur. This will eventually lead to localised necking and failure. The ability to determine where this localised necking happens is important to forming processes.

The measurements obtained from the experimental work covered in this thesis will be used to validate the models being produced. Due to packaging steels being so thin, measurements have been difficult to obtain. This thesis has addressed these issues so that experimental work can be carried out with these thin steel grades.

Comprehensive studies have been undertaken regarding necking and failure during sheet forming processes. Such papers include (Doege et al, 1997), (Manabe et al, 2007), (Courbon, 2003) and (Chang and Wang, 1997), where tooling parameters effects material

behaviour has been investigated. The emphasis recently has changed from examining the tooling properties to analysing the material properties. Anisotropy of the material has become the focus since the introduction of computational models, (Barisic and Pepelnjak, 2008). This has led to the full circle effect, figure 1.3, with regard to introducing computer models to simulate material processes.

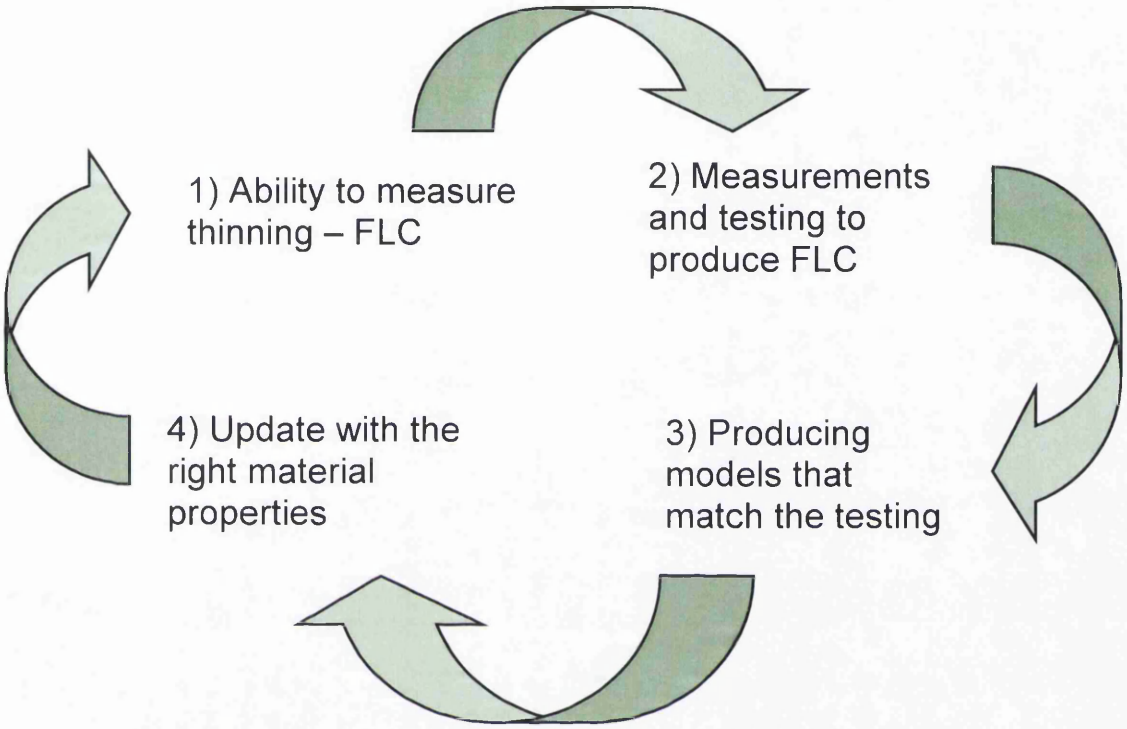

Figure 1.3. A simplified diagram of the "full circle" that this project will follow.

1. The ability to analyse localised necking (thinning of the material) has become an important factor in steel manufacturing. The way a material is chosen for a forming process is based on the amount of strain the material must withstand during the manufacturing stage. A Forming Limit Curve (FLC) is used to help decide which material will be chosen. The ability to predict an accurate forming limit curve is difficult based on a large number of factors.

2. Before and FLC can be predicted, actual measurements are needed. Materials are tested through a procedure and from these experiments a FLC of the materials can be produced. These experimental results will be used when the computer model is finish to validate the effectiveness of the computer model.

3. In order to predict a FLC, a computer model will be produced that matches the experimental procedure. The model will be produced using FEM software and will match the physical size and movement of the experimental test method.

4. Well defined conditions are needed where the onset of localised necking may be measured for all materials under the same conditions. These are the yield criterion, the flow rate and the strain rate. Firstly the yield criterion, which is a mathematical expression that attempts to predict the state of stress that will induce yielding of the material. Secondly the flow rate, which represents the relationship between stress, measured by the load applied to the material, against the strain, measured by the deformation of the material. Thirdly is the strain rate, which is the rate of change of strain over a time period.

The successful model will be used as an aid to produce a FLC of any given material. This concludes the full circle which takes us back to the ability of measuring thinning.

1.4 Aims and objectives

In collaboration with TATA and RSL, the aim of the thesis is, through experimental validation, to predict localised thinning of packaging steels during the Nakazima test experiment by computer modelling to help better understand material behaviour during forming processes. The project is to develop a numerical tool which can predict the behaviour of packaging steels under strain path conditions, this is broken down into the following areas:-

1. Establish a simplified experimental test method to measure strain path dependant failure limit of packaging steels.

2. Generate a computer model in which the strain results are very closely matched to the experiment test method.

1.5 Project importance and benefits

The project is important because being able to successfully model the FLD of metal materials gives a better understand of the material behaviour which means process improvements can be introduced. Understanding the process more will help reduce the failure rates during manufacture and increase the throughput, increasing profit margins. Also

understanding the material behaviour is essential for the production of quality packaging products without any imperfections.

Being able to predict how the material reacts using a FLD, means if the safety margin is large, this can be reduced by reducing the amount of material used. This would save money. Potential process improvements could also be simulated, without the need of changing the machinery, which will save time, manpower and money. This is the same for new steel grades. These could be simulated to predict how they would perform over the conventional grades currently used in the process, again without the cost of resources and machine time.

The computer model would not replace the experimental testing it would be used in conjunction with the experimental results to help identify which materials would be best suited for the relevant manufacturing process. With a working model different material properties can be entered to view the benefits of the potential material. This can be change on the production line once instead of changing the production line many times to produce the materials for testing at high costs.

Chapter 2

LITERATURE REVIEW

Chapter 2

LITERATURE REVIEW

CHAPTER 2 – LITERATURE REVIEW

2.1 Introduction

To ensure that the reader understands the work undertaken, the following literature review will give a detailed overview of some of the fundamentals, passed research work and experimental techniques used in this project.

2.2 History of Steel Packaging

The origins of steel packaging began in 1795 when a French Directoire offered a prize of 12000 francs to anyone who could present the government with a new, effective means of preserving food. A man called Nicholas Appert thought of the idea of packing food in bottles of wine, since wine kept for tens of years within a bottle. In 1809, 15 years after he started his research, he came up with a solution. Food could be preserved if it was sufficiently heated and sealed in an airtight container. For this Appert was rewarded with the 12000 francs (Can Manufactures Institute, 2002).

In 1810 an English man called Peter Durand took Appert's idea and instead to using glass he elected to use tin. Tin also could be sealed airtight and its main advantage was it did not break as easily as glass, making it more durable in transportation. The "Can" as it is known today was born. The first tin cans were hand made by three pieces of tin. One skilled workman could produce 10 cans per day. In 1849 with the help of the introduction of machinery to can manufacture, can production was increased from 10 cans to 60 cans per day. Over then next 70 years can processes were improved and by 1920 production of cans was up to a rate of 250 cans per minute. In more resent years the tin material was replaced by tin plated steel. Then around 1965 a new manufacturing method was introduced which involved two pieces of materials. Two pieces meant reduced material use during production resulting in less waste and increased profits.

To distinguish between the two types of can manufacturing processes they were quickly called 3 piece and 2 piece cans, reflecting the number of material pieces used during the manufacturing. There is a large difference between 3 and 2 piece can manufacture, one is not a

modification of the other process, they are two different manufacturing methods. The 3 piece can is made by a rectangle piece of tinplated steel having two of its opposites ends welded together to form a cylinder then two further circular pieces placed at either end. However in 2 piece can manufacture a flat circular steel blank is forced into a die producing a cup with a lid attached at the open end to form the can. The latter process requires that the material has certain properties which allow it to be deformed under manufacture.

2.3 Formability

The general term formability is used with sheet metal processes which has no intentional change in the thickness of the material during the manufacturing process. The formability of a material, in this projects case sheet steel, is the measurement of the amount of deformation the sheet can withstand before excessive thinning or fracture occurs. Determining how much a material can deform is necessary for designing a product that can be reproducible in a mass produce industry such as beverage can manufacture (Gedney, 2006). Formability of the material is affected by microstructure, mechanical properties and formability parameters.

2.4 Material Characteristics

2.4.1 Elastic behaviour

When a sufficiently high enough load is placed on a material it can deform. Its length, cross sectional area and volume is changed. For example, a material under tension stretches, its length increase and its cross-sectional area decrease. The opposite applies under compression. Therefore there is a relationship between load and deformation. A load is the external force that acts on the body, and the internal force which resists this load per unit area is called stress.

$$\sigma = F/A \quad (1)$$

Where F is the force and A is the cross-sectional area of the material. The amount of extension or deformation after the load is applied, compared to its original length, is called strain.

$$\varepsilon = \Delta l/l_o \quad (2)$$

Where Δl is the extension and l_o is the original length. Equation (2) measures the strain along the length of the bar. Under forming processes the formability is also measured by.

$$\varepsilon = \Delta w/w_o \qquad (3)$$

Where Δw is the extension and w_o is the original width respectively. If the strain (extension) is measured at each stress (load) step a stress-strain (load-extension) graph can be obtain. Figure 2.1 shows a stress-strain curve for a material under tension. The material increases in length until the material fractures.

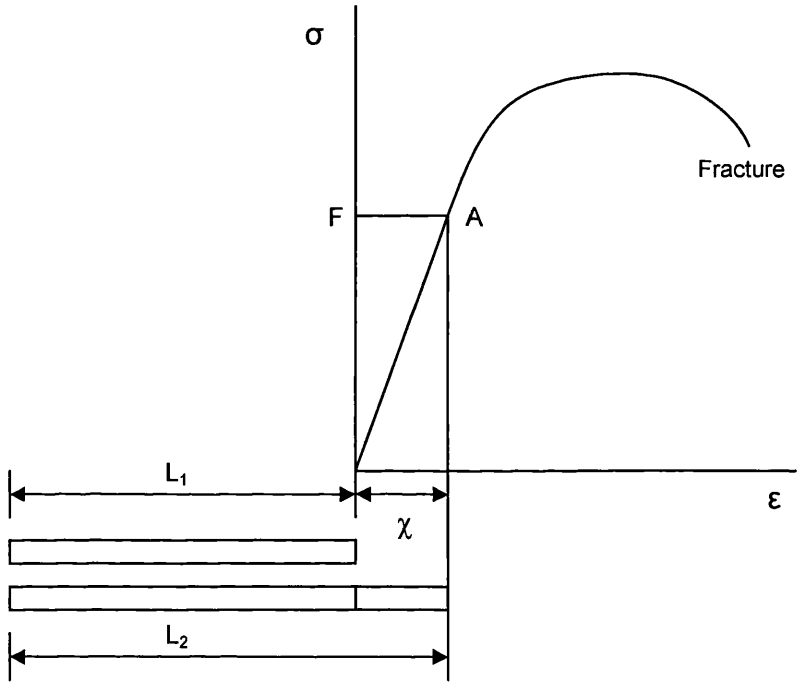

Figure 2.1. Stress-strain graph of a steel bar. As the load is increased the length of the bar also increases.

A material is said to be elastic if that, after being unloaded it returns to its original length. Figure 2.1 shows a bar of elastic material of length L_1, and the same bar of length L_2 when a load is applied to it. The extension χ increases as the force applied to the bar increases. When the load is removed the bar returns to its original length L_1, the extension is zero. The extension is proportional to the load, provided that the load is not too great, exceeding point A on figure 2.1.

$$F = (\text{contact}) \times \chi \qquad (4)$$

Where the value of the constant depends on the material and the dimensions of the bar.

$$\sigma = E\,\varepsilon \qquad (5)$$

E is the Youngs Modules. Equation (5) is known as linear elasticity or Hooke's Law and states that

"*The extension produced in a (linearly) elastic material is directly proportional to the load which produces it.*"

Figure 2.2 shows part of a stress-strain graph for a steel bar. Between OA the graph is straight (linear) and obeys Hooke's Law. Beyond point A the graph is curved, since the load is no longer proportional to the extension Hooke's Law does not apply. Point A is called the proportional limit. If the bar is loaded beyond the proportional limit the metal my still be elastic to some point B which is known as the elastic limit, if unloaded the bar will return along a parallel path, shown in figure 2.2 by the red line, back too its original length. This is commonly known as the 0.2% elastic limit.

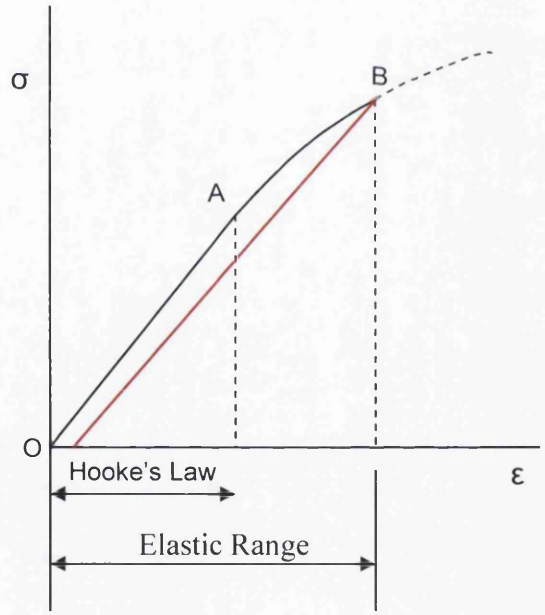

Figure 2.2. The elastic range of a material, OB, may be greater then the range which obeys Hooke's Law.

2.4.2 Plastic behaviour

Plastic deformation occurs when the extension in the material exceeds the elastic limit, point B in figure 2.2. Figure 2.3 shows that if a bar of length L_1 is extended by X beyond the elastic limit B, when the bar is unloaded there will be a permanent extension left, length Y. The material is said to have been plastically deformed.

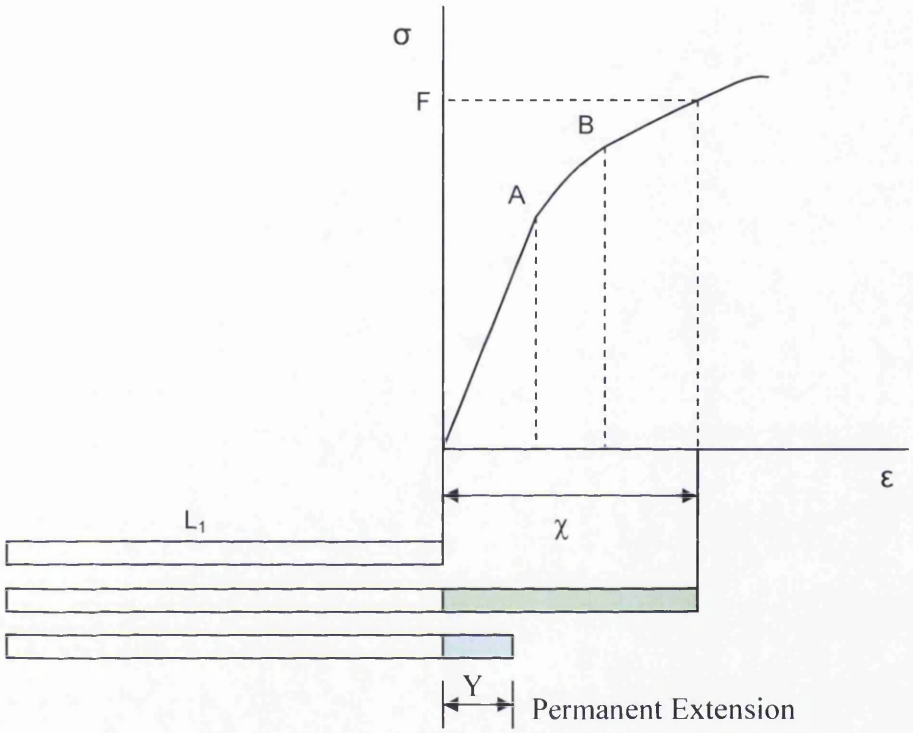

Figure 2.3. If a material is taken beyond the elastic limit then it will not return to its original length.

Figure 2.4 shows a load-extension curve for a steel bar under tension until failure occurs. After the elastic limit has been reached at point B, the material begins to yield. Yielding is when the material continues to extend to a point C without a further increase in load. This point is called the yield point. The yield point of any material is important during forming processes because it tells us the stress at which permanent deformation in the material to be formed begins. After the yield point the material enters a phase called strain hardening, the area CD of figure 2.4.

Point D is the maximum load the material can withstand and is called the ultimate tensile strength. Between points OD the material extends uniformly along its length. After point D the material will being to thin which will lead to failure if the load continues.

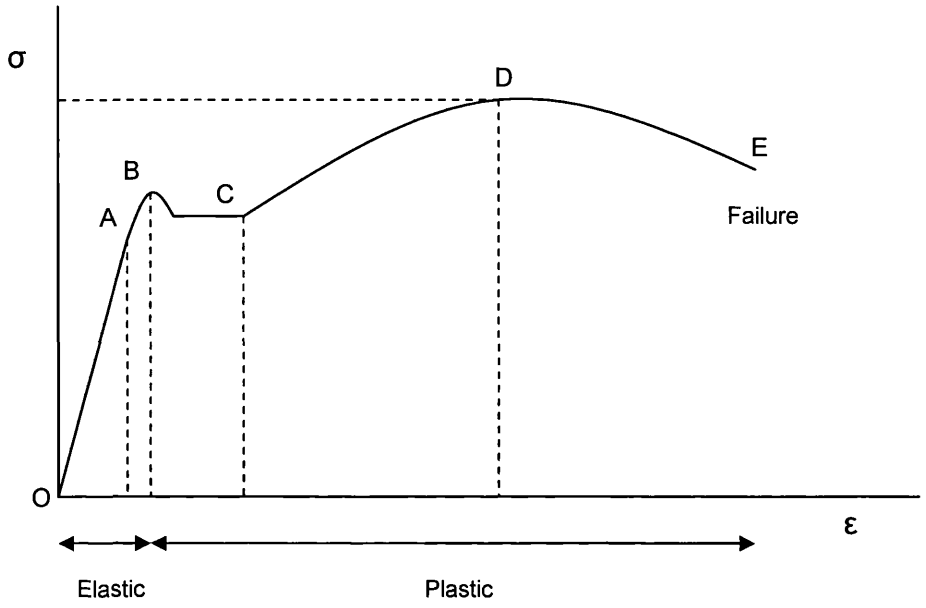

Figure 2.4. Stress-strain graph of a steel bar until failure at point E.

Beyond point D, in figure 2.4, materials start to rapidly thin in one area, which will lead to failure, point E. Depending if the material is brittle or ductile the necking can be large or small.

There are many types of failure due to excessive thinning. The common of these are tearing and cracking. Tearing is when the shear stress is too large for the material to take and the material rips or tears. Cracking is where the material has been thinned which produces necking of the material which leads to failure. Wrinkling occurs at the flange area because of the material becomes to thin and the material is unable to keeps it structure. Wrinkling in not a failure due to excessive thinning it is caused by thinning. The material has insufficient strength during compression within the material and this compression within the material causes the wrinkles to form.

2.4.3 Dislocations

Dislocations, which are defects within the material structure, are distributed throughout any metal. They are produced when the material is formed. During elastic deformation the whole material is being stretched therefore the dislocations stay in place within the material structure. However during plastic deformation, the dislocation first starts by moving through the crystal lattice on a primary glide system (the dislocation move in the same direction). When the material is plastically deformed, the dislocations within the material start to move through the crystal lattice and join other dislocations at grain boundaries. This produces areas of low and high densities

within the material. When enough of these dislocations link together they propagate into fractures which lead to failure of the material.

This movement of dislocation within the material is important as it affects the mechanical properties. This is why the strain paths of multi-step processes are very difficult to predict compared to single step processes. This is what affects the FLC on FLDs as described in section 2.3. The following three sections are laboratory experiments that can be used to model strain path dependency.

From a microscopic perspective a metal is a polycrystalline aggregate each crystal being of differing shape, size and orientation having formed from individual nuclei when the metal was originally cast. Recrystallised polycrystalline material, where no previous deformation has been applied to it, will commonly behave in an isotropic manner. Deformation, for example by forming, orientates the crystals causing the material to be anisotropic. On the atomic scale, deformation within these microstructure crystals is the breaking and remaking of interatomic bonds of many atoms as they move relative to one another.

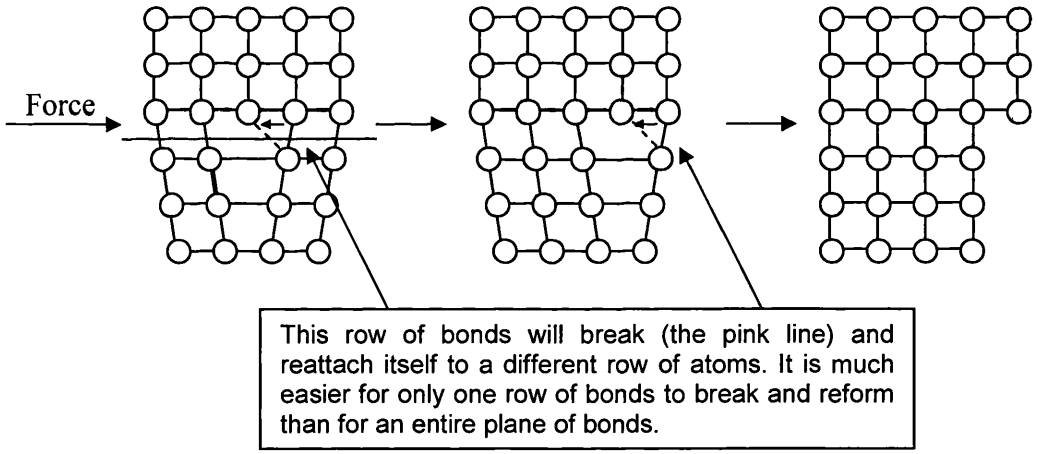

Figure 2.5. The movement of dislocation through the crystal lattice.

For crystalline materials such as metals this process is called slip and involves the movement of dislocations, figure 2.5. This dislocation movement occurs from points B to E in figure 2.4. Between points B and C the dislocations start to move through the crystal lattice, between points C to E is when the dislocations join other dislocations at grain boundaries.

2.4.4 r-Value

The plastic strain ratio or *r*-value, as it's usually referred to, is the measure of the property controlling the deep drawability of sheet metals. Man (2002) defines the r-value as:

"A measure of plastic anisotropy frequently used for prediction of performance in deep-drawing."

And goes on to clarify later that,

"As plastic anisotropy in sheets metals is caused mainly by the preferred orientations of grains within the polycrystalline metal."

The r-value is the ratio of the true strain in the width direction of a specimen piece, against the true strain in the thickness direction when a sheet material is pulled in uniaxial tension. Figure 2.6, illustrates this,

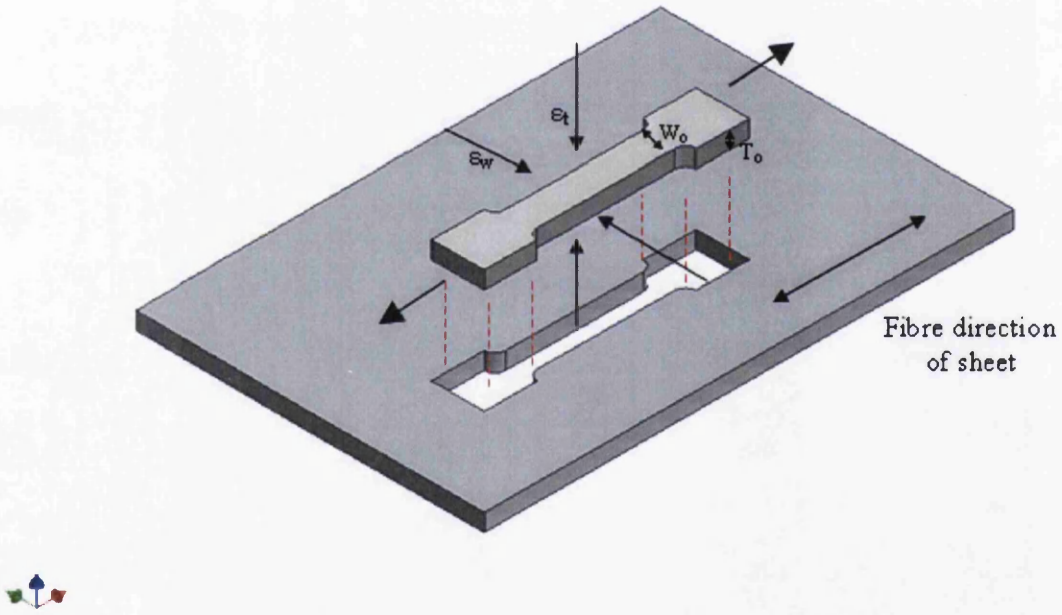

Figure 2.6. An illustration of a tensile test specimen that has been cut parallel to the strip rolling direction.

True strain in the width direction

$$\varepsilon_w = (w_i - w_f)/w_i \qquad (1)$$

True strain in the thickness direction

$$\varepsilon_t = (t_i - t_f)/t_i \quad (2)$$

Where (i) and (f) are the initial and finished measurements respectively. Using (1) and (2) the *r*-value is

$$r = \varepsilon_w/\varepsilon_t \quad (3)$$

If *r* is greater than 1, a sheet will strain in the plane of the sheet in preference to thinning, so the drawing properties are better as the *r*-value increases.

The *ř*-value is the normal anisotropy

$$\check{r} = \tfrac{1}{4}(r_0 + 2r_{45} + r_{90}) \quad (4)$$

and the planar anisotropy Δr is calculated by

$$\Delta r = \tfrac{1}{2}(r_0 - 2r_{45} + r_{90}) \quad (5)$$

Where the subscripts in equations (4) and (5) indicate the orientation of the specimen axis with respect to the rolling direction.

2.4.5 n-Value

The *n*-value or strain hardening regards the sheet metal forming. The larger the *n*-value the more the material can elongate before necking of the material. The necking produces thin surface areas which can lead to failure.

The *n*-value can be obtained by two equations, firstly using the Holloman equation, which is a power law relationship between the stress (σ) and the amount of plastic strain (ε). Where the K is the strength coefficient.

$$\sigma = K\varepsilon^n \quad (6)$$

Or it can also be determined by the Ludwik's equation which is similar but includes the yield stress (σ_y)

$$\sigma = \sigma_y + K\varepsilon^n \quad (7)$$

The constant K is structure dependent and is influenced by processing while n is a material property normally lying in the range 0.2-0.5. Using Holloman equation (6), the strain hardening can be rearranged to

$$n = d\log(\sigma)/d\log(\varepsilon) \quad (8)$$

This value for *n* can be calculated from the slope of a log(σ) - log(ε) plot. Rearranging equation (8) the rate of strain hardening at a given stress and strain can be calculated.

$$d\sigma/d\varepsilon = n\sigma/\varepsilon \quad (9)$$

The rate of strain hardening or the strain rate sensitivity index is also called the *m*-value (Kumar, 2002)

2.5 Plasticity

2.5.1 Introduction

The reader should be now aware of plastic deformation and the various stages materials undergo as a stress is gradually increased until failure, covered in section 2.4.2 Plastic behaviour. The theory of plasticity is used to calculate the stresses and strains in a deformed material after the material has yielded, point C on figure 2.4.

Plastic deformation is a time independent deformation, i.e. the deformation is permanent. A perfectly plastic material is one that does not strain harden. A Viscoplastic deformation on the other hand is a time dependent. This means that the permanent deformation has a variable of the strain rate (Mielnik, 1991).

2.5.2 Yield Surface

In uniaxial tension, yielding will occur when the yield point is exceeded. In forming processes there are combinations of stresses acting of the material. When each yield point is formed together a yield surface is produced figure 2.7. To take this into account a yield criterion is needed. A yield criterion is a mathematical expression that attempts to predict the state of stress that will induce yielding under any combination of strain conditions.

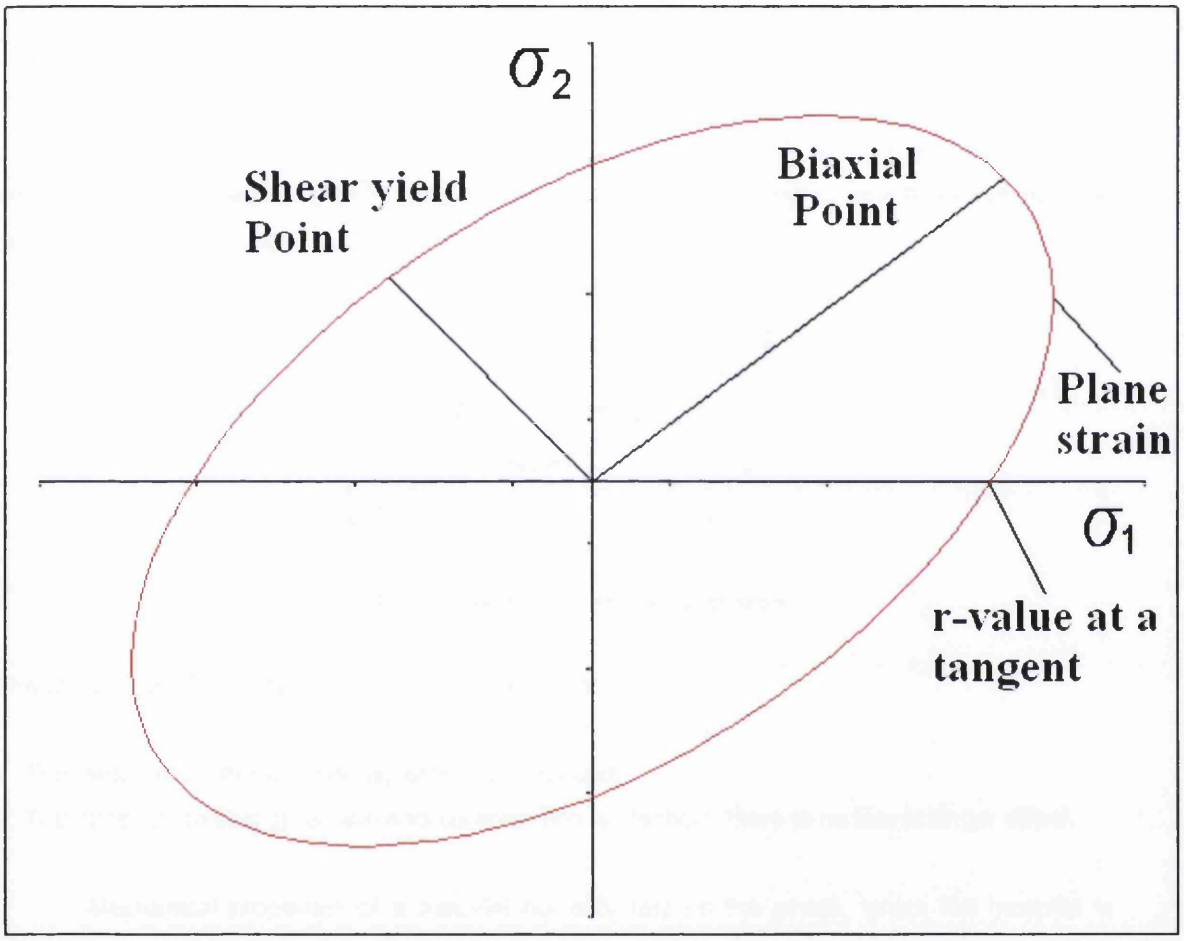

Figure 2.7. Illustration of a yield surface

2.5.4 Isotropic

In uniaxial tension, yielding will occur when the yield point has been exceeded. However in forming processes there is a combination of stresses acting on the material from an infinite number of directions, each direction has a yield point which when formed together produce a yield surface. To take into account the different combination of stresses, a yield criterion is needed.

When the stress state lies on the surface the material is said to have reached its yield point and the material is said to have become plastic. Further deformation of the material causes the stress state to remain on the yield surface, even though the surface itself may change shape and size as the plastic deformation evolves. Any mathematical expression that attempts to predict the state of stress that will induce yielding, or the onset of plastic deformation is called a yield criterion. A generalised from for any equation is shown as follows

$$f(\sigma_x\ \sigma_y\ \sigma_z\ \tau_{xy}\ \tau_{yz}\ \tau_{zx}) = C$$

Where σ is the stress, τ is the shear stress and x,y,z being the axis which the stress of shear stress is being applied. The yield surface is usually expressed in terms of a three dimensional principal stress space 1 2 3 as shown in figure 2.8.

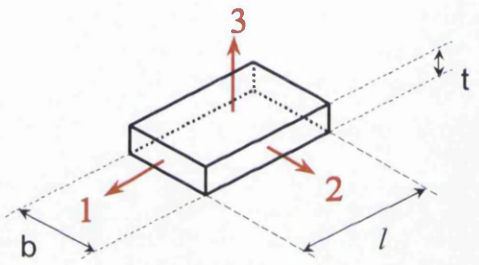

Figure 2.8. Three dimensional principal stress space.

These yield criterions have the following assumptions

1. The material is a homogeneous, isotropic continuum.
2. The onset of yielding in tension and compression is identical, there is no Bauschinger effect.

Mechanical properties of a material not only rely on the stress, which the material is currently undergoing, it also is measured by the deformation that the material has previously had. An example of this is when a material is plastically deformed, the yield stress in most materials is lower when deformed in the reverse direction. If the stress in the material in the reversed plastic flow has the same as the initial stress when first deformed then the material hardens isotropically. However for most materials, the reverse stress is lower than the forward stress. This anisotropic stress was first found by Bauschinger (1881) and since has been called the Bauschinger Effect, Figure 2.9.

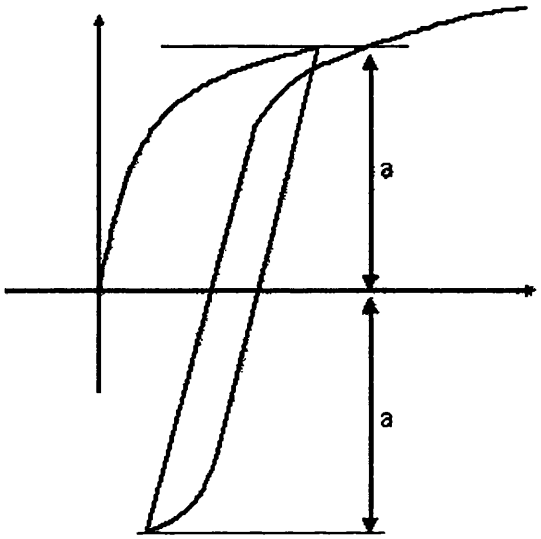

Figure 2.9. Graph of an anisotropic material showing the Bauschinger Effect

The loss of strength means the material is softened and is important if the working stress that is applied to a part is in the opposite direction to the manufacturing stress. Being able to predict the Bauschinger Effect and understands how it affects the material during and after manufacture can result in products with improved mechanical properties. Before going into anisotropic materials, there is a need to look at isotropic mathematic expressions. The two most common types of isotropic yield criterion is Tresca and von Mises

2.5.4.1 Tresca

The maximum shear stress theory also known as the Tresca yield criterion after the French scientist Henri Tresca. This assumes that yielding occurs when the shear stress τ exceeds the shear yield strength (Mielnik, 1991). For uniaxial tension, yielding will occur when the yield strength is reached. The pure shear, yielding will occur when the valve is half the yielding stress.

- $\sigma y = \sigma 2$
- $Tmax = 1/2\sigma y$

2.5.4.2 Von-Mises

The von mises yield criterion (also known as Prandtl–Reuss yield criterion). Figure 2.10 shows the von Mises yield surface in two-dimensional space compared with Tresca criterion.

$$\Phi = (\sigma_1 - \sigma_2)^2 + (\sigma_2 - \sigma_3)^2 + (\sigma_3 - \sigma_1)^2 = 2\sigma_0^2$$

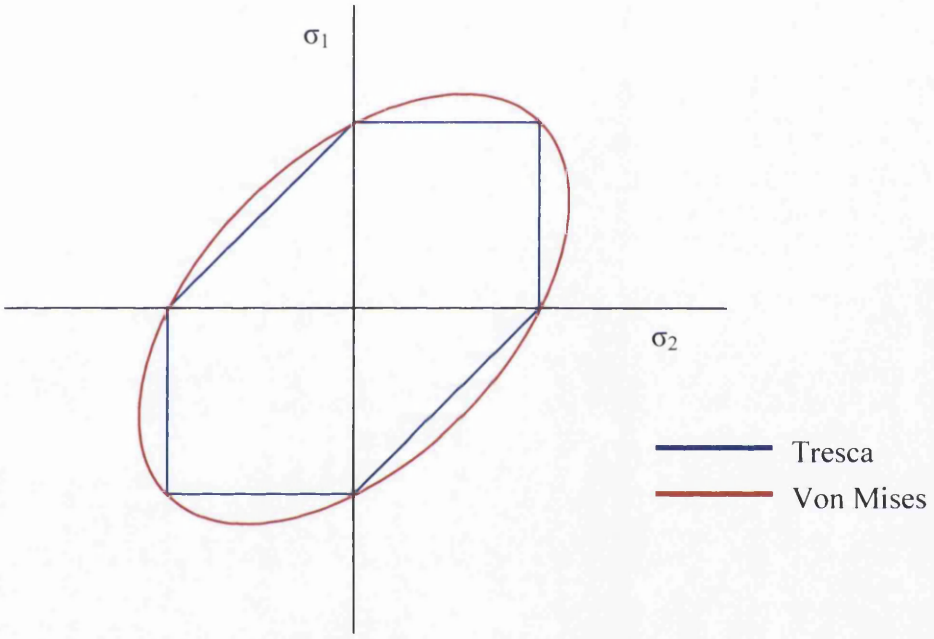

Figure 2.10. Illustration comparing the Treca and Von Mises yield surface

2.5.4.3 Other isotropic yield criterion

The reader should be aware that there are many different isotropic yield criterion including

- Mohr-Coulomb
- Drucker-Prager
- Bresler-Pister
- Willam-Warnke

Each one is a mathematical model that describes how a material will respond under stress. The Drucker-Prager is another isotropic yield criterion that is used in determining material failure under plastic deformation. Mohr-Coulomb, Bresler-Pister and Willam-Warnke are mainly used for brittle materials such as concretes.

2.5.5 Anisotropic

When a metal is subjected to large plastic deformations the grain sizes and orientations change in the direction of deformation. As a result the plastic yield behaviour of the material shows directional dependency. Under such circumstances, the isotropic yield criterion such as von Mises and Tresca are unable to predict the yield behaviour accurately.

2.5.5.1 Hill 48'

Rodney Hill has developed several yield criteria for anisotropic plastic deformations. The earliest version was a straightforward extension of the von mises yield criterion and had a quadratic form. This model was later generalized by allowing for an exponent *m*. Variations of these criteria are in wide use for metals, polymers, and certain composites.

The quadratic Hill yield criterion. has the form

$$F(\sigma_{22}-\sigma_{33})^2+G(\sigma_{33}-\sigma_{11})^2+H(\sigma_{11}-\sigma_{22})^2+2L\sigma_{23}^2+2M\sigma_{31}^2+2N\sigma_{12}^2=1\ .$$

Here *F, G, H, L, M, N* are constants that have to be determined experimentally and σ_{ij} are the stresses. Figure 2.11 shows the difference between the Von-mesis and Hill yield surface.

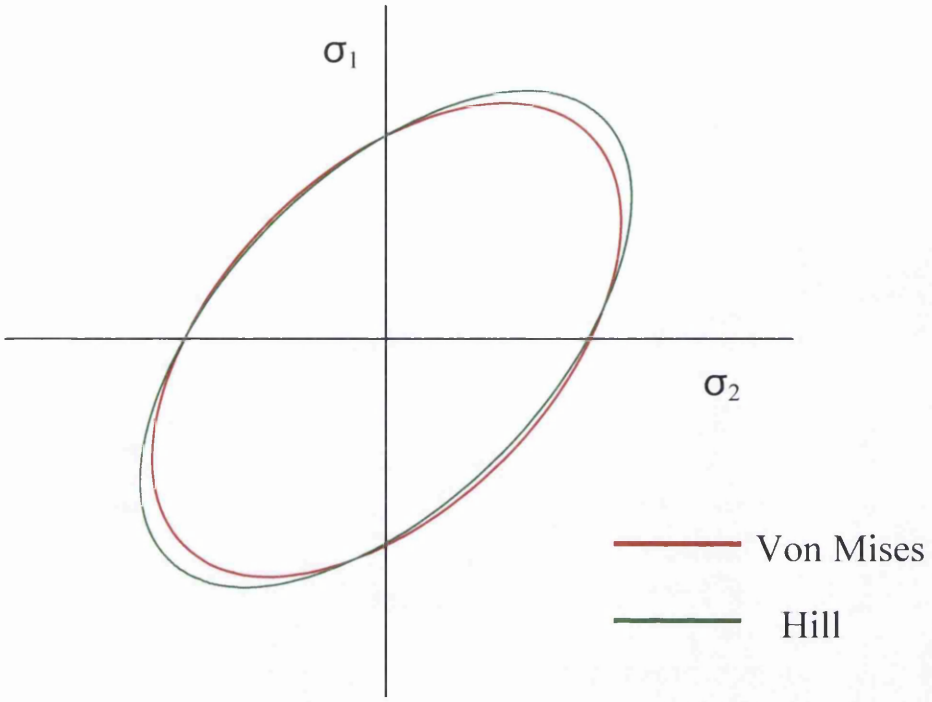

Figure 2.11. Illustration comparing the Von Mises and Hill yield surfaces.

On the yield surface the Hill model over predicts the plane strain and equibiaxial points Hill model, however the Hill model takes the r-value into consideration. The Hill model also underestimates the uniaxial point.

2.5.5.2 Barlats Yield Criterion

There are several Barlat models, including the 89, 91, 96, 00 and 04. Each of which has its own advantages and disadvantages to this project. The Barlat 89 was the first yield criterion developed by Barlat. It lacks accuracy compared to later versions developed.

The Barlat 91 was an improvement on the 89 model. It uses only 4 parameters to fit the yield locus. Uses either the yield stresses or the r-values of the material. This is the same with the Hill model. Ideally a yield criterion should include both for increased accuracy. The Hill yield criterion was already being used in this project.

The Barlat 96 is a yield criterion that takes into account both the yield stresses and the r-vaules hence has an increased accuracy over the 89 and 91 model. This yield criterion has 6

parameters to fit the yield locus. The Barlat 00 is a yield criterion which is only available in 2D plane stress. The models being developed for this thesis are 3D and so this criterion would not work. The Barlat 04 takes into account 18 parameters to fit the yield locus and would be very accurate. However obtaining all of the 18 parameters is long and difficult.

From the yield criterion available the Barlat 96 has been chosen as the third yield criterion. This is because it is more accurate then the Hill model and realises on 6 parameters that are available. RSL implemented the yield criterion within its code. The manual, including how the yield criterion is calculated, can be found in Appendix A.

Figure 2.12 shows the yield surface of the four yield criterion. The Von-mises, Hill and Barlat yield criterion will be used when the computer model is generated.

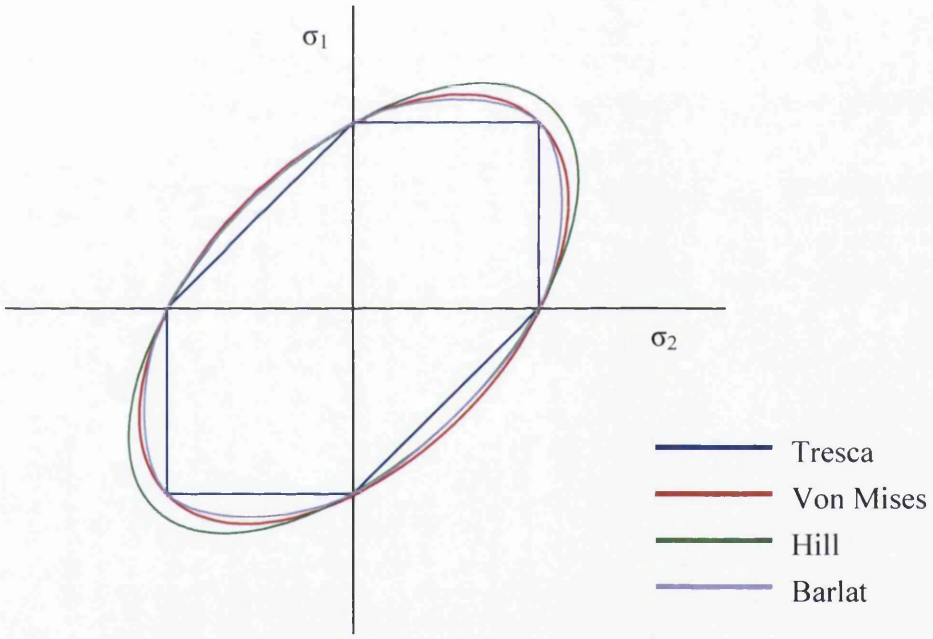

Figure 2.12. Comparison of the various yield surface based on different yield criterion.

2.5.7 Strain Rate Hardening

As what has been discussed earlier, yielding is where plastic deformation occurs. An increase in stress is needed to produce an increase strain level. This is known as strain or work

hardening. For a viscoplastic material the hardening curves are not significantly different from those of rate-independent plastic material.

Although the difference between plastic and viscoplastic hardening curves are not significantly different there are however differences, these are:-

- At the same strain, the higher the rate of strain the higher the stress
- A change in the rate of strain during the test results in an immediate change in the stress–strain curve.
- The concept of a platic yield limit is no longer strictly applicable.

The ideal of separating the strains into its elastic and plastic parts is still applicable.

$$\varepsilon = \varepsilon_e + \varepsilon_{vp}$$

where ε_e is the elastic strain and ε_{vp} is the viscoplastic strain. Take for example a piece of material that is under a initially load of 0.1/s. The strain rate is increase to 100/s instantly, held for a period of time and then instantly dropped back to 0.1/s, figure 2.13 shows how the stress strain graph alters. Even though the change in strain rate is instant they is a delay between the strain rate change and the stress response. This delay is modeled quite accurately by stress models such as the Perzyna model.

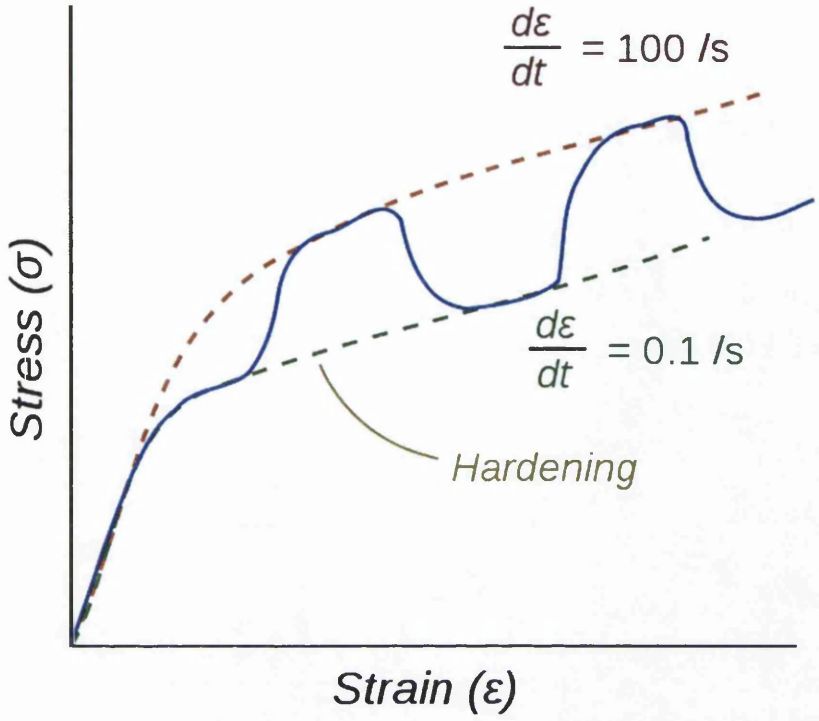

Figure 2.13. Illistration of how the change in strain rate affects the strain hardening curve

One strain rate dependent plasticity model is the Perzyna formulation. In the Perzyna formulation the plastic strain rate is expressed by the following term.

$$\dot{\varepsilon}_{vp} = \begin{cases} \dfrac{f(\boldsymbol{\sigma}, \boldsymbol{q})}{\tau} & \text{if } f(\boldsymbol{\sigma}, \boldsymbol{q}) > 0 \\ 0 & \text{otherwise} \end{cases}$$

where $f(.,.)$ is a yield function, σ is the stress, q is a set of plastic strain variables and T is a time.

The quantity $f(\boldsymbol{\sigma}, \boldsymbol{q})$ represents the evolution of the yield locus. The yield function *f* is expressed as an equation, which has been explained earlier, an example would be the Hill or Von Mises (Mielnik 1991). There are numerous flow stress models are used the computational plasticity. The models use a combination of temperature and strain rate dependency. The following below is a sample of the models in current use:-

- The Zerilli–Armstrong model.

- The Mechanical Threshold Stress model.
- The Johnson–Cook model.
- The Steinberg–Cochran–Guinan–Lund model.
- The Preston–Tonks–Wallace model.

2.6 Measuring Strain within a Material

2.6.1 Introduction

In order to determine when a material will fail, a measurement system is needed to calculate when this occurs. The ability to measure when thinning, necking, is occurring within the material is vital. As described earlier, thinning starts at the point the ultimate tensile strength, when the extension, strain, in the material has reached its maximum. A graph is needed where the strain, in both directions, within the material can be shown. This graph is called a Forming Limit Diagram.

2.6.2 Forming Limit Diagrams

A FLD is used to predict the failure of a material. Keeler and Backofen (1964) and Goodwin (1968) introduced the FLD to predict the onset of necking within the material prior to failure. Usually, a FLD are based on one strain path, either a single bending motion or linear elongation, where the ratio between the major and minor principal strains is constant throughout the deformation process (shown as the arrow on figure 11). The major corresponds the equation (2) and the Minor corresponds the equation (3)

Cao et al, (1999) describes a FLD as,

"The maximum strains that can be sustained by sheet materials prior to the onset of localised necking are generally referred to as the forming limit strains. A plot of the major and minor limit strains in the principal strain space constitutes a FLD."

2.6.3 Forming Limit Curves

A forming limit curve (*FLC*) is determined to predict to what extent sheet metal materials can be formed in a strain state by deep drawing or stretch forming or combinations of deep drawing and stretch forming. FLC's define the boundary between strain states that are always free of necks from those that are prone to necking under plane stress condition. The shape and location of the FLC are a characteristic of the metal that is independent of the forming process or the work piece shape.

The FLC indicates that a material can be safety formed until the major strain meets a point on the FLC (figure 2.14). Beyond this curve will result in failure of the material, usually tearing. The FLC is different for each type and variation of material and also charges depending on the manufacturing process.

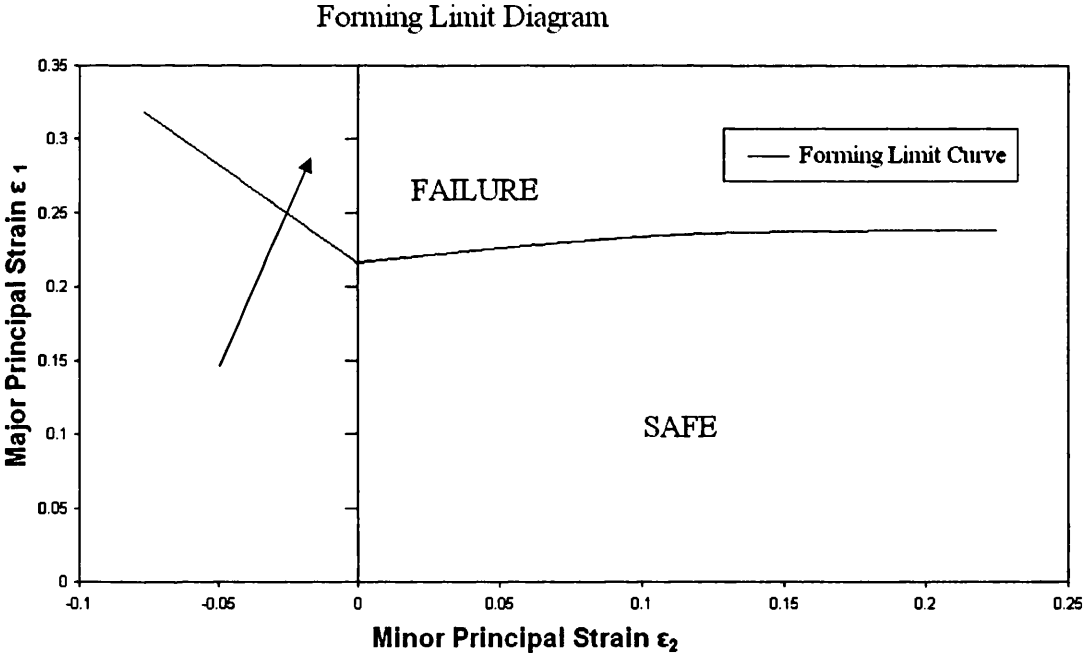

Figure 2.14. An example of a forming limit diagram (FLD) with a forming limit curve (FLC), (Cao et al, 1999)

However, there is not much understanding of how materials failure during the DRD and DWI processes. These processes are not linear due to being multi-step forming operations. There are several bending and elongation stages during the manufacture which changes the linear strain path. Changes to a linear strain path can substantially increases or decreases the level of the FLC. This makes it very hard to predict the FLC in regards to these processes. There are many ways to change the linear path including, geometry of the tool, friction, multi-step operations and material springback. Therefore being able to predict non-linear strain paths for

FLDs is an important tool to manufacturing companies to increase manufacturing efficiency. FLDs are not just for determining when materials will fail, figure 2.15 explains the how the FLC can be used to determine the properties of the material

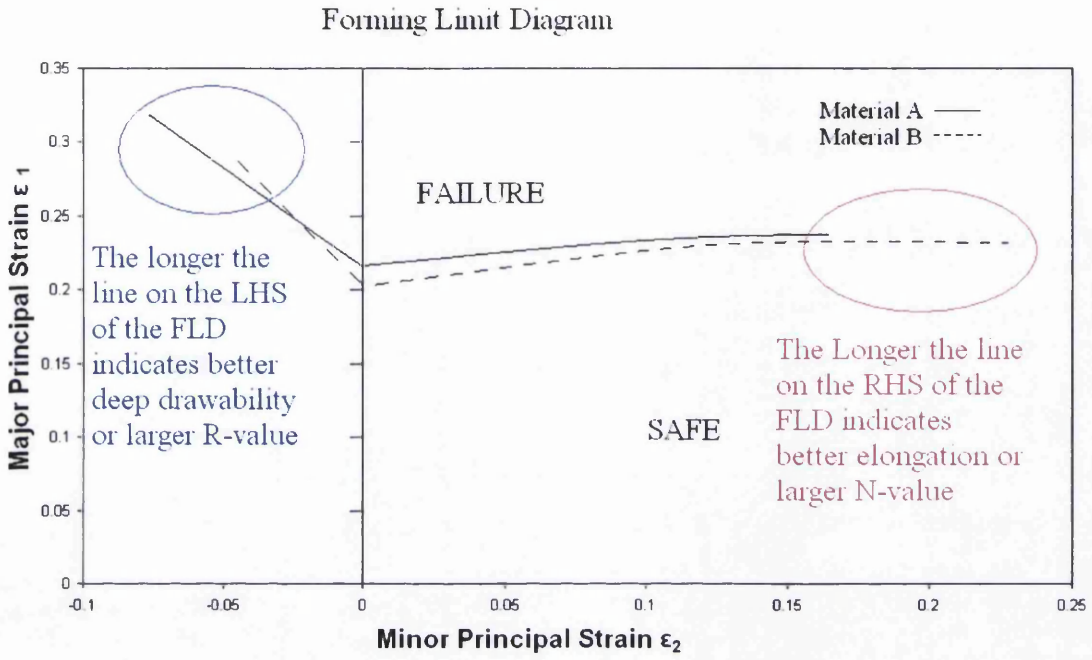

Figure 2.15. An explanation of the FLD

The right hand side of the graph indicates the N-valve. The long the line the better elongation the material has. The left hand side of the graph indicates the R-valve. The R-valve influences the deep drawability of the material.

Kumar (2002) examine the formability parameters that affect the drawing process using forming limit diagrams. The parameters were the strain hardening coefficient (*n*-value) and the normal anisotropy (*r*-value). Kumar took different thicknesses of low carbon steel sheets, and examined the affect the *n* and *r*-value had on the deep drawing process. The conclusions showed that the major principal strain level was increased with sheet thickness, the biaxial tension zone is largely dependant on the *n*-value, the length of the curve on the left hand side of the graph is increased with larger *r*-values and the slope of the forming limit curve is affected by the $\bar{r}$-value.

2.6.4 Construction of an FLC

During sheet metal forming three dimensional stress states will occur. Figure 2.16 shows a piece of material that has length, l, width, b and thickness, t. The three dimensional strains are

show as 1, 2 and 3 respectively. Ɛ1 the major strain in the sheet's plane, Ɛ2 the minor strain in the sheet's plane and Ɛ3 is the thickness strain.

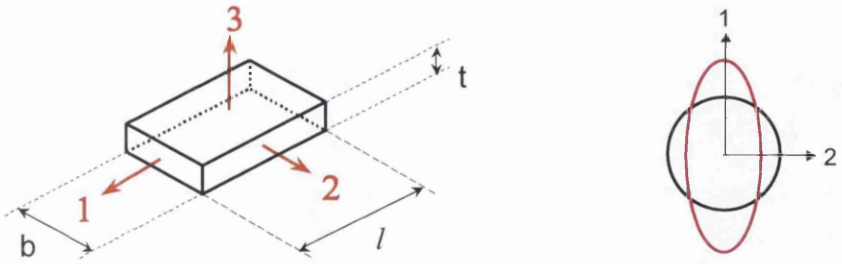

Figure 2.16 and 2.17. Strains directions that act on materials and illustration showing how a uniaxial force deforms the material repectively.

If a circle was applied to the surface and the uniaxial force applied along its length which deformed the piece, the circle would be deformed into an oval, figure 2.17. Depending on the direction the force was applied the circle would deform differently giving different shaped ovals. Knowing how this oval has deformed from the starting circle the major and minor strains can be measure. These strains are plotted on a graph giving a FLD, figure 2.18.

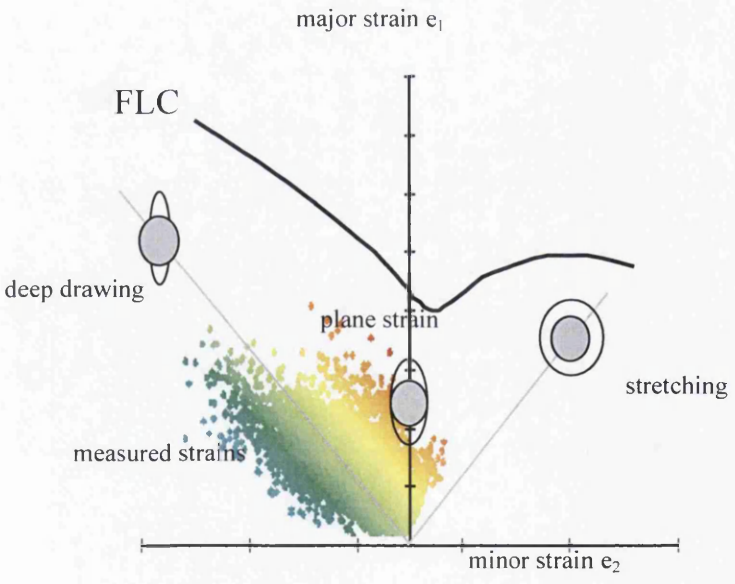

Figure 2.18. FLD showing the deformed grid.

These circles are usually applied in a grid pattern on a sample. There are two main ways to determine the FLC of a sheet metal material, these are the Nakazima and Marciniak test.

2.6.4 Limitations of FLD's and FLC's

There are limitations on the applicability of a FLC, one is the samples that are formed to determine the FLC must be formed under plane stress conditions, bending within the material is not ideal. Bending causes stress gradients over the thickness and it violates the plane stress requirement. Figure 2.19 shows that when the punch has plastically deformed the material the two side will undergo different loads. The top face of the material undergoes tension and the bottom face undergoes compression. This difference of tension one side and compression the other side introduces a stress gradient across the thickness of the material which contravenes the plane stress requirement.

The thicker the material is, the stress gradients will have a higher influence, on the other hand, as the thickness of the material thins to zero, the stress gradient has also lowers. To reduce bending within the material, either use a thinner material, or increase the radius of the punch. Increasing the radius of the punch reduces the compressive load on the material, reducing the stress gradients.

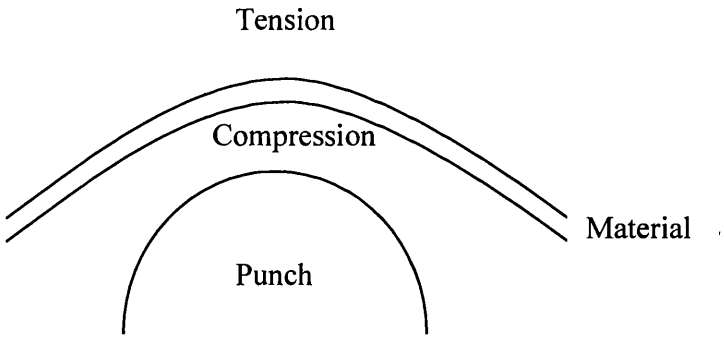

Figure 2.19. Stress gradients over the thickness

Another limitation is that too obtain a true FLC, the FLC is determined under isothermal conditions. Meaning the temperature should be the same for all the samples that are tested. A change in temperature would effect how the material would react under load.

2.7 Friction

2.7.1 Introduction

Fiction is an important issue in sheet metal forming processes due to the motion of the sheet metal surface during deformation. Other then the mechanical properties of the sheet metal, friction has the largest influence on the development of stress and strain across a formed part. Therefore being able to control the friction during the process can minimize the amount of surface damage and defects throughout the formed part.

2.7.2 Friction during Sheet Metal Forming

Excessive friction also has a negative effect on the life of the tool, in this case the punch, blankholder and die. Problems generated by friction include, heat which increases tool wear and reduces tool life, wearing between the tool and the work piece which produces damage surfaces, pick-up and galling of the tool, these all contribute to the damage or failure of a material under forming (Ebrahimi and Najafizadeh, 2004). Gaard et al (2006) defines galling as:-

"The transfer and accumulation of adhered sheet material to the tool surfaces."

During the cup operation of the draw redraw process, the flat blank material is placed between the die and the blankholder with a certain force. The punch moves downwards to produce the cup. The blankholder force and the fiction between the blank and the die and the blankholder, determines the ease in which the blank can flow into the die. If the blankholder force is too high the blank is unable to flow into the die which can lead to damage surfaces and necking of the material, in some cases this necking can produce fracture by tearing. However, if there is insufficient force, the blank has too much freedom when being drawn which produces wrinkling (Yagani et al, 2007).

Commonly a forming window (figure 2.20) is used to show the safe combination of blankholder force and drawing ratio. By using this window, material can be successfully drawn without tearing or wrinkling. The safe working window can be increased greatly by lowering the friction (TATA RD&T, 2007).

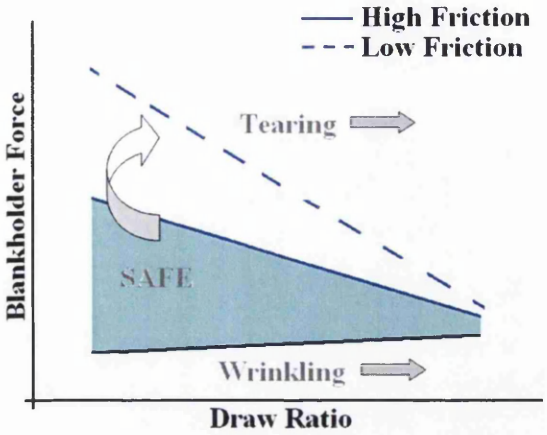

Figure 2.20. Graphical representation of the safe working window for drawing.

Although lowering the friction is advantageous, it is not always the best idea to reduce it to its absolute minimum value. Friction can be used beneficially to control the material flow rate into the die. Generally to control the friction acting on the material being formed lubricants are used. Lubricants are used to limit and control the friction, not too eliminate it altogether (Ebrahimi and Najafizadeh, 2004).

2.7.3 Controlling and Utilising Friction

Various ideas have been produced to limit, control or utilise the friction in the attempt to reduce the damage to the part under forming. Fratini et al, (2006) did research into using different lubricants to help produce a constant flow rate into the die. Using no lubricant (dry), grease and Teflon they studied to reduce the stick-slip phenomena, which can inflict surface damage to the blank during forming, and in some cases lead to failure. By reducing this phenomena would reduce surface damage and reduce the risk of tearing and wrinkling. They concluded that using Teflon was the best of the three options.

Maslennikov, (1957) examined the potential of increasing the drawing ratio with the use of friction. He used rubber pads which moved with the material into the die, this increased controlled friction increased the drawing ratio from a factor of 2 to 3. There were large problems produced by this high drawing ratio included high chance of flange fracture if the sheet material was to thin, sheets with large thickness or high strength could not be draw successfully and the process required a high compressive load by the blankholder that wore the rubber ring. It was also found that the rubber pads needed to be replaced after 100-10,000 draws, depending on the

sheet material. With manufacturing techniques producing 250 cans and upwards per minute it would be unfeasible to use them. Because of the problems the idea of using friction in increase the drawing ratio was forgotten about for a while.

Thiruvarudchelvan and Tan (2005) about 50 years later used a similar method to Maslennikov to increase the draw ratio. They modified a draw redraw rig to use friction to increase the drawing ratio. Although the rig and the method of the experiments were different they used the idea of friction to increase the draw ratio.

Chapter 3

EXPERIMENTAL TECHNIQUES AND RESULTS

CHAPTER 3 – EXPERIMENTAL TECHNIQUES AND RESULTS

3.1 Introduction

In chapter 2, thinning of materials during forming was discussed and the ability to measure thinning, in the form of FLDs was reviewed. In order to produce a computer model, experimental results are needed to validate it. The following chapter shows the experimental procedures and results obtain from the testing carried out.

3.2 Erichsen Test

3.2.1 Introduction

Before testing was carried out on the Nakazima testing machine, several steel grades were tested on an Erichsen testing machine. This initial testing was carried out primarily to determine crack direction, secondly to examine how different lubrications affect the materials under testing and thirdly to examine the ductility of the steel grades.

The crack direction of the material is important later in the Nakazima test. This is so the crack propagates in the direction of lowest limit strain for steel this is parallel to the rolling direction. This is outlined by the International Standard ISO 12004-2. Both the Erichsen and Nakazima test experimental procedures indicate that the thickness of the material being tested should be between 0.3mm to 4mm. The materials under testing have a thickness of less than 0.3mm which is not in the limit set by the international standards. As the thickness of a material becomes thin, fiction has a high influence, inducing necking of the material. Different lubrications will be used to help reduce this early necking to obtain cracks that are straight over the top of the bulge. Ductility will be measured by the height of the bulge each material reaches upon failure. This will be used to help decide which materials will be taken further for the Nakazima test.

3.2.2 Materials Utilised

There were fifteen materials tested, a list of the materials can be found in Table 3.1. There were a range of the current packaging steel grades as well as some DR grades and other grades including a new HSLA grade.

Material	Thickness (mm)	Code	Order Number	Storage Number
T52 BA	0,21	TS 245	80989A	20080230
T57 BA	0,21	TS 275	80873K	20080235
T57 CA	0,21	TH 340	88349A	20080231
T59 CA	0,21	TH 390	80991A	20080232
T61 CA	0,21	TH 415	80995A	20080233
T65 CA	0,21	TH 435	88915M	20080234
DR 550 BA	0,21	TS 550	80116H	20080216
DR 550 CA	0,22	TH 550	80353C	20080225
DR 550 CA	0,17	TH 550	80730A	20080214
DR 550 CA	0,17	TH 550	80680A	20080226
DR 620 CA	0,17	TH 620	88426P	20080227
T48 BA	0,18	TS 300		20061810
FN81 DR25 BA	0,21	TH 55N		20070251
FN81 DR16 BA	0,24			20070252
1N86 SR	0,20			20080212

Table 3.1. List of materials used for them Bulge Test.

3.2.3 Procedure

The experiment was carried out to International Standard ISO1520 2006(E)-cupping test and to TATA's document number PCK P&P 025D revision 4. Figure 3.1 shows the equipment used for the experiment. The experiment was carried out at TATA's packaging research centre in Ijmuiden Holland.

Figure 3.1. Erichsen testing equipment

There are two procedures to the International Standard ISO1520 2006(E). The first is to draw the material to a predetermined depth and use a microscope to examine the material for cracks or the onset of localised necking. The other procedure, which is the one being use for this experiment, is to determine the minimum depth of draw to cause failure of the material, i.e. draw the material until a crack propagates on the surface. At this point the depth of the draw will be measured. The bulge depth needs to be measured to the nearest 0.1mm and the thickness of the materials to the nearest 0.01mm.

There were four types of experiments done using various lubrications. The first type was to do the test dry without any lubrication. The second type was to use a viscous liquid. The third test was done with a PET sheet between the material and the ball of the cupping equipment. The final experiment was to use a Teflon sheet instead of the PET sheet. The apparatus was cleaned after each test to ensure a fair test and to avoid the build up of excess lubrication which could have affected the results. Each of the four experiments was repeated three times to confirm the results obtain. Table 3.2 shows the test number of each of the materials against the test conditions.

Test Number	Test Conditions
1	No Lubrication
2	No Lubrication
3	No Lubrication
4	Viscous Liquid
5	Viscous Liquid
6	Viscous Liquid
7	PET Sheet
8	PET Sheet
9	PET Sheet
10	Teflon Sheet
11	Teflon Sheet
12	Teflon Sheet

Table 3.2. Test numbers corresponding to the test condition.

The cupping test equipment conformed to the International Standard ISO design shown in figure 3.2.

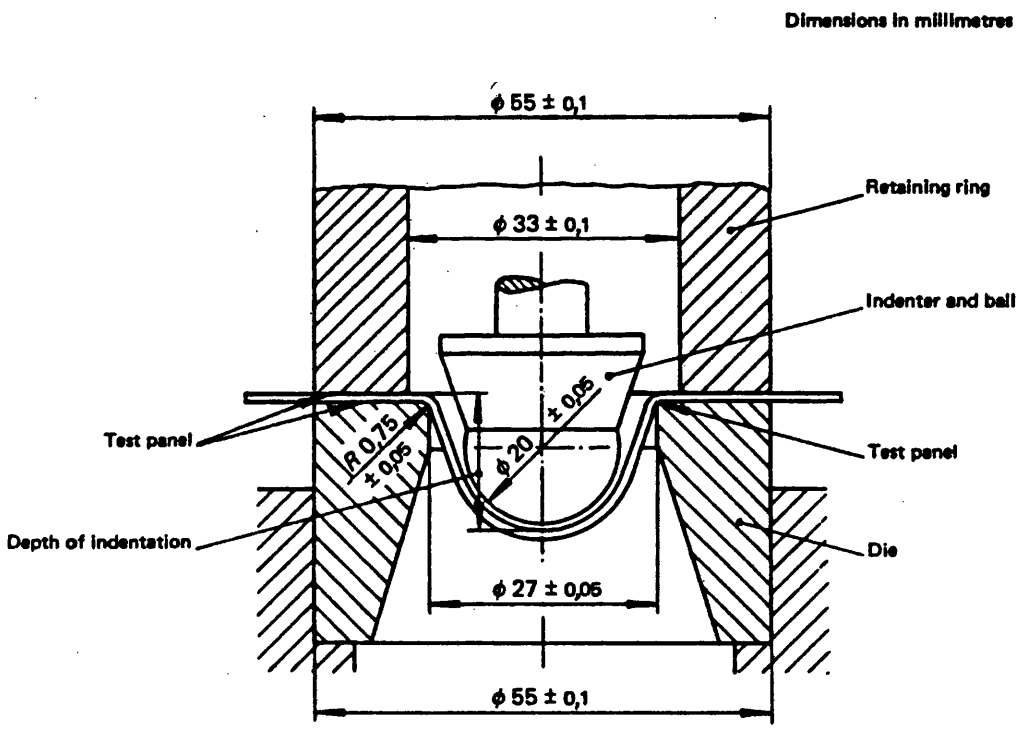

Figure 3.2. International Standard design for ISO1520 2006(E)-cupping test

3.2.4 Results

The results obtain from the Erichsen testing are shown in Table 3.3. All

Test No.	1	2	3	4	5	6	7	8	9	10	11	12
Material	Height crack was formed (mm)											
T52 BA	8.21	8.11	8.42	8.60	8.60	8.74	9.80	9.78	9.80	9.64	9.51	9.47
T57 BA	7.27	7.83	7.30	8.00	8.30	8.55	8.52	8.95	8.80	9.56	9.54	9.56
T57 CA	9.00	8.64	8.51	8.35	8.80	8.65	8.25	8.02	8.01	8.08	8.05	7.90
T59 CA	9.10	8.70	8.60	8.85	9.01	8.90	8.44	8.56	8.70	8.60	8.62	8.51
T61 CA	9.00	9.05	8.65	8.80	8.95	8.96	8.46	8.25	8.42	8.30	8.46	8.66
T65 CA	7.00	8.05	7.75	7.82	8.00	8.05	7.70	7.72	7.45	7.21	7.61	7.58
DR 550 BA	5.57	5.59	5.24	5.62	5.60	5.37	4.25	4.81	4.72	4.62	4.58	4.39
DR 550 CA	6.30	6.60	6.62	6.50	6.61	6.57	5.76	5.81	5.77	5.85	5.67	5.71
DR 550 CA	7.15	7.62	7.17	7.60	7.70	7.82	7.76	7.43	8.17	7.74	7.75	7.61
DR 550 CA	5.70	5.51	5.72	5.60	5.81	5.80	5.29	5.32	5.05	5.21	5.28	5.22
DR 620 CA	5.25	5.05	5.17	5.07	5.26	4.97	4.63	4.57	4.24	4.49	4.49	4.23
T48 BA	7.22	6.51	6.36	7.95	7.98	8.53	7.86	8.10	7.86	7.50	7.87	8.27
FN81DR25BA	5.70	5.76	5.51	5.61	5.89	5.86	5.01	4.66	4.92	4.70	4.86	4.87
FN81DR16BA	5.06	5.66	5.17	6.52	6.57	6.63	6.10	6.28	6.16	6.01	5.90	6.11
1N868R	8.24	8.41	8.89	8.93	8.70	8.75	7.60	7.31	8.00	7.79	8.19	8.03

Table 3.3. Experimental results for the Erichsen Testing.

3.2.5 Discussion

The general crack directions of all the materials were parallel to the rolling direction. There were four tests in which the material did not fail in the rolling direction. Two of the test T57 BA test 8 and T57 CA test 1 (figures 3.3 and 3.4) the material failed 45° to the rolling direction. The T57 CA could have happened because of friction. The test was carried out without lubrication which would affect the material movement during cupping because of the high friction. This could produce a high area of stress not along the rolling direction resulting in a crack at the 45° angle to the rolling direction. The T57 BA test was carried out using the PET sheet, the lubrication should have allowed the material to move during testing resulting in the crack propagating along the rolling direction. With the crack not propagating along the rolling direction the likely reason for this would be a defect within the material.

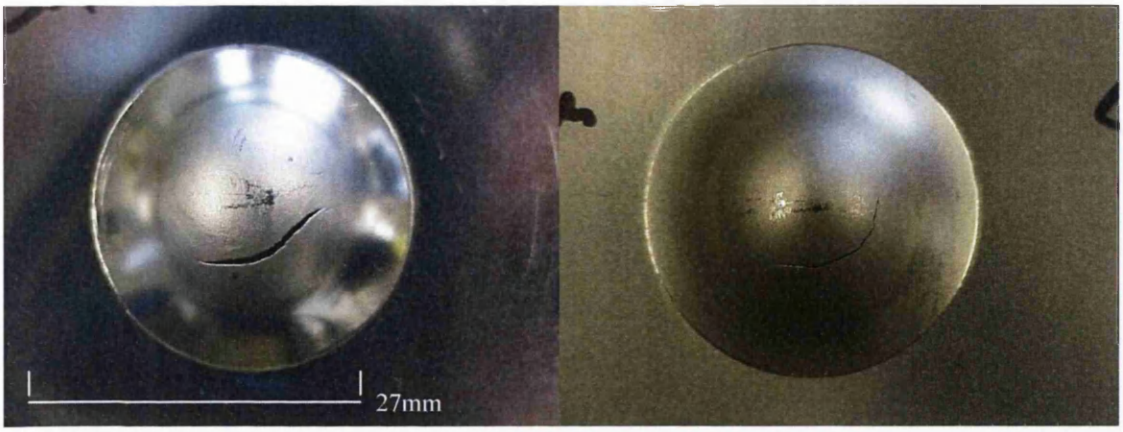

Figures 3.3 and 3.4 showing materials T57 BA and T57CA that cracked at 45° to the rolling direction respectively.

The other two tests, T59 CA test 6 and one of the DR 550 CA test 5 (figure 3.5 and 3.6) fail perpendicular to the rolling direction. These two tests failing to crack parallel to the rolling direction could have happened because of imperfections within the material which would result in slip plane orientation different to the rolling direction resulting in the crack propagating perpendicular to the rolling direction.

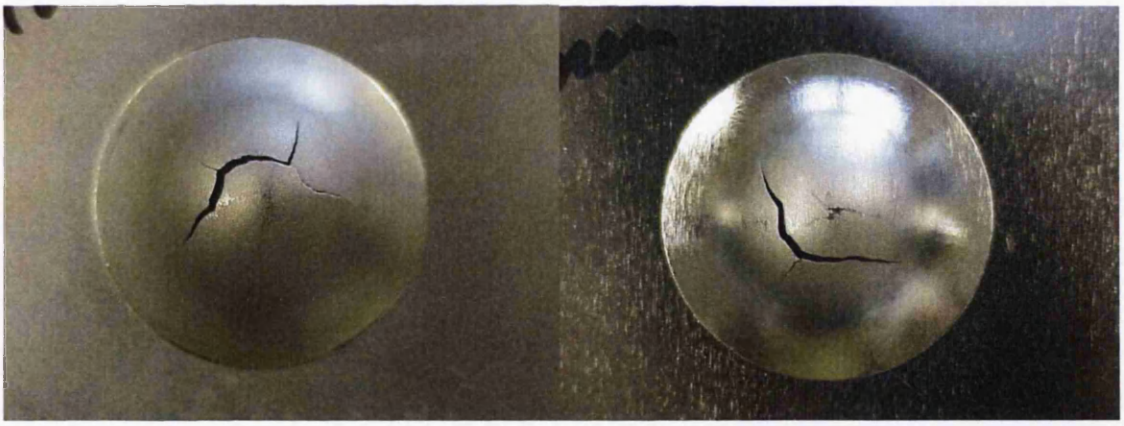

Figures 3.5 and 3.6 showing materials T59 CA and DR 550 CA that cracked perpendicular to the rolling direction respectively.

Materials T48 BA, T52 BA and T57 BA behaved similarly. Under dry testing the crack propagated from 4.5mm-6mm from the centre of the bulge. There was necking around the top area of the bulge in a circle to which the crack was propagating around, this can be seen in figure 3.7. The crack can be seen around the right side of the bulge while the arrows on the left side indicating where the necking around the top area of the bulge was. The viscous liquid had three effects on the materials. Firstly the crack propagated closer to the centre of the bulge, between 4mm-5mm. Secondly the bulge height was increased and thirdly the crack did not propagate around the top of the bulge as much as under dry conditions. After it had crack part of the way

around the bulge the crack straightened. Adding a small sheet of PET material between the steel grade and the ball increased the bulge height further. The crack also moved towards the centre of the bulge, the cracks were between 3.5mm-4.5mm from the centre. The necking around the top of the bulge that was seen with the previous types of test was not seen and the crack was straighter to the rolling direction. The Teflon sheet had two main advantages over the PET sheet, the crack propagated closer to the centre of the bulge and the crack was much straighter resulting in a good tare.

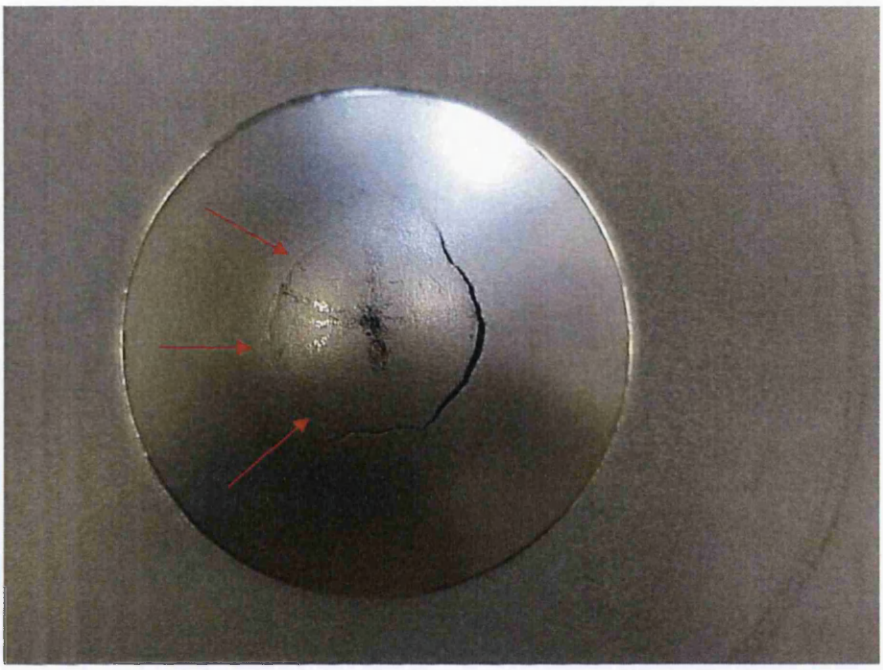

Figure 3.7. Material T52 BA showing necking and crack propagation around the bulge under dry conditions.

T57 CA, T59 CA, T61 CA and T65 CA grades performed similarly. Although the bulge height differed slightly from the T57 CA to the T65 CA the pattern of how the material behaved were the same. The bulge height decreased as the lubrication was changed, however the initial crack and the straightness of the tare moved from 3mm-4mm with no lubrication to within 1mm of the centre of the bulge height, this is seen from figures 3.8 to 3.11. Another note was with no lubrication the failure of the material was brittle where as with lubrication there was necking in the material before the crack propagated to a tare.

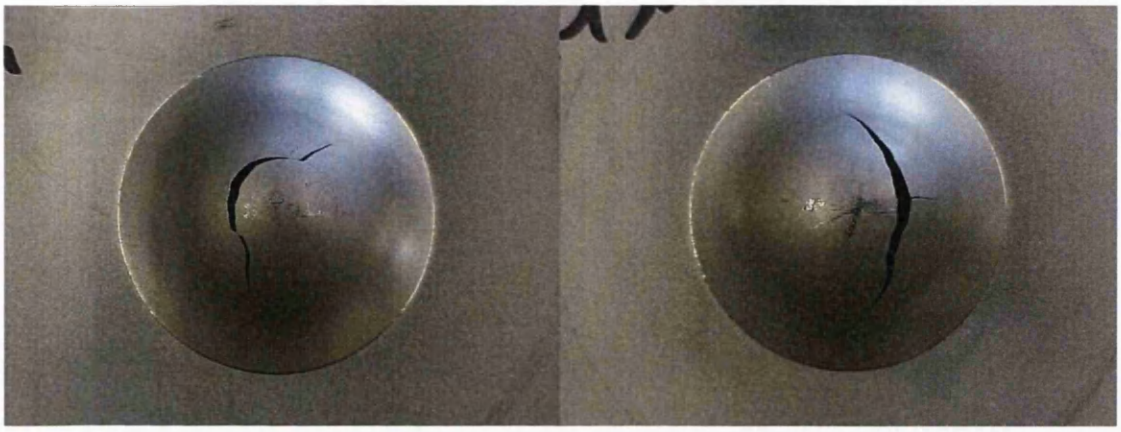

Figures 3.8 and 3.9 show the results of the tests under dry and viscous liquid respectively.

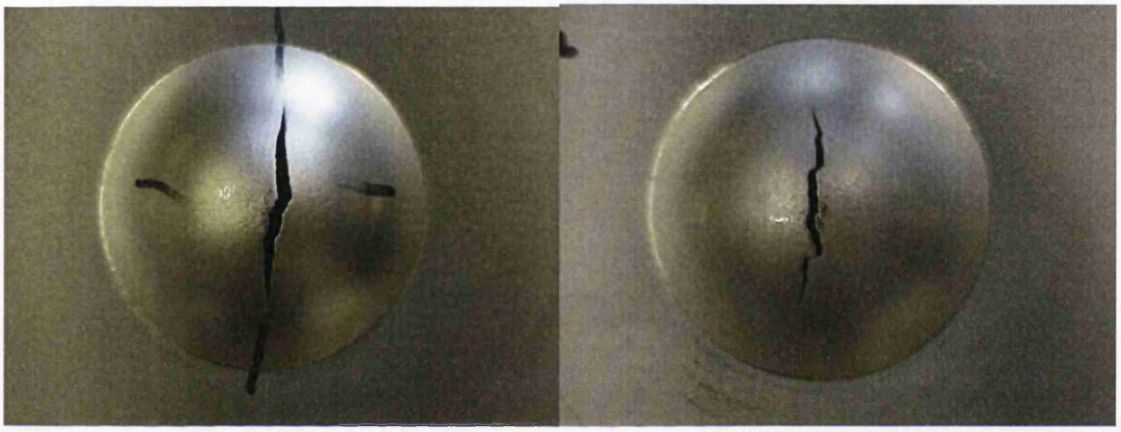

Figures 3.10 and 3.11. Tthe results of the tests with PET and Teflon sheets respectively.

With the DR 550 BA, the three DR 550 CA and DR 620 CA grades, the bulge height decreased. With no lubrication and the viscous liquid the bulge height remained the same, with the crack propagating closer to the centre of the bulge using the viscous liquid, figures 3.12 and 3.13. However when the PET and Teflon sheets were used the bulge propagated over the centre of the bulge but there was a reduction in bulge height over about 0.5mm-1mm, figures 3.14 and 3.15.

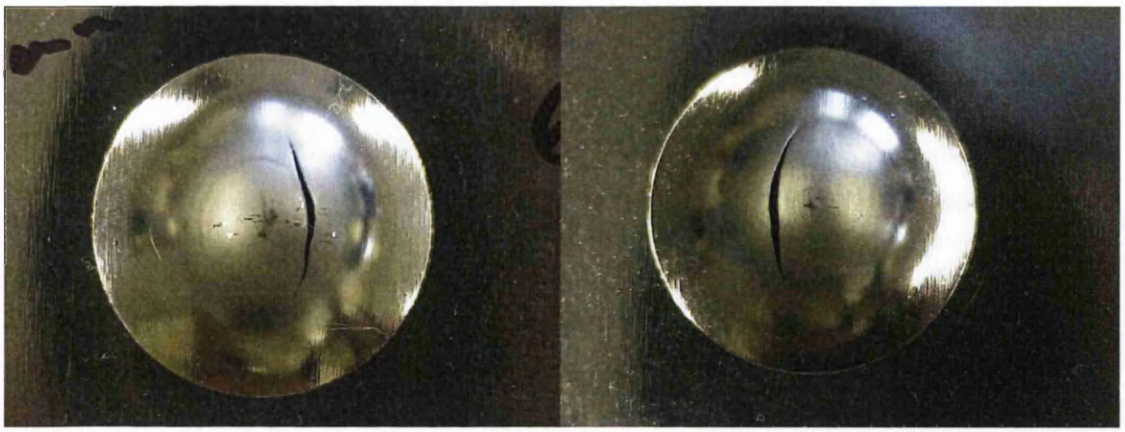

Figures 3.12 and 3.13. showing the necking ring around the bulge under dry conditions, and the viscous liquid which reduces the necking ring and results in the crack initialising closer to the centre of the bulge respectively.

Figures 3.14 and 3.15 showing the PET and Teflon sheets helped to propagate the crack at the centre of the bulge and formed a straight tare.

FN81 DR25 BA and FN81 DR16 BA behaved similarly with the bulge height. Both increased the bulge height with the introduction of the viscous liquid, with DR25 increasing slightly of about 0.2mm-0.3mm where as the DR16 grade increased over 1mm. Then they behaved like the other DR grades, with the introduction of the PET and the Teflon sheets the bulge height was reduced about 0.5mm-1mm. However with such a large increase in bulge height of the DR16 grade compared to the DR25 grade, the DR16 grade increased its bulge height overall, where as the DR25 decrease over all. With both materials the crack propagated closer to the centre of the bulge as the lubrication was increased. However the DR25 grade propagated its cracks much closer to the centre then the other.

1N86 SR which is a new HSLA grade of steel performed well. The bulge height was above 8mm which shows good ductility. The cracks propagated along the rolling direction and the tare was smooth and straight. Under dry and viscous conditions the material cracked within 2mm

of the top of the bulge and using the PET and the Teflon sheets made the cracks propagate right over the centre of the bulge.

The two DR 550 CA grades with thickness of 0.17mm had different results. The DR 550 CA grade with the higher bulge depth is believed not to have been treated correctly during manufacture. This material has been sent off for tensile testing to obtain results to which material it is. The thought currently is that is will be similar to the T65 CA.

Something that has been previous been identified by TATA is that as the thickness of the material decrease it becomes more difficult to obtain good centre cracks. The Erichsen test showed that obtaining good centre cracks was difficult. With regards to the Erichsen testing friction was found to be the main influence on the crack location and how it propagates after.

Friction has a directed affect on with failure mode occurs. Under low friction the material can move over the punch resulting in a biaxial failure mode occurring at the centre of the bulge. The material is aloud to stretch resulting in the crack propagating at the centre of the bulge. As the friction between the material and the punch increases, the material does not move over the surface of the punch resulting in an area of high stress off centre to the bulge. This is the necking ring seen in figure 3.7. As a crack propagates it follows the necking around the bulge to a point and then crack at a tangent. Because the crack propagates along this necking ring at a tangential point, the failure can be considered somewhat uniaxial to a degree. Figures 3.16 and 3.17 show the differences under different friction conditions.

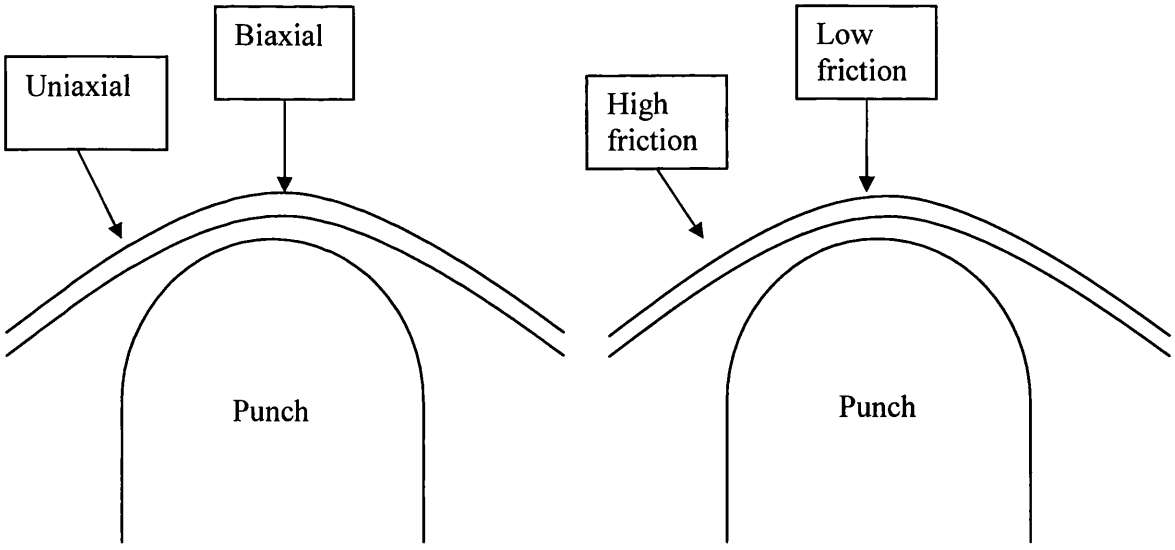

Figures 3.16 and 3.17. Illustrations of altering strain condition and friction around the punch

A general discussion point that can be taken, looking at figures 3.18 and 3.19, is that the "better" or lower the frictional conditions during testing will result in a biaxial test taking place. This will result in the failure of the material at the centre of the bulge. Therefore this will be similar with the Nakazima test, therefore it will be important to get the frictional conditions right

Figures 3.18 and 3.19 show this, the only parameter that is different is the lubrication (friction.) Figure 3.18 has no lubrication and produced a crack ring. This occurs because without any lubrication the material does not stretch over the centre of the punch. This makes the material thin off centre producing a necking ring, the crack propagates and follows the necking ring around producing the circular crack shown in figure 3.18. Figure 3.19 has lubrication in form of Vaseline spray and Teflon pad. The lubrication allows the material to stretch over the punch resulting in a centre crack.

Figure 3.18, material T57CA with no lubrication produces a circular crack.

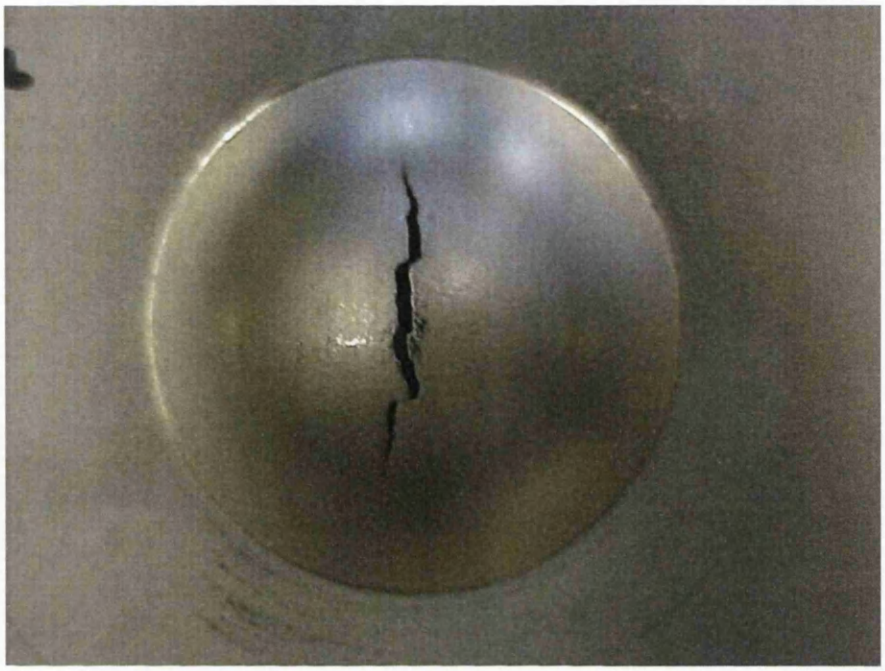

Figure 3.19, material T57CA with Vaseline spray lubrication produces a centre crack.

3.2.6 Erichsen Conclusion

The crack propagated along the rolling direction for all of the steel grades. This indicates that the grades will be suitable for Nakazima testing to obtain the FLCs of the materials.

Lubrication affects where the crack propagates from in relation to the centre of the bulge. Using PET and Teflon sheet resulted in improve crack straightness and producing cracks at the centre of the bulge. This information will be helpful when experimentation takes place with the Ericsson test.

The DR grades had the poorer results with regards to bulge height, indicating that their ductility not up to the current packaging steels. However the crack propagation and straightness with regards to the centre of the bulge was better. The new HLSA grade performed as well as the current packaging steels with its ductility and produced good centre bulge, straight, smooth cracks like the DR grades.

The DR 550 CA grade which is believed not to have been treated correctly during testing will be reviewed when the results of the tensile testing are available.

3.3 Preliminary Nakazima Test

3.3.1 Introduction

There are two main test methods for obtaining FLCs, these are the Nakazima and Marciniak test methods. Barisic and Pepelnjak (2008) used the Marciniak test method and tried to determine a FLC for a Tinplate steel of 0.24mm thickness. Their main problems were the frictional conditions and edge cracking when the blank was formed. The edge cracking resulted in no centre cracks being formed in the required area. To address this problem the blank's geometry was altered until centre cracks could be obtained as well has examining different lubrications.

Obtaining centre cracks on the blanks are important for several reasons. Firstly it shows the friction has been limited. Fiction will cause the crack to form on the side of the blank, meaning friction will affect the amount of strain within the material on failure. Secondly it shows that plane stress conditions have been met. Thirdly that the crack has been produce by a straight strain path, no bending or shear has influenced the material under failure.

The difficulties encountered by Barisic and Pepelnjak with regards to edge cracking were a combination of friction properties and tool geometry. The difference between the Marciniak and Nakazima test experiments are shown in figures 3.20 and 3.21. The Marciniak has a flat top punch where as the Nakazima has a domed punch. In both cases to obtain a centre crack the blank must be allowed to stretch freely over the punch. If the friction between the blank and the punch is great enough where they move together, there will be a high stress area which will produce necking and the resultant failure will be in another area not at the centre of the blank. In Barisic and Pepelnjak case either or a combination of the friction between the blank and the flat top punch or around the radius of the top of the punch was great enough to cause a high stress area around the Die radius. This resulted in edge cracking of the blank. The Nakazima punch geometry has one large radius, so as long as the friction properties allow the blank to stretch over the punch, edge cracking should be avoided.

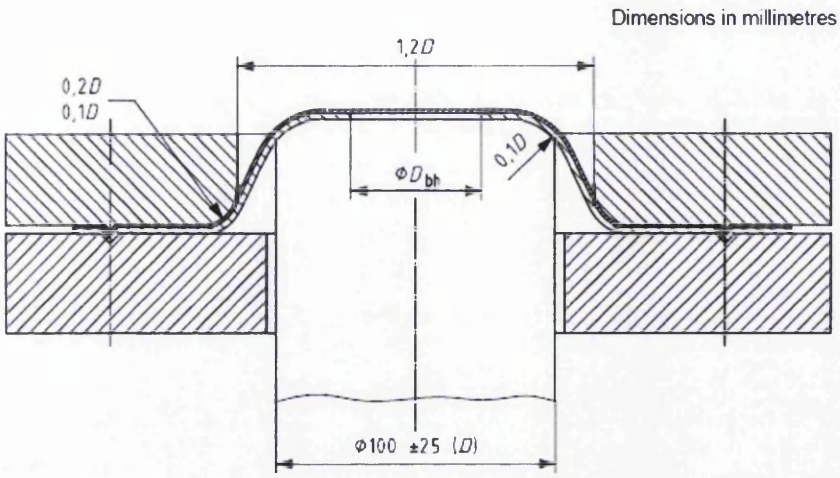

Figure 3.20. Illustration of the cross section of the tool used for the Marciniak testing.

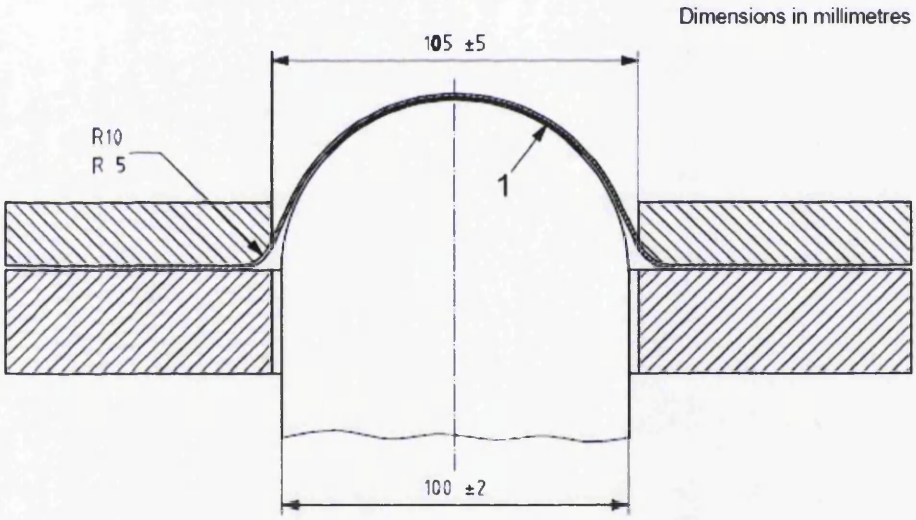

Figure 3.21. Illustration of the cross section of the tool used for the Nakazima Testing.

The Nakazima testing method was chosen because of the problems with obtaining centre crack using the Marciniak test method. Also this was the only type of machine available within TATA.

The international standard ISO 12004-2 was used to carry out the process. The difference between the international standard and the equipment used for this project was the punch radius

was 75mm and not 100mm. Due to machine availability the 100m punch machine was unavailable. The 75mm punch machine was available which was the punch radius specified in the previous version ISO 12004. When the new ISO standard was brought into effect, TATA did a comparison between a 75mm and 100mm punch, various steel grades and thicknesses were used (Tea 2007). There conclusion stated that the tests that were carried out:-

"Resulted in quite the same forming limit curves for the 75 mm diameter punch and the 100 mm diameter punch."

Figure 3.22 shows a result comparing a 75mm and 100mm punch. The slight variation in results would be down to equipment and blank errors. However both would produce a FLC of similar paths. This gives a level of confidence that the results obtained from testing will be comparable to results obtain if the 100mm punch had been used.

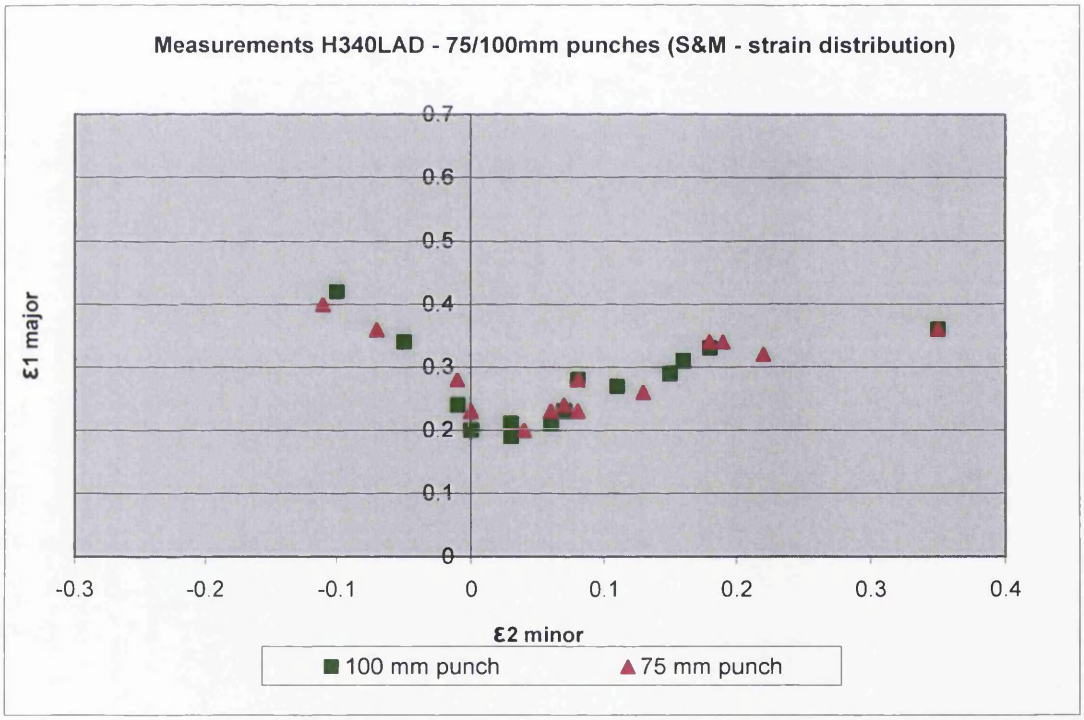

Figure 3.22. Comparison of measurements of H340LAD between 75mm and 100mm punches.

The reason the ISO standard changed from 75mm to 100mm was to decrease the effectiveness of bending within the material. As described earlier about the limitations of FLC, bending within the material causes stress gradients over the thickness and it violates the plane stress requirement that the Nakazima test needs. TATA's comparison of the two different punch

sizes showed that the results would be similar. Also the materials that are being tested in this thesis are 0.21mm thick. Typically the thickness of material used in the Nakazima test is between 1-3mm. This is much thinker and hence bending would have more of a higher influence. Having a material thickness of 0.21mm would reduce the bending influence without the need to increase the punch size.

Before samples could be produced which would be used to determine the FLDs and FLCs of the selected materials, preliminary testing was carried out. The aims and objectives of this preliminary work were as follows:-

- Obtained correct crack direction at the centre of the sample.
- Determine if IF steel masks are needed.
- Determine the severity of the edge cracking.
- Obtain the friction conditions to obtain best crack.
- Obtain correct parameters for machine set up.

Four different Halterwidths 50, 80 ,110 and 166 blanks were used for the preliminary testing to give and range of the sample sizes need and to see if different size gave different results during forming.

3.3.2 Materials Utilised

The material selected for this was T52 BA. It was chosen because it performed the worse of the material during the Erichsen testing with regards to obtaining cracks at the centre of the bulge. This was because of the materials directionality, the material is made with smaller grain sizes compared to the other materials. Figures 3.23 and 3.24 show two materials, T52-BA and T61-CA respectively. Material T61-CA has a large grain size when treated and rolled. This is shown in the direction of the material. When a crack is formed it propagates along the direction of the material. Material T52-BA has a small grain which reduces the material directionality. This produces the difficultly in obtaining cracks at the centre of the bulge.

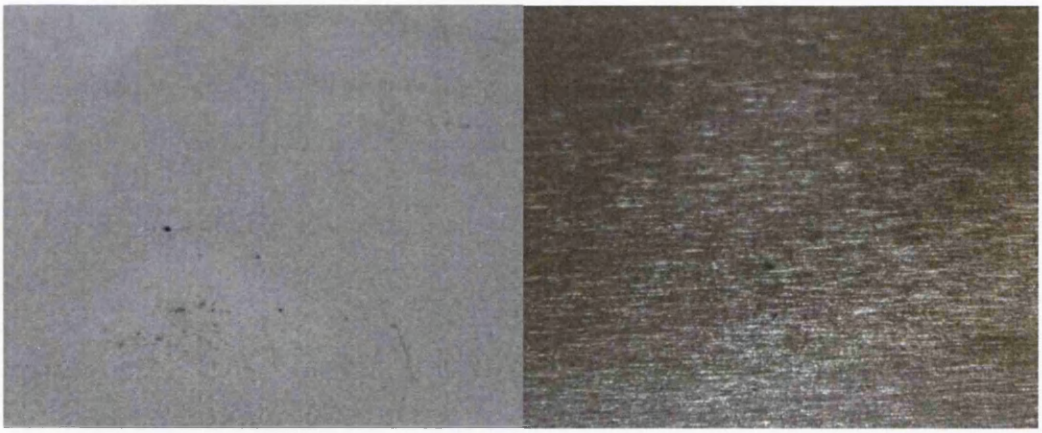

Figure 3.23 and 3.24. Materials T52-BA and T61-CA respectively.

Previous initial work carried out by TATA on thin grade steels have proven that obtaining good FLCs are difficult, this is also outlined in Baristic and Pepelnjak. One solution that has given improved results has been to use an Interstitial Free (IF) Steel masks (Roelofsen and Schouten, 2006). The experiments carried out will using both with and without an IF steel mask.

The blanks for this project were laser cut and not machined cut. This laser cutting was done outside TATA. Machine cutting can introduce material defects on the edges which may propagate once the blank is being formed. When the laser cuts the blank out, the edge is subject to heat. On inspection, under a microscope, this heated edge can be seen. The heat would have heat treated the edges which may have helped preventing edge cracking.

The other method being discussed for cutting the blanks in future was a water jet cutting machine. Examination will need to be preformed be determine that the water cutting does not introduce cracks to the blanks that can lead to failure during forming.

Upon delivery of the blanks, it was found that some of the blanks had been cut in the incorrect rolling direction. This would have results in incorrect crack direction on the formed blanks. It is important that the rolling direction of the blanks are checked prior to testing.

3.3.4 Results and Discussion

The Blankholder Force was first examined. The maximum blankholder force that the machine could produce was 330kN. Because of the thickness of the material it was believed that this maximum force could damage the material and cause premature failure between the blankholder and die. To begin with the blankholder force was set to 165kN, half of the maximum

force. The blankholder force was insufficient and allowed the blank to be drawn and not stretch. This is shown in figure 3.25, it also produced an erratic crack.

Figure 3.25. Blank that was drawn and not stretch due to insufficient blankholder force.

The blankholder force was increased to 70% of its maximum force, 231kN. This again resulted in the blank being drawn and not stretched also producing an erratic crack, figure 3.26.

Figure 3.26. Blank that was drawn and not stretch due to insufficient force.

The blankholder force was finally increased to its maximum force of 330kN, this prevented the blank begin drawn and allowed the blank to stretch. Figure X shows the blank that has been stretched to from the crack and not been drawn during forming. This stretch allows the crack to form in the correct place on the top of the bulge, figure 3.27, and not to one size figures 3.25 and 3.26.

Figure 3.27 Blank that has been stretched and not drawn

The next Blankholder type was examined. There were two different types with a rough grooved and a smooth surface. Using the grooved surface resulted in some of the 50, 80 and 110 halterwidths blanks cracking at the edge, where the die radius begins, figure 3.28. This was the problem outline earlier that Barisic and Pepelnjak had encountered. The crack started due the high blankholder force being using to prevent the blank from being drawn. The force with the grooved surface of the blankholder damage the blank where the blank and die radius meet. The two ideas to prevent this was to either use a blankholder with a smooth surface, which could result in the blank being drawn and not stretch, the other was to increase the die radius, to see if a larger radius would prevent the blank from damage.

Figure 3.28. 80 halterwidth blank that has failed due to edge cracking

To begin with the die radius was changed, figure 3.29. This did give the required effect and did not result in edge cracking. However this change in radius went outside the tolerance shown in figure 3.21. Therefore the other option of changing the blankholder surface to a smooth one was examined.

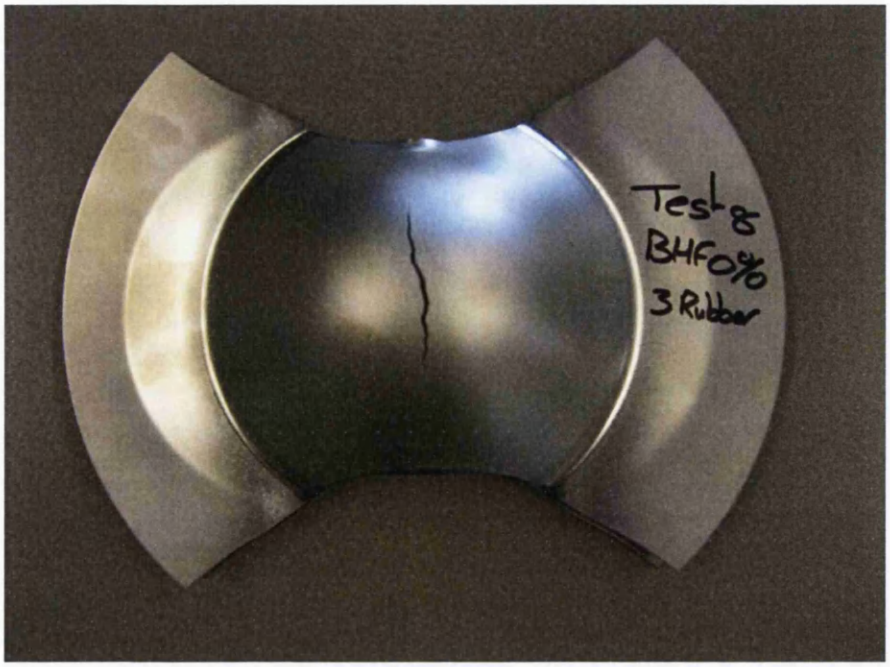

Figure 3.29. 80 halterwidth blank formed using a larger radius.

The smooth blankholder also give the required effect, figure 3.30, producing a centre crack at the top of the bulged. The surface of the formed blank was examined to determine if the blank had been drawn during the forming process however the surface did not show any signs. The decision was made that the smooth blankholder was to be used instead of the larger die radius.

Figure 3.30. 50 halterwidth blank formed using a smooth blankholder.

Friction was then examined with and without the IF steel mask. The two friction method used was the old and new international standards using 3 rubber pads and a combination of Teflon – Vaseline – Teflon – Vaseline – rubber pad respectively.

The two frictional methods had no change in results using the IF steel mask. Both produced centre cracks in the correct orientation. The decision was made to use the three rubber pads. This was because the old International Standard which used a 75mm punch used the three rubber pads. Therefore the method is only different because we are using an IF mask. Using the other frictional method would have two changes, the friction and IF mask. Therefore the friction was not changed so the examination into using an IF mask could be examined.

Without using an IF steel mask the results were different. The three rubber pads did not allow the blank to stretch over the punch and cracks were not obtained in the centre of the bulged. Using the new frictional method using a layer of Teflon – Vaseline – Teflon – Vaseline – rubber pad allowed the blank to stretch over the punch and gave centre cracks, figure 3.31. Since the IF steel mask was not used the only change to the International Standard using the 75mm punch would be the lubrication.

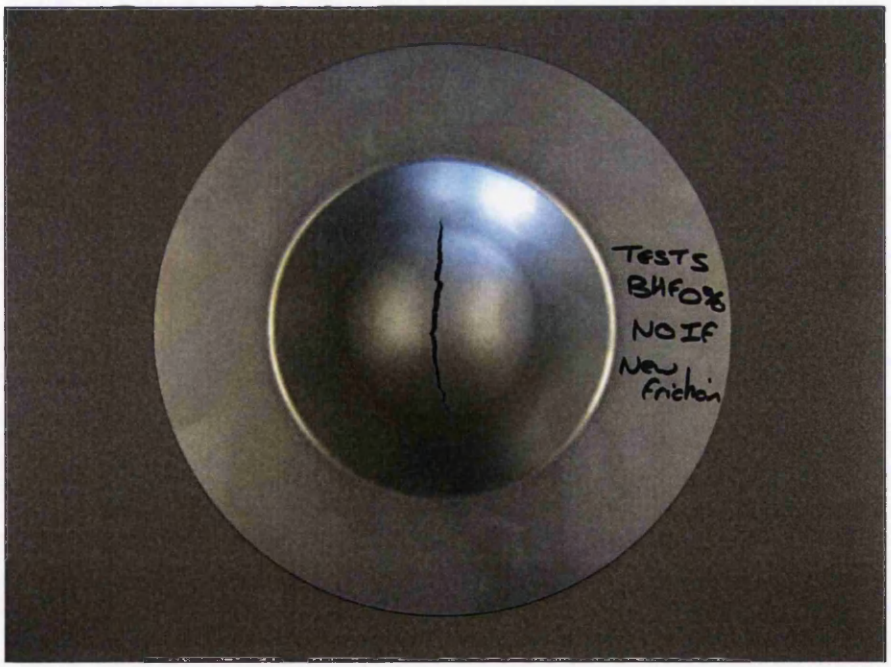

Figure 3.31. 166 halterwidth formed blank using the new lubrication method.

On closer examination of the blank, figure 3.32, due to the thinness of the material the rubber pad had produced a mushroom shape effect. This produced necking in the area indicated

by the red circles. It is unclear if this would affect the results as the crack and the strain needed at the point of failure as the crack as been formed at the top of the bugle. This will be examined later once the experiment has been done.

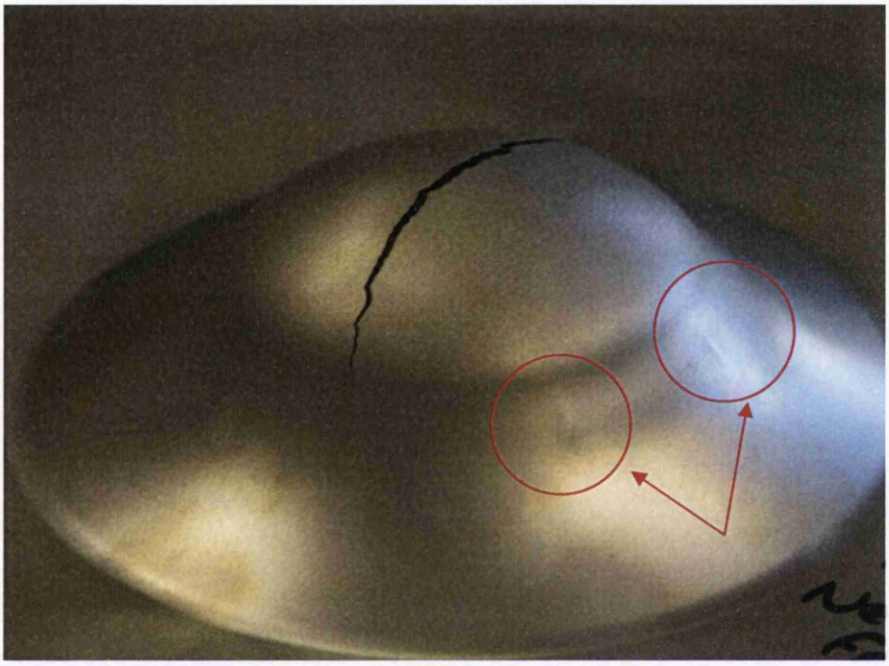

Figure 3.32. Mushroom shaped effect caused by the lubrication.

Another task was to measure the repeatability of the test. Figures 3.33 to 3.36 show halterwidths of 50, 80, 110 and 166 all with centre cracks at the top of the bulge in the required area outlined by the international standard.

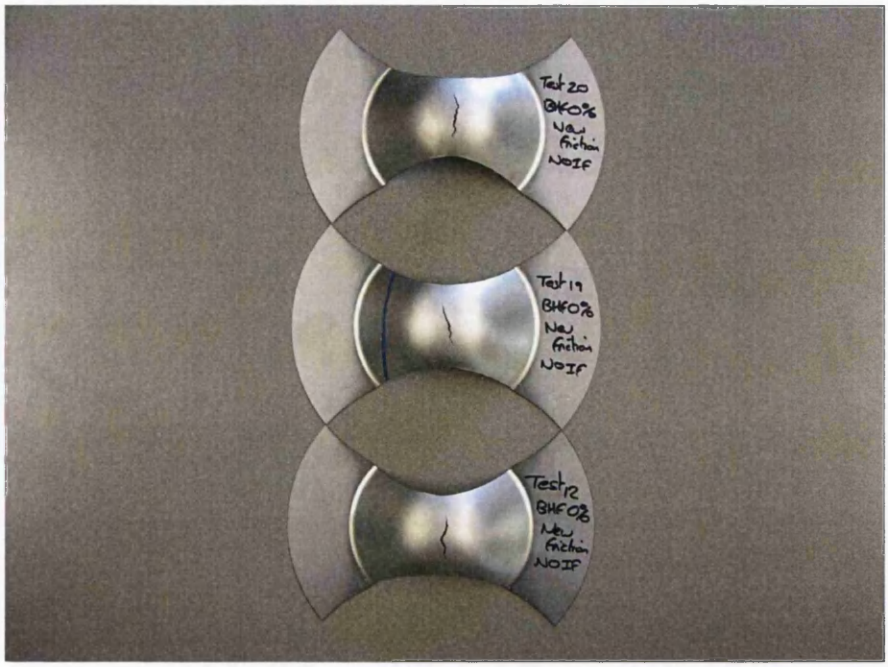

Figure 3.33. Set of three 50 halterwidth bank successfully stretch until failure.

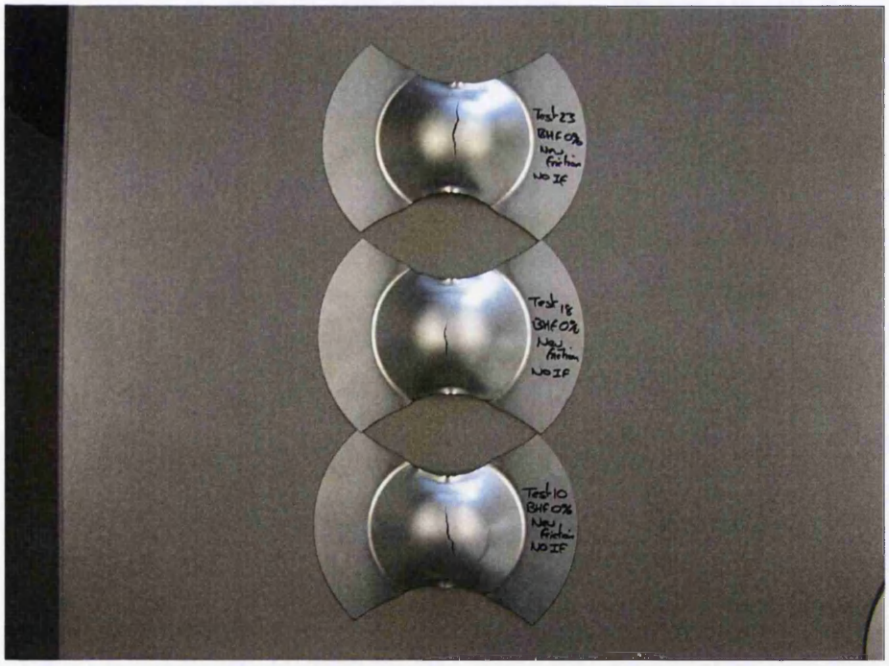

Figure 3.34. Set of three 50 halterwidth bank successfully stretch until failure.

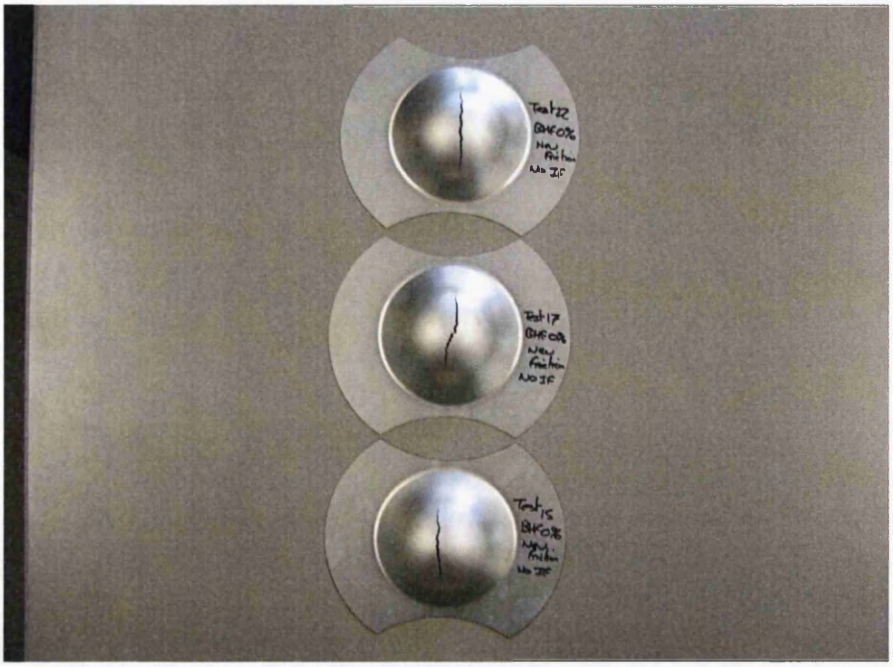

Figure 3.35. Set of three 50 halterwidth bank successfully stretch until failure.

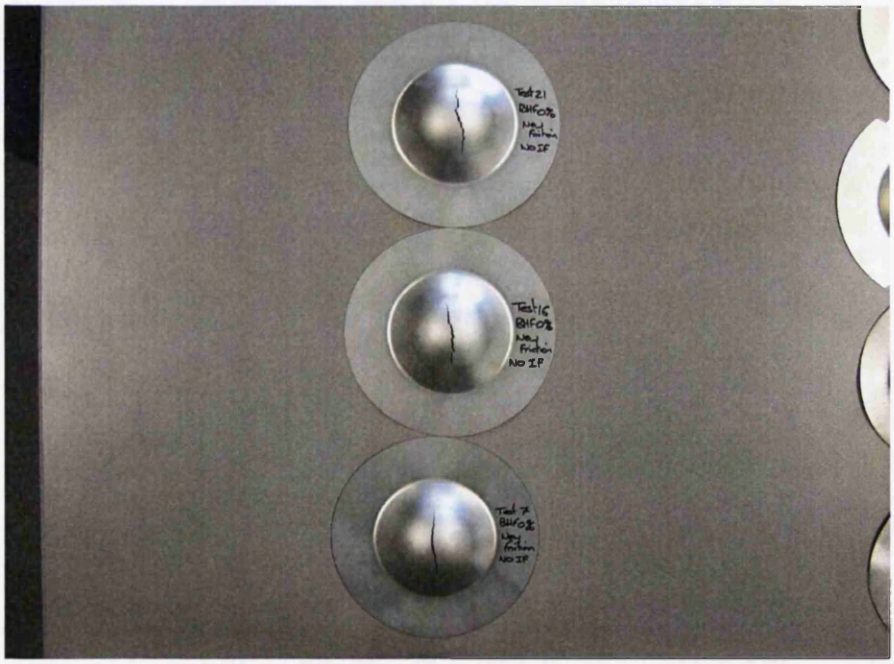

Figure 3.36. Set of three 50 halterwidth bank successfully stretch until failure.

3.3.5 Conclusions

A blankholder force of 330kN is required acting on the blank. With a weaker blankholder force the blank is aloud to move under the blankholder and is drawn into the die. This is deep drawing and not stretching. With a stronger blankholder force results in compression of the material under the blankholder. This weakens the area between the blankholder and die resulting in tearing.

Each blank needs to be checked before testing to make sure that the blank has been cut to the correct rolling direction.

The new lubrication conditions result in good centre cup cracks, therefore the IF steel masks are not needed. However because there is no proof that there is a difference between the two lubrication types, the experiments will be carried out both with and without the IF steel mask. A comparison then can be made whether there is a difference in the FLC. If there is this would show that the IF steel mask is having an influence on the results.

The best lubrication is Teflon – Vaseline – Teflon – Vaseline – Rubber pad. This is the same international standard for the automotive testing. The current international standard says that the thickness of the material must be between 0.5mm and 2/3mm. Because the packaging steel grades have thicknesses of around 0.2mm this international standard can not be applied to the experiments going to be undertaken. However there is currently no international standard for the Erichsen testing with packaging steel grades. Because of this the IF steel mask was used before to thicken the material. However this rises the question about the frictional conditions between the IF steel mask and the Blank. This is why both tests are being carried out. With the IF steel mask to increase the thickness and without however with extra frictional properties and without the IF steel mask however failing on the standard because of the material thickness.

During the testing there was no edge cracking occurring once the blankholder had been changed from the grooved surface to the smooth one.

From this preliminary testing a test method procedure can be produced to how the blanks should be formed. This has been done in case of further testing that may follow this project.

3.3.3 Procedure

The procedure is applicable to the activities of the Product and Product Applications department (PPA) of the IJmuiden Technology Centre of TATA Research, Development & Technology. For thin sheet metal materials (of 0.3mm thickness or less) of steel as well as aluminium alloys an FLC can be determined according to this procedure.

Determination of an FLC shall be done according to the principle of the Nakazima test using a hemispherical punch of 75mm. A measurement grid with defined dimensions is applied to the surface of unformed blanks made of the sheet metal. The blanks will be deformed by the hemispherical punch until just after fracture.

At least eleven combinations of forming conditions (halterwidths) will be obtained with different widths of the blanks. The deformations of the grid on the samples are measured and subsequently the strains. The procedure for fitting this data is described in ISO 12004-2 section 5.

The strain points for local necking found are plotted in a diagram. A line is drawn through the strain points by means of non-linear regression. The result is a forming-limit curve (FLC) of the sheet material tested.

The grid should be applied using an electro chemical method in accordance to TATA's document AUT STN 201D, photochemical according to AUT STN 202D or other methods of grid application with initial grid accuracy better than 1%. The grid pattern should be of a round dot of 1.0 mm in diameter, an example is shown in figure 3.37.

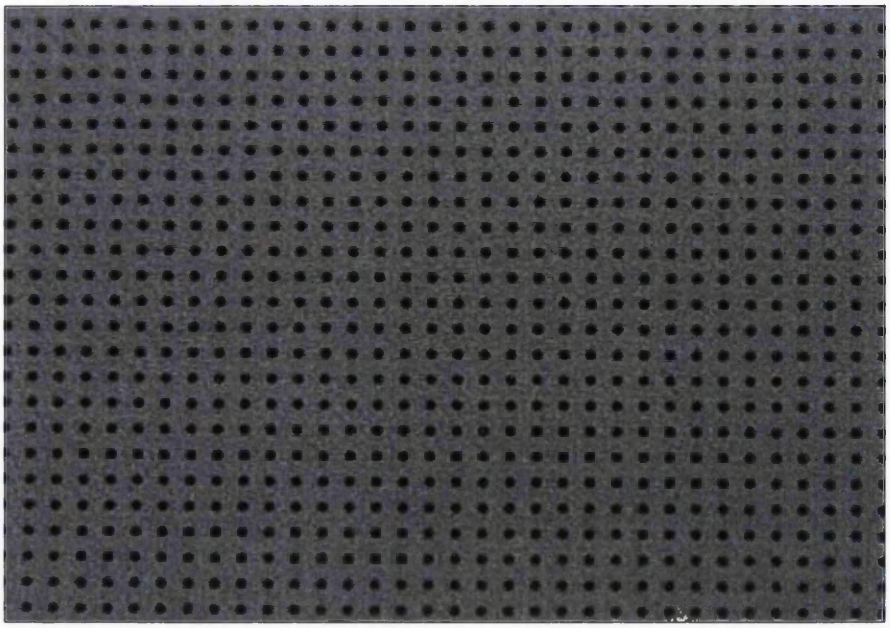

Figure 3.37. 1.0mm round grid pattern

The testing equipment is as follows:-

- Blanks (with optional IF steel mask)
- Lubrication
- Blanking tools and press
- Nakazima tooling

3.3.3.1 Blanks

Due to the sheet thickness of less then 0.3 mm, tested materials will be tested with and without an IF steel mask, figure 3.38. The thickness of the mask should be 1mm. The blanks can be of all types of steel and aluminium alloys. The IF Steel Mask is made from material IF DC06, automotive steel.

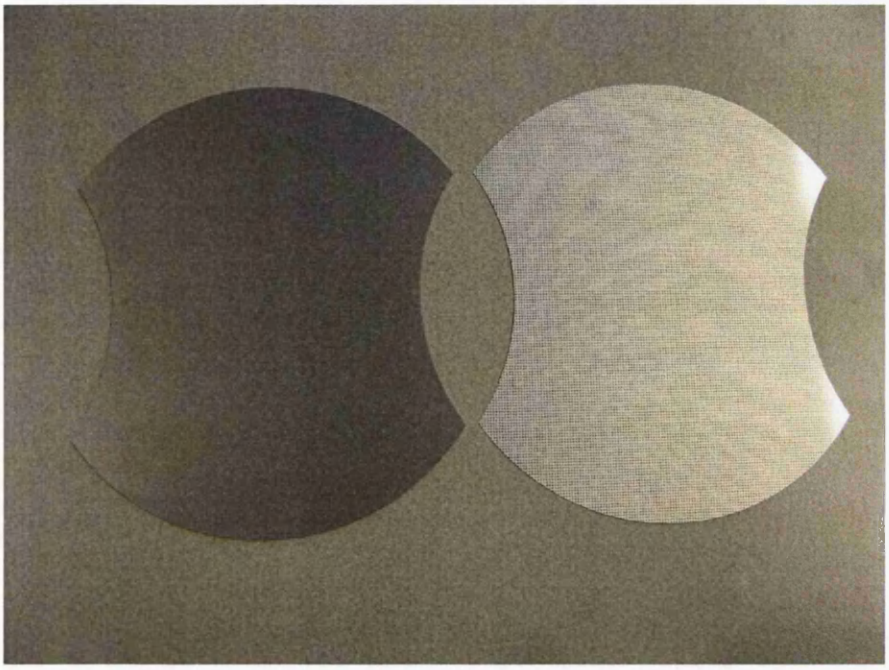

Figure 3.38. IF Steel Mask (left) with packaging Steel with 1mm Grid (right).

The manufacture of the blanks is shown in figure 3.39. Avoid taking material from the coil edges leaving at least one blank width out, about 200 mm. Care needs to be taken when marking the rolling direction so that the blanks are cutting correctly. For steel the length is taken perpendicular to the rolling direction of the sheet. For aluminium the length is taken parallel to the rolling direction. The blank geometry is show in figure 3.40.

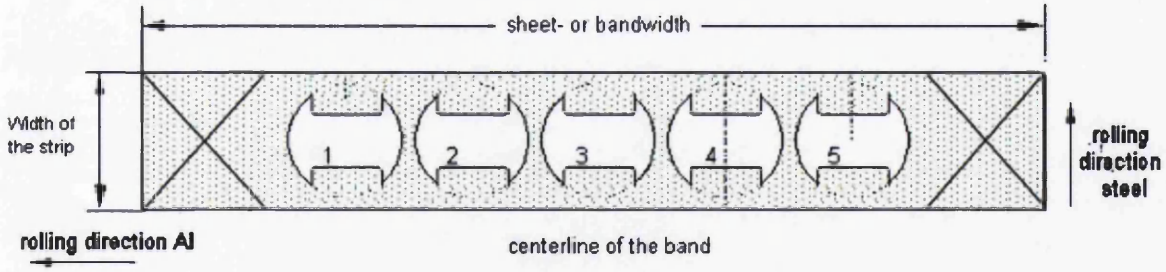

Figure 3.39. Direction of blanking

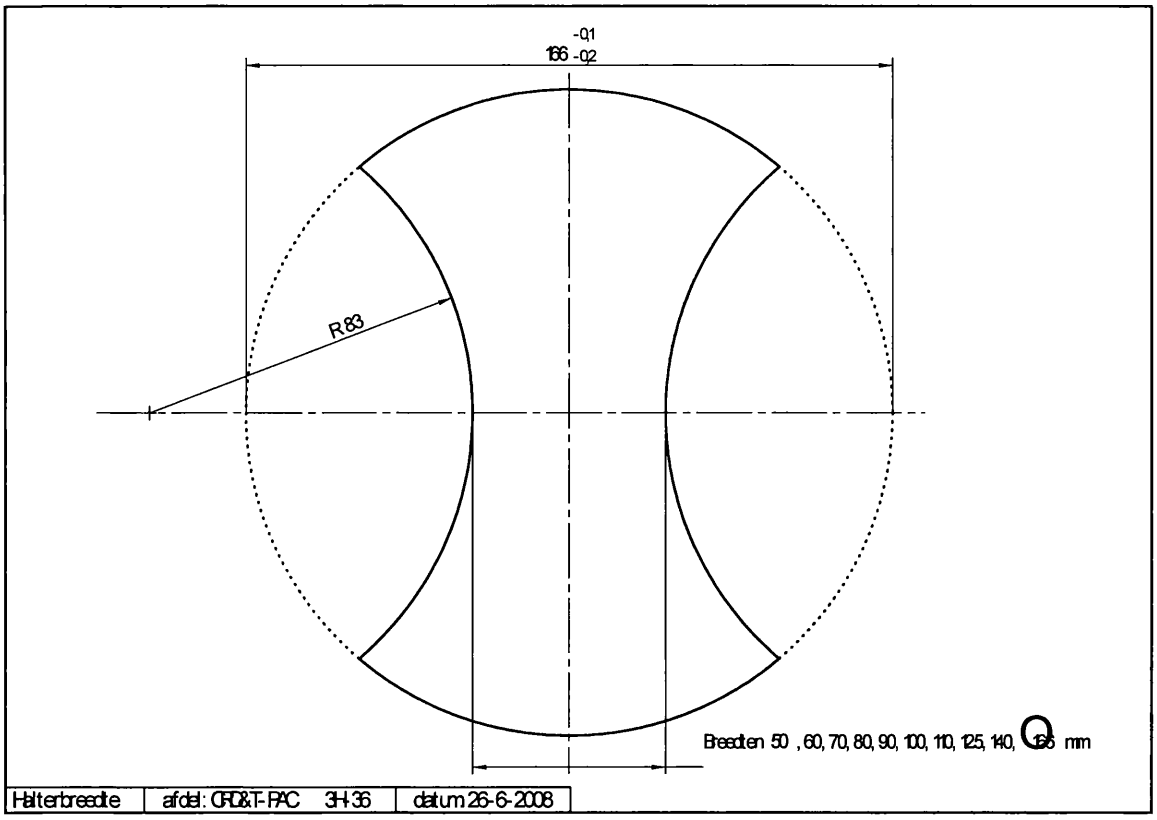

.Figure 3.40. Sample shapes showing the different Halterwidths

The minimum of eleven shapes per FLC is needed and for each width at least three formed blanks should be produced. The aim is to have a uniform distribution of halterwidths blanks from uniaxial to biaxial. There will be eleven blank shapes used for form the FLC. The sizes, or halterwidths, are 50, 60, 70, 80, 90, 100, 110, 125, 140, 166 partial and 166 full. The halterwidth is the width of the material a the centre of the blank. Halterwidth 50 to 90 represents the strain conditions from uniaxial to plane strain, and from 90 to the 166 full represents the strain conditions plane to biaxial. The difference between 166 partial and 166 full is different blankholder shapes are used. The 166 full blankholder constrains the blank all the way round and is the biaxial strain condition where as the 166 partial blankholder holds the blank across part of the blank, shown as blankholder 2 in figure 3.44. The blanks should be laser cut to produce a smooth edge. The sample may not crack from the edge of the sample when formed.

3.3.3.2 Lubrication

There are two lubrication systems being used, however during the process to produce one FLC the lubrication system may not be changed. The recommended lubrication type is a system when using an IF steel mask is the three rubber pads, figure 3.41.

Figure 3.41. Three layers of rubber pads.

The rubber pads are Erlan 70 °SH PUR. When not using an IF steel mask, the lubrication system that should be used is the Teflon – Vaseline – Teflon – Vaseline – Rubber pad, which is the system used in International standard 12004-2. Due to the use of Vaseline, the punch needs to be cleaned after every formed blank to ensure a fair test. In either case the lubrication needs to the positioned between the punch and the IF steel mask, figure 3.42 showing the three rubber pads placed between the punch and the IF steel mask. It is recommended to test the lubrication using a few sample blanks to see if the cracks are being produced at the top of the bulge.

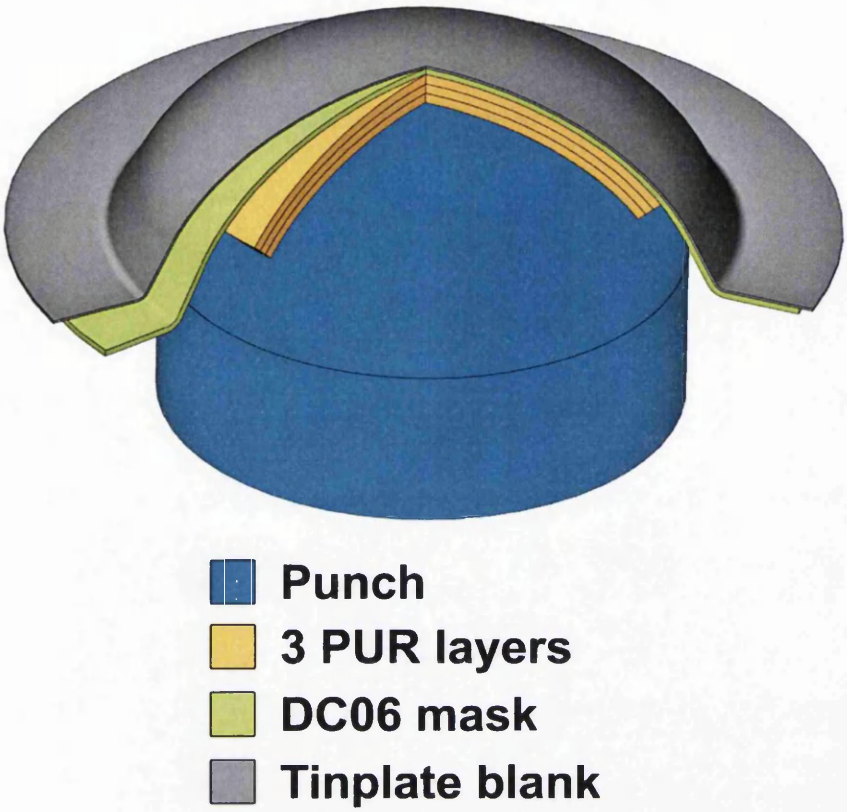

Figure 3.42. Position of the lubrication between the punch and the IF steel mask.

3.3.3.3 Blank tooling

The blankholder's that are used should have a smooth surface. A grooved surface will result in tearing of the blank. The die radius used for the test has a radius of 7.5mm should be used. This is in accordance with ISO 12004-2. The punch size of 75mm should be used, until the 100mm punch machine becomes readily available. When this happens a comparison should be preformed and compared against the results obtained from the 75mm punch.

3.3.3.4 Nakazima Testing

A full Work Instruction can be found in the packaging database about how the experiment can be done under TATA's regulations. The apparatus used was the Nakazima testing machine based at the automotive and packaging research centre in Ijmuiden Holland, figure 3.43. The Positioning of the blanks against the blankholder is shown in figure 3.44. To mount the blank it is recommended to take out the die and the support ring together for better positioning of the IF steel mask, blank and lubrication.

Figure 3.43. Nakazima testing machine, packaging research centre in Ijmuiden Holland.

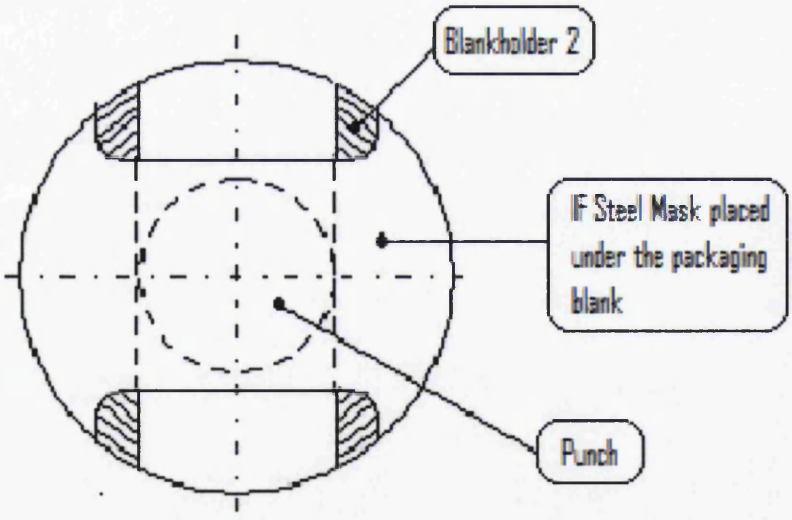

Figure 3.44 Position of sample on the blank holder (partly serrated)

The Blankholder force of 330 kN needs to be applied. Draw in must be prevented as much as possible. Draw in can be checked by viewing the blank holder side of the sample after

punching. Scratched indicate draw in. It can also be checked if the outer diameter of the sample remains the same. The Punch speed should be a constant 85mm/min (+/- 30mm/min)

Termination of the test should occur as soon as the fracture occurs, this can be done automatically by the test machine be presetting a high to stop or manually by stopping the machine once the crack has appeared. This may be best done manually as presetting a high to stop can be can result in un-cracked blanks or over cracked blanks which are split across the blank. The crack may not be more then 15 mm offset from the top. The crack may not start from the edge of the blank. If the sample has not failed in a correct way this has to be noted. At least three results should be done on each halterwidths to be confident in consistency Once the blank has been formed it should be marked to help identify it.

The drawn blank should be marked with, the material code, the halterwidth size, whether or not an IF mask was used and test number that can be identified to a test batch. The dome height rounded on 1 decimal can be written on or noted else where, this is only used for indication.

3.4 Nakazima Test

3.4.1 Introduction

Once the procedure had been finalised the main Nakazima testing could take place. Each material was tested with and without an IF steel mask.

3.4.2 Materials Utilised

From the fifteen materials that were tested using the Erichsen method seven have been selected for the Nakazima method. Five were chosen because there are current packaging steel grades, T52 BA, T57 BA, T57 CA, T61 CA and T65 CA. The other two DR 550 BA and DR 550 CA were chosen because they are not current packaging steel grades and would give a good contract against the other five materials, table 3.4

Material	Thickness (mm)	Code	Order Number	Storage Number
T52 BA	0.21	TS 245	80989A	20080230
T57 BA	0.21	TS 275	80873K	20080235
T57 CA	0.21	TH 340	88349A	20080232
T61 CA	0.21	TH 415	80995A	20080233
T65 CA	0.21	TH 435	88915M	20080234
DR 550 BA	0.21	TS 550	80116H	20080216
DR 550 CA	0.22	TH 550	80353C	20080225

Table 3.4. List of steel grades used for the experimental work.

3.4.4 Discussion

In total there were 14 complete sets of blanks formed. One for each of the seven materials with and without an IF steel mask. With the preliminary work that had taken place centre cracks were obtained for all halterwidth sizes. Figures 3.45 and 3.46 show complete sets of formed blanks for T61 CA and T52 BA respectively, these were formed using an IF steel mask.

Figure 3.45. Set of banks using an IF steel mask for material T61 CA.

Figure 3.46. Set of banks using an IF steel mask for material T52 BA.

3.5 Argus Measurement Procedure

3.5.1 Introduction

In order to produce an FLD of a specific material, the blanks that were formed during the Nakazima test need to be examined to obtain the strain values. The grid on the blanks that have been deformed under the forming process are examined to obtain the strain value, this will be done using the ARGUS system. ARGUS is used to measure the strain of a formed material shape.

3.5.2 Procedure

The formed blanks from the Nakazima Test are placed together in sequence as shown in figure 3.47. Various markers are added on and around the blanks to produce a marking system. It is important to make sure that the markers are spread evenly around the blanks. Photographs are taken using a position strategy. The photographs should approximately be taken from the positions shown in figures 3.48 and 3.49. It is important that at least 5 markers are visible in each photograph. This is because the photographs are used to produce a 3D strain model. The markers are used to allow the software to build this 3D model and the software needs a minimum of 5 markers per photograph.

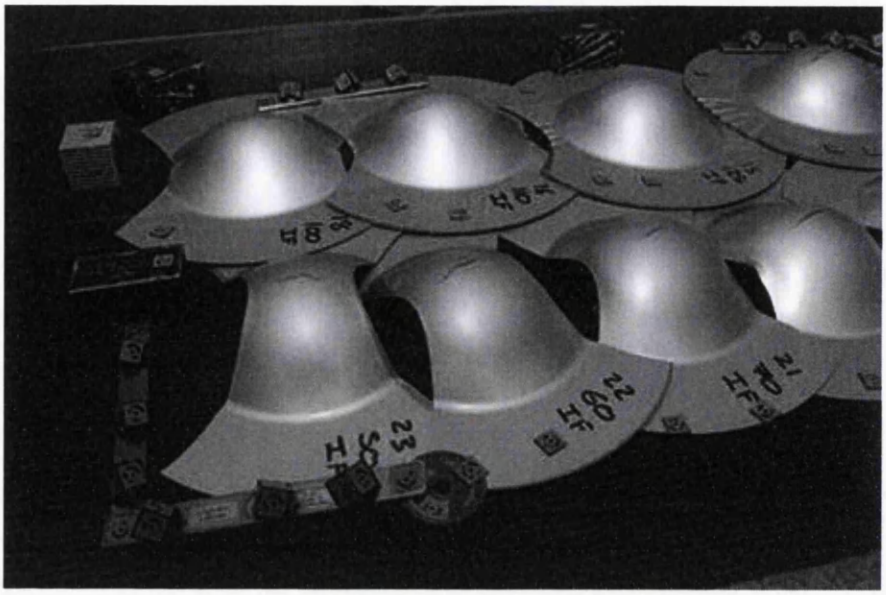

Figure 3.47. Set of blanks with markers in place.

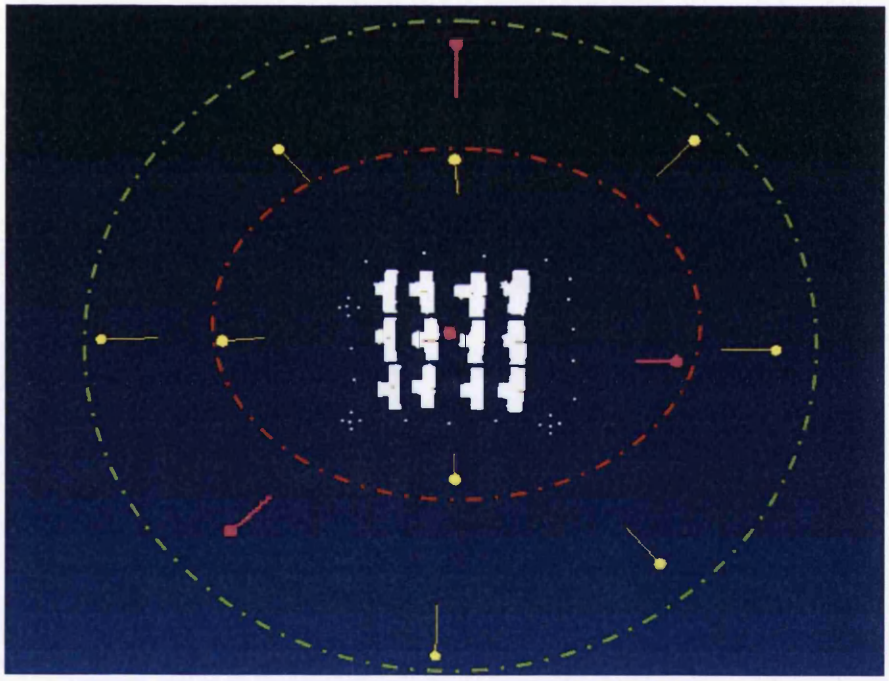

Figure 3.48. Camera positions vertical view

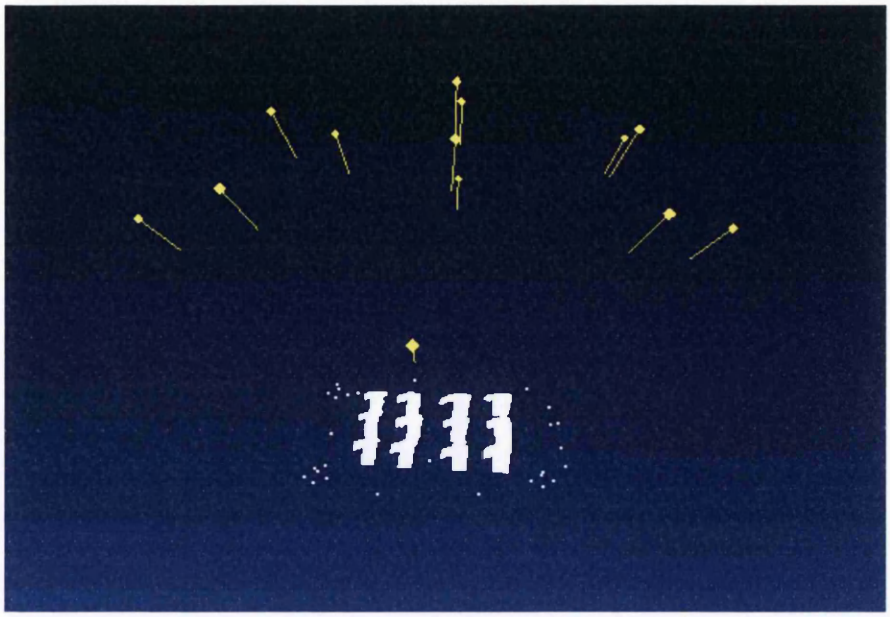

Figure 3.49. Camera positions horizontal view

The photographs are compiled using the ARGUS software to create a 3D image of the blanks. The deformed grids on the blanks are examined and each point on the grid is calculated to work out its strain value. This results in a 3D strain model of the blanks as shown in Figure 3.50.

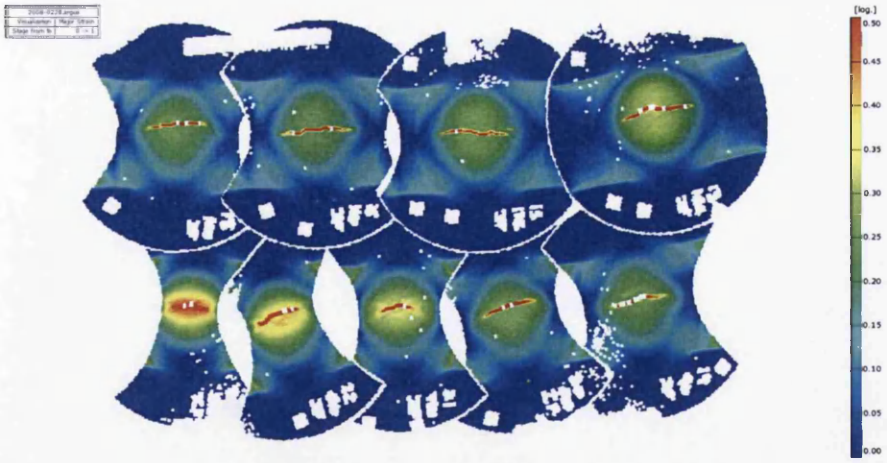

Figure 3.50. 3D image of the formed blanks showing the strain

To determine the major and minor strains, a cross section is needed from each of the calculated blanks. Five cross sections are taken to obtain accurate results as show in figure 3.51.

The results of the cross sections are converted to a graph so they can be examined to determine the major and minor strain values in that blank.

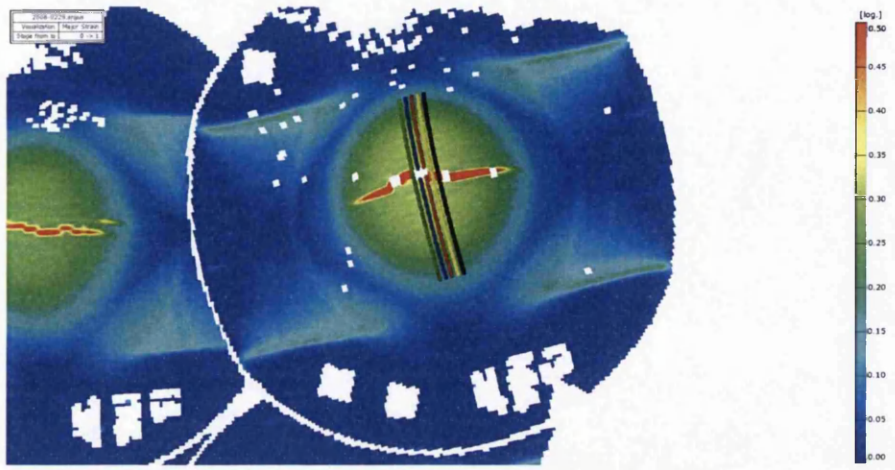

Figure 3.51. Blank showing the five cross sections taken

The top and bottom groups of lines represent the major and minor strains respectively, as shown in Figure 3.52. The "spike" in the graph indicates the crack in the material. The mid point of the spike is taken as the major strain point and a measurement is taken below as the minor point. This is done for each of the blanks in the set.

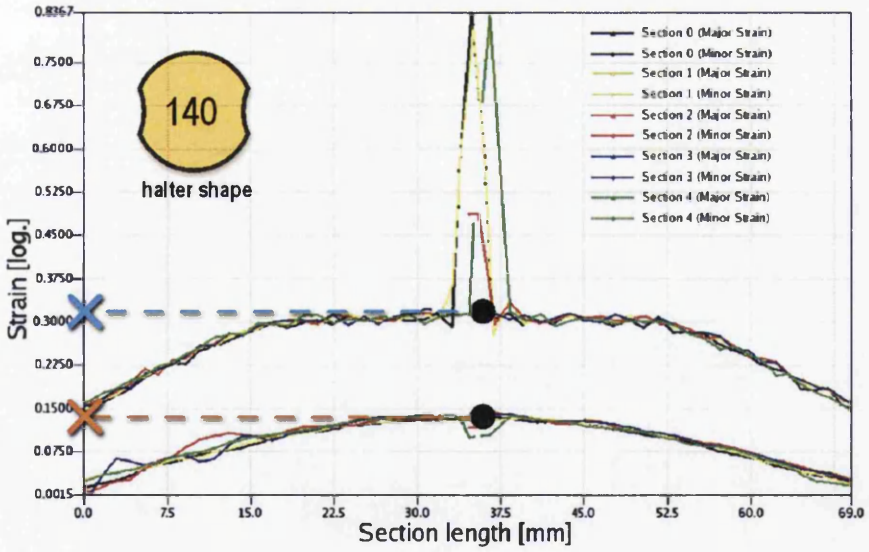

Figure 3.52 Major and minor strain 140 halterwidth averaged over 5 cross sections

The measured Major and Minor points for each of the 11 blank sizes are entered onto a graph to form a FLD. A line is extrapolated which is the FLC, figure 3.52. There were 14 sets of blanks undertaken during the testing, all have been determined.

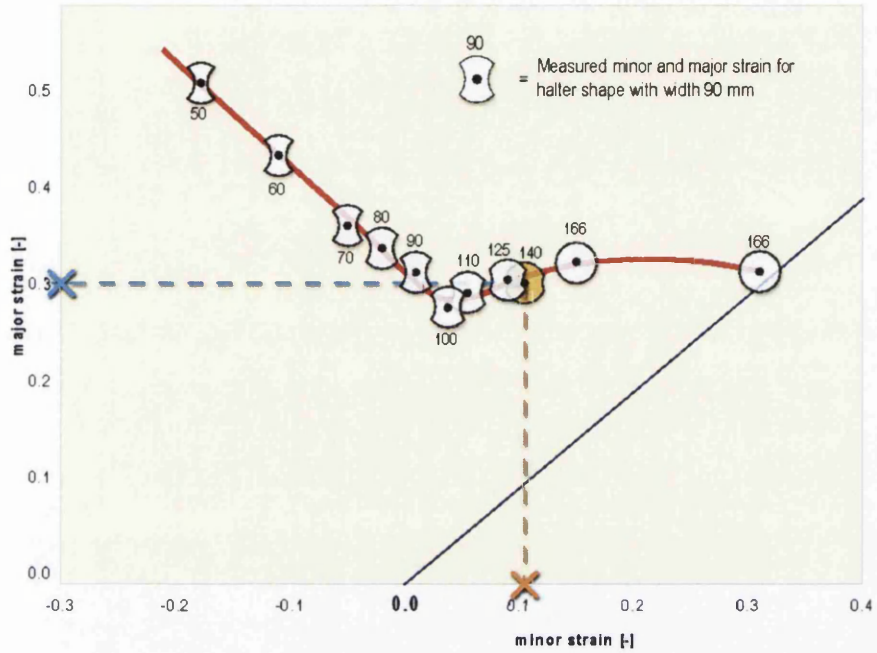

Figure 3.53. Forming limit curve based on the major and minor strains of each halterwidth

3.6 Nakazima Results

3.6.1 With IF Steel Mask

The follow graph, figure 3.54, shows the results of the sets of materials that used the IF steel mask.

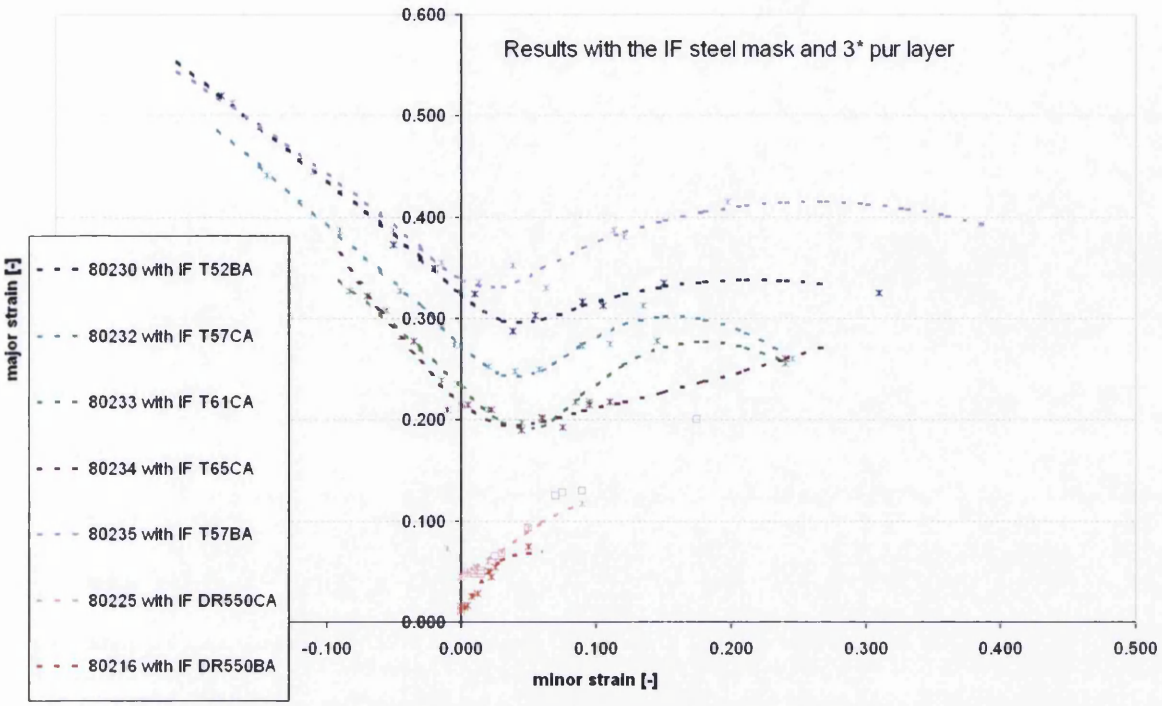

Figure 3.54. FLC results for Nakazima test using IF steel mask.

The use of the IF steel mask appears to have given good results for the five packaging steels. The biaxial tests, 166 blank fully constrained, are around the 45° line from the origin. The halterwidths size 50, 60, 70, 80 and 90, that represent forming conditions uniaxial to plane strain respectively, gave the characteristic 45° line. The plane strain position, represented by the 90 halterwidth blank, should be occurring when the Minor Strain has a valve of zero. However the plane strain results show that this condition is occurring when the Minor strain has a valve of between 0.02-0.05.

The FLC's of the two DR steel grades indicate that the material is unable to be formed under conditions from uniaxial to plane strain. Forming the material under these conditions would results the material failing. Conditions from plane to biaxial strain show that these DR grades do not have the elongation properties that match the current packaging steels.

3.6.2 Without IF Steel Mask

The follow graph, figure 3.55, shows the results of the sets that did not used the IF steel mask.

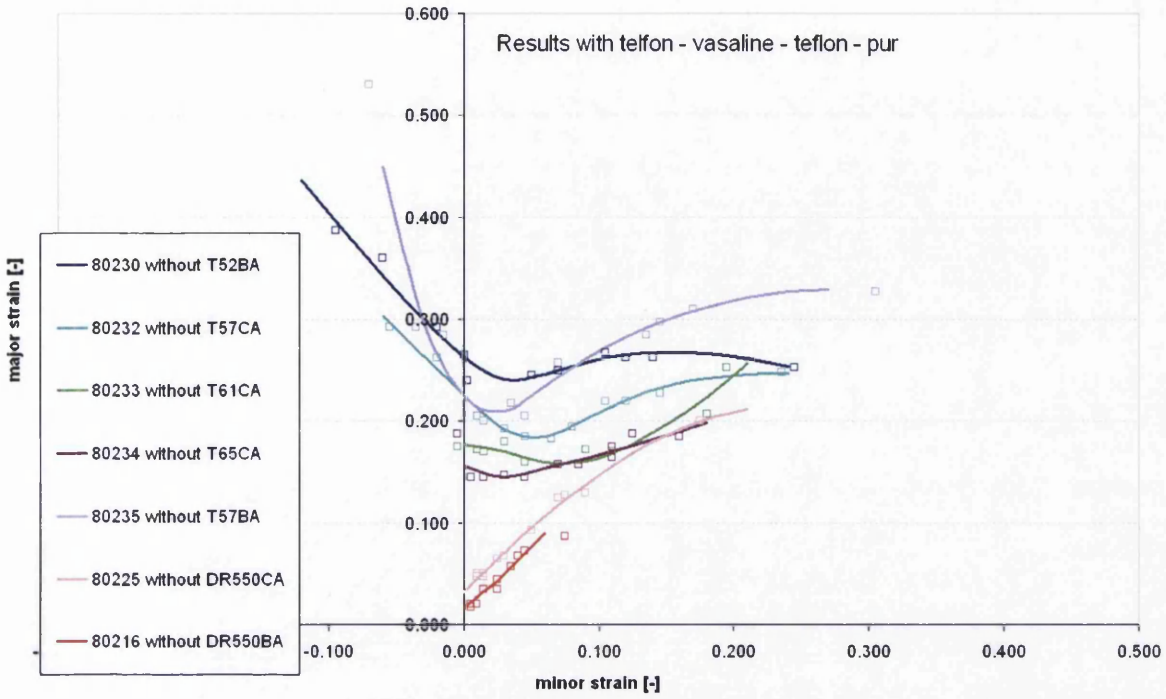

Figure 3.55. FLC results for Nakazima test without using IF steel mask.

Two packaging grades, T61CA and T65 CA, failed to produce any results under uniaxial to plane strain conditions while the other three grades, T52 BA, T57 BA and T57 CA showed reduced deep drawability without using the IF mask. The biaxial points were still at the 45° line from the origin.

Again like the IF mask results, the DR grades did not perform well under uniaxial to plane strain conditions. The grades did show improved stretching properties without using the mask. The DR550 CA grade performed similarly to some of the packaging grades under full biaxial conditions.

3.7 Discussion

Comparing the graphs, with or without the IF steel mask shows that the IF mask has an influence on FLD. The IF steel mask influences the left hand side of the graph more then the right hand side. The IF steel mask effectively increases the R-valve of the material grades. This allows the uniaxial to plane strain to perform better. Without the mask, the R-valve is effectively reduced which is why the FLC of the materials in this area are poor. In the case of T61CA and T65CA the R-valves are reduced to a point that no uniaxial to plane strain condition can be measured.

Each material has been graphed so that comparisons between using and not using the IF steel mask can be seen. Figure 3.56 shows the results of the T52 BA material, the IF mask has increased the level of strain needed to cause failure of the material. On an average the level has been increase by 0.5. There has been an increase in the deep drawability and the amount of stretch, elongation

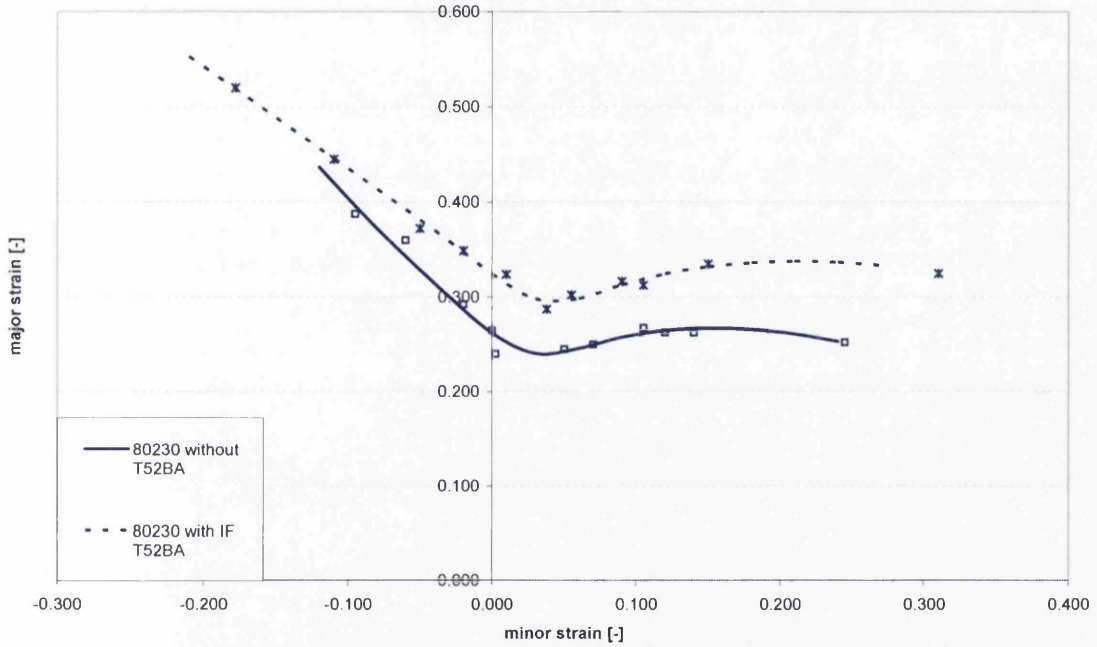

Figure 3.56. FLC results of T52 BA

Figure 3.57 and 3.58 shows the results of T57 BA and T57 CA respectively. Like T52 BA there has been increased in the amount of strain before failure, using the IF mask. There was also an increase in the deep drawability and amount of elongation.

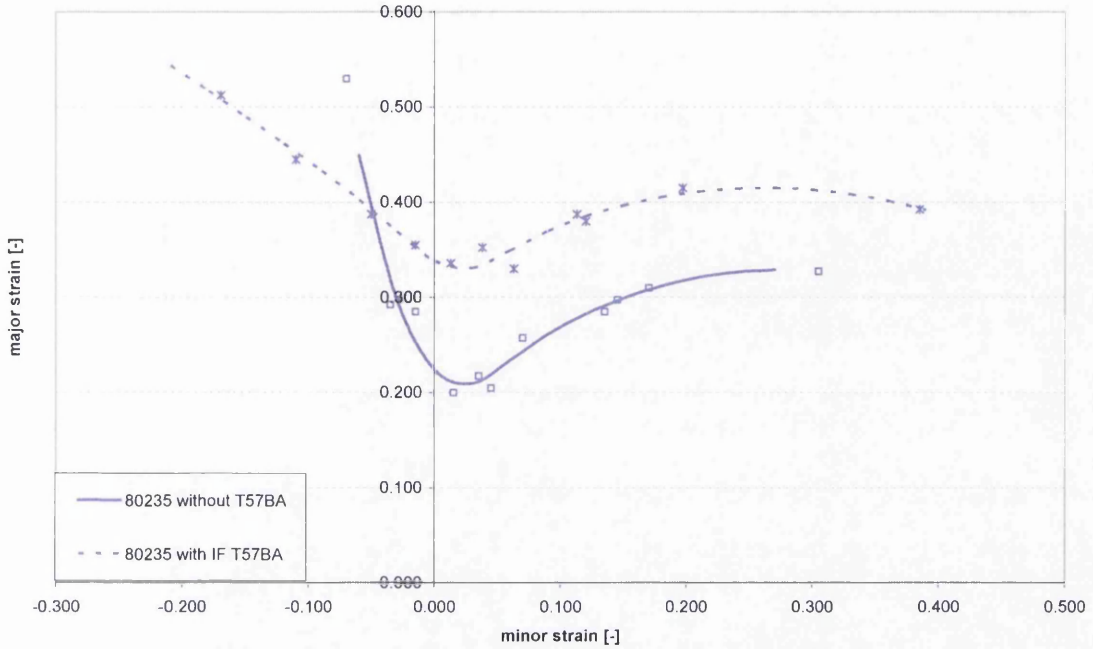

Figure 3.57. FLC results of T57 BA

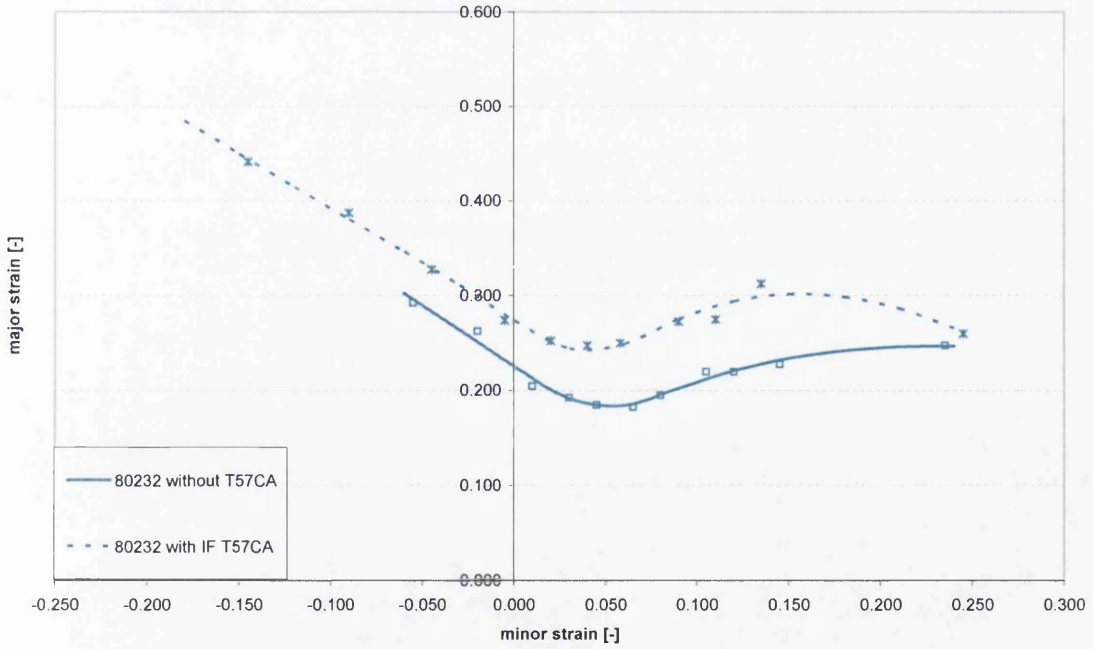

Figure 3.58. FLC results of T57 CA

Figures 3.59 and 3.60 show the results of materials T61 CA and T65 CA respectively. In both cases the material has lost its ability to be formed under uniaxial to plane strain conditions

when the IF mask is not used. Again like the other materials the IF mask increases the amount of strain needed to cause failure.

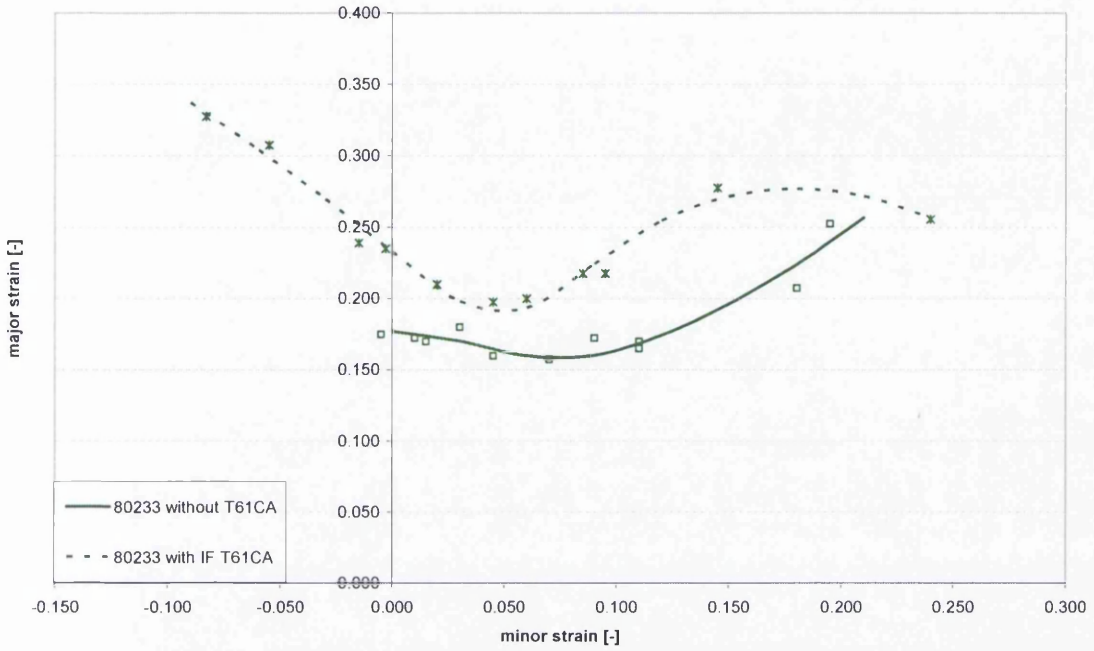

Figure 3.59. FLC results of T61 CA

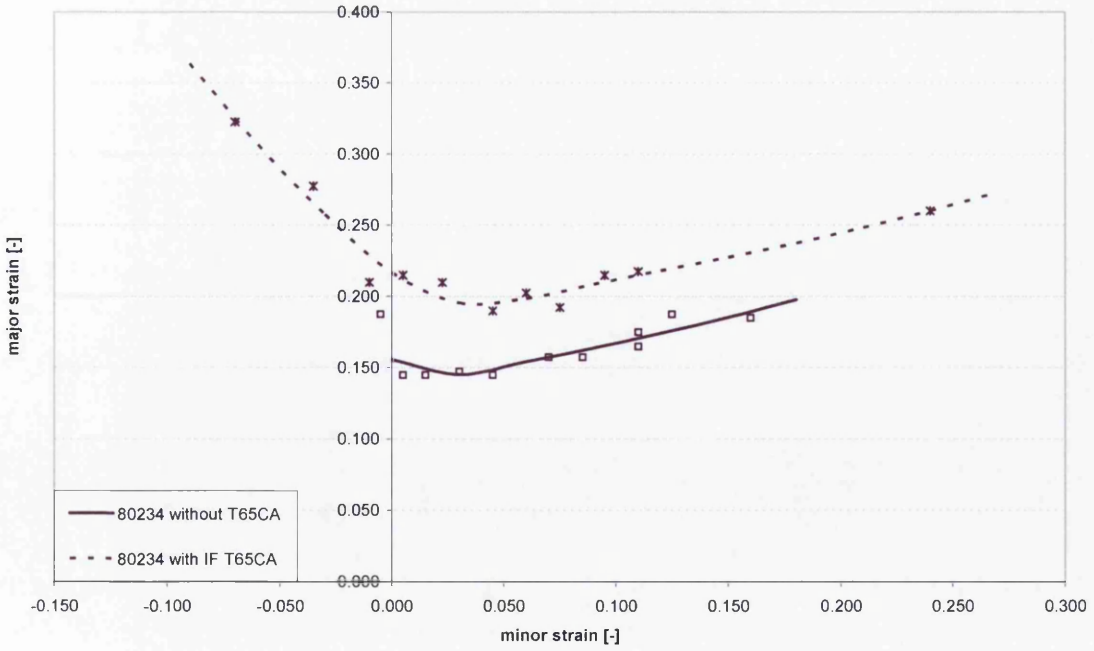

Figure 3.60. FLC results of T65 CA

The two DR steel grades showed similar results with and without the IF mask. In both cases the 166 full blank without the IF mask showed a great improvement. This appears to be the complete opposite compared to the other results which show using the IF mask increases the strain level to failure, figures 3.61 and 3.62.

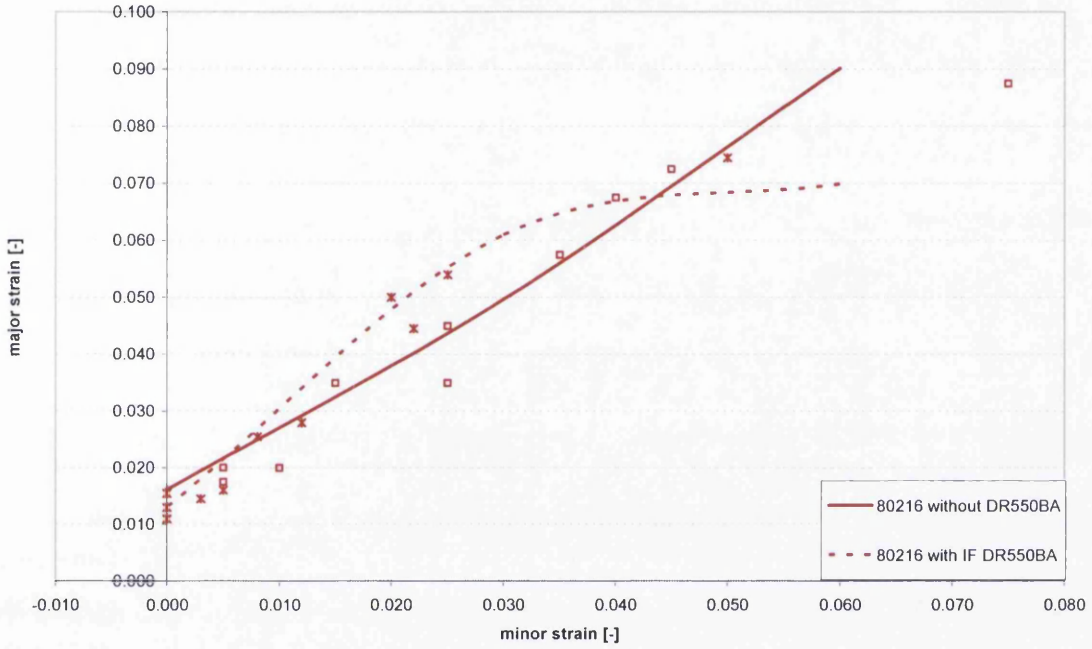

Figure 3.61. FLC results of DR550 BA

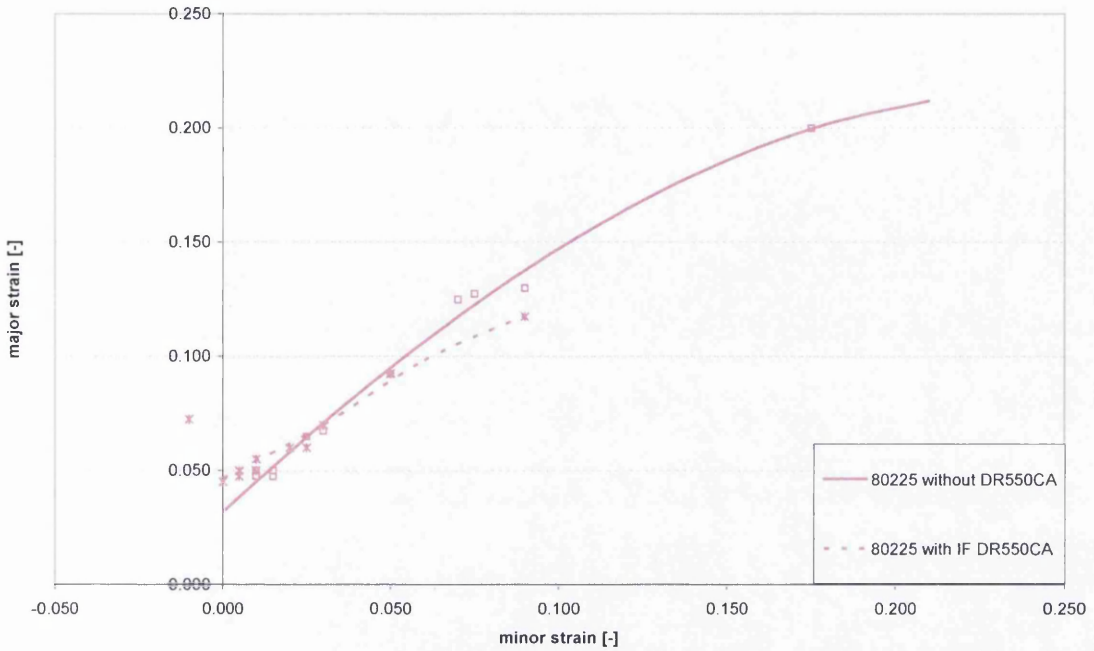

Figure 3.62. FLC results of DR550 CA

With the current packaging steel grades, T52 BA, T57BA, T57 CA, T61 CA and T65 CA using the IF mask increase the amount of strain needed to cause failure. With regards to the packaging steels the plane strain point stays around the same minor strain, even if the IF mask is used or not. There is a difference in the major strain using the IF mask which increase the strain level. This give the impression that the closer to the plane strain condition the IF mask only affects the Major strain.

The closer the condition to the uniaxial strain the IF mask increases the deep drawability of the material. To a lesser degree the same can be said about the biaxial strain condition. The IF mask increases the elongation ability of the material.

This shows that the mask influences the blank during forming, increasing the level of strain. Due to the thickness of the IF mask compared to the packaging material. The packaging material is of secondary magnitude to the IF mask. Also due to the thinness of the material could the rubber pad, used in the lubrication on the non IF mask tests, also be affecting the FLC and to what extent.

Something that was not done was to do a FLC of just the IF mask without any packaging materials. This result could be compared against the results supplied in figure 3.54 to better understand the affect the mask has on the blanks.

On further examination of the blanks there were odd results supplied by the 140 halterwidths. In some cases the results were no better the 125 halterwidth and in some there was an increase in the minor strain level however a decrease in the major strain level. It is unclear why, it may show that as the halterwidth increase the minor strain has less influence on the result until a full biaxial test is preformed.

The DR550 BA material is currently being use to manufacture beaded cans. Figure 3.63 shows the FLC of the DR550 BA with IF mask. Much in the same way this project has outlined obtaining FLC using a grid patterned material with the Argus system, the can was produced using DR550 BA material with a grid system. Upon completion the can was photographed the grid pattern analysed to obtain strain values. These are the yellow points in figure 3.63.

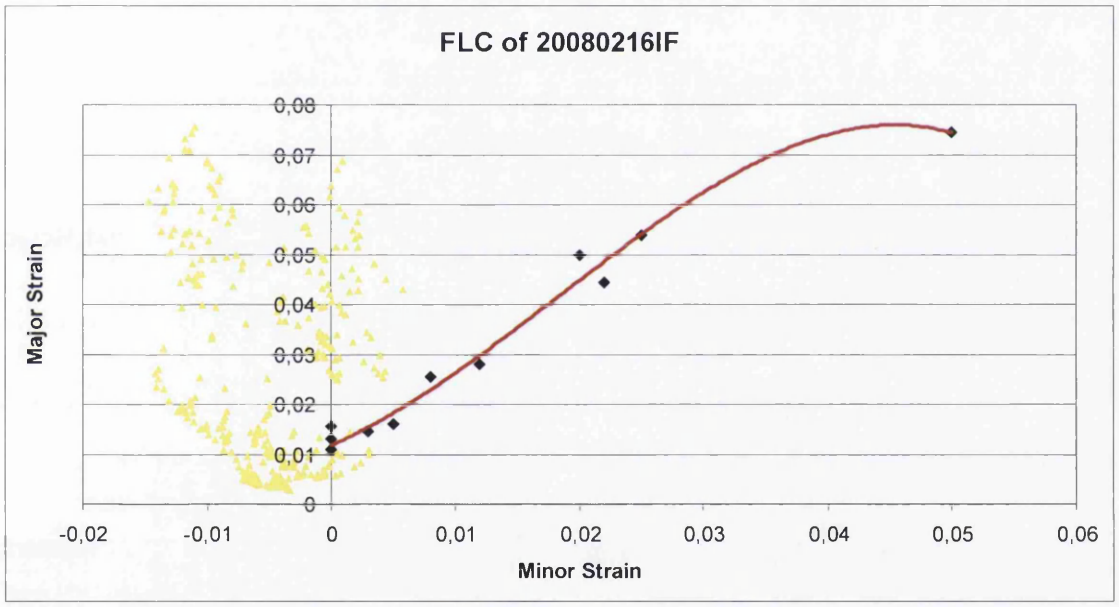

Figure 3.63. Strain valves of a beaded can against the FLC produced from the same material.

The questions raised were, why are there strain valves above the FLC that was produced? And why are there valves that indicate the can has been formed under uniaxial to plane strain conditions when the FLC indicates that this was not possible? The FLC indicates that any strain combination of strain valves above the line or under uniaxial to plane strain should mean that the material will fail, yet these beaded cans are being produced.

The answer to this was touched on in the literature review about the limitations of FLCs. The FLC must be produce under plane stress conditions. Take figure 3.64 for example, a piece of material of thickness T, being bent around a radius r.

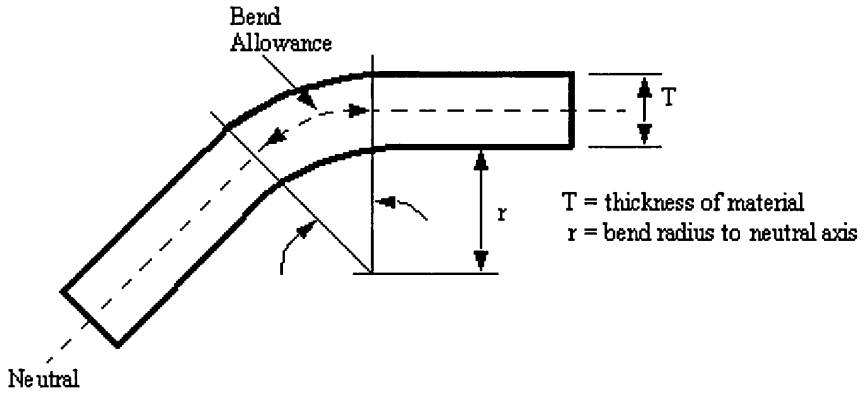

Figure 3.64. Illustration of a piece of material being bent through a radius.

The following formula can be used to determine the strain if the stretch of the material is by bending only and there is no frictional conditions.

$$\frac{r+t}{r+\frac{1}{2}t} = \varepsilon = \ln(1+e)$$

This equation can be used to give an idea how the beaded cans strain valves are higher then the FLC that was produce for the DR550 BA material. If the material thickness was 0.2mm and the radius' used were 75mm, which was the punch radius used for the FLC, and 2mm the radius used to produce the beaded cans, the following strain valves are obtained.

$$\frac{2+0.2}{2+\frac{1}{2}\times 0.2} = \frac{2.2}{2.1} = 1.0476 \xrightarrow{\ln} 0.0465$$

$$\frac{75+0.2}{75+\frac{1}{2}\times 0.2} = \frac{75.2}{75.1} = 1.00133 \xrightarrow{\ln} 0.00133$$

Bending causes stress gradients over the thickness and it is thus violating the plane stress requirement. This causes the strain valves to increase as the radius decreases, bending has a higher influence as the radius the material be being stretch around reduces in size.

To show this using the results obtained, the Erichsen testing method was used again. The seven materials were formed using gridded material. The bulges produced were applied to the ARGUS system to obtain the major and minor strain valves. There were no different blanks sizes used, only the fully constrained 166 halterwidth blank results form the produced FLC will be used. This test is the same as the Erichsen test with a larger radius punch. The 166 fully constrained results used from the Nakazima test were of the non-IF mask.

Table 3.5 and figure 3.65 shows the results for all seven materials. The Erichsen results which used a smaller punch radius compared to the Nakazima test, 20mm and 75mm respectively, resulted in increased strain valves.

	Erichsen testing			Nakazima testing	
Material	major	minor		major	minor
T52 BA	0.31	0.285		0.25	0.245
T65 CA	0.28	0.25		0.19	0.18
T57 CA	0.29	0.28		0.245	0.235
T57 BA	0.35	0.32		0.325	0.305
T61 CA	0.28	0.265		0.205	0.18
DR550 BA	0.24	0.21		0.09	0.075
DR550 CA	0.11	0.11		0.195	0.175

Table 3.5. Results of Erichsen V Nakazima for biaxial strain test.

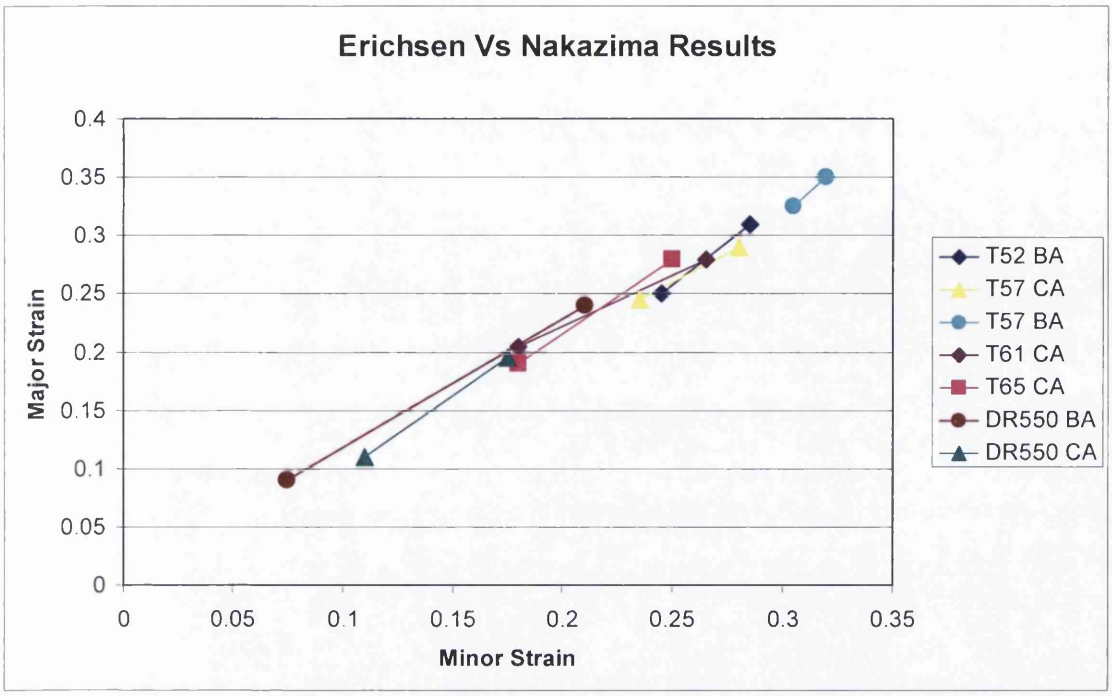

Figure 3.65. Comparing Erichsen v Nakazima results of the biaxial test.

The next area to examine is the inability to produce results under uniaxial to plane strain conditions for the DR grades and packaging materials T61CA and T65 CA when the IF mask was not used. On examination of the blanks, figures 3.66 and 3.67 are examples of formed DR550 CA and T65 CA 50 halterwidth blanks respectively, it was found that the crack had not been produce at the centre of the bulge but still within the 15mm of the centre which the ISO 12004-2 specifies. The red lines in figures X and X indicate the centre of the blank.

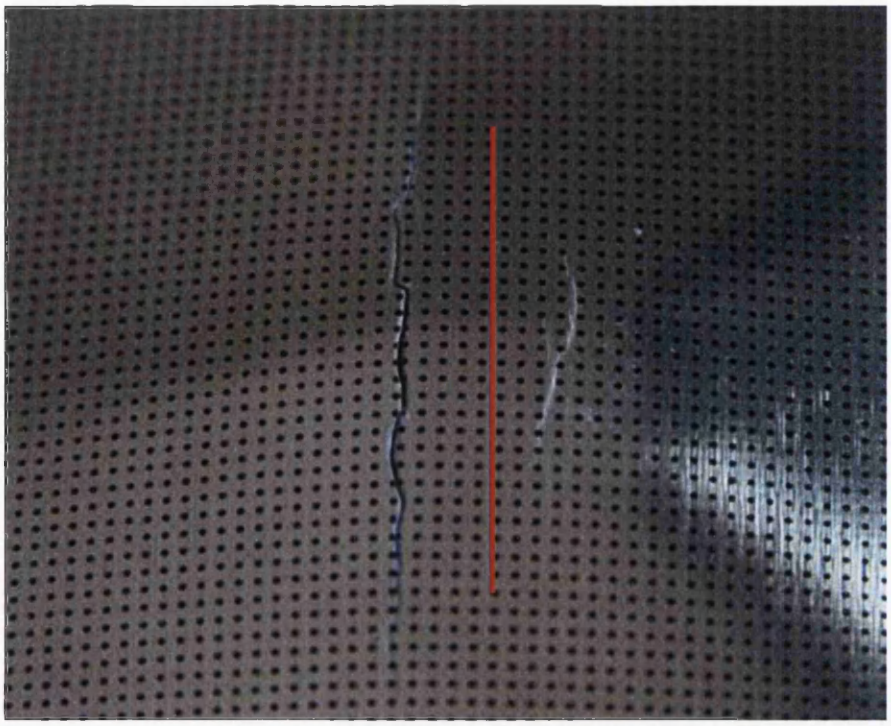

Figure 3.66. DR550 CA showing crack position compared to the centre of the blank.

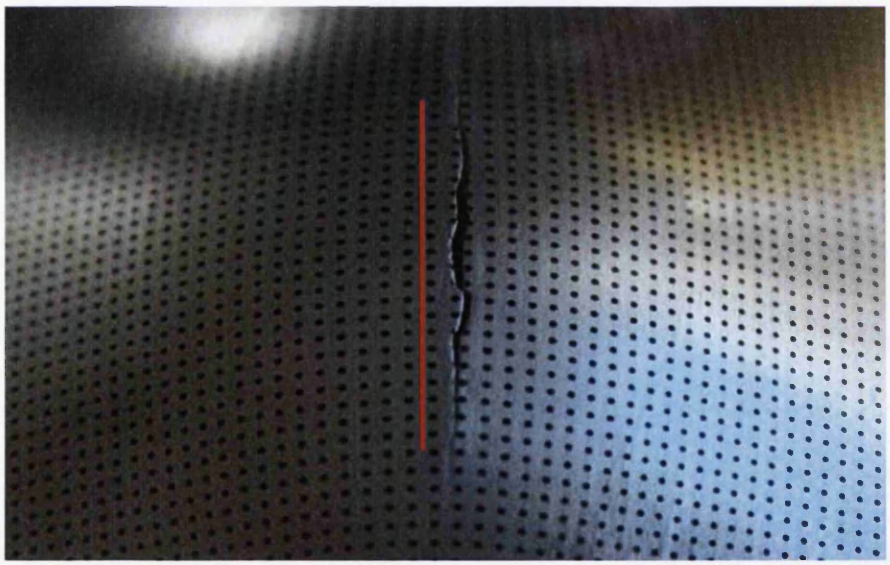

Figure 3.67. T65 CA showing crack position compared to the centre of the blank.

As the material hardens the crack appears further away from the centre of the bugle. The IF mask influences the packaging steeling allowing uniaxial to plane strain conditions. The IF mask does not affect the DR grades uniaxial to plane strain conditions as the material is much

harder compared to the packaging steels. Due to this hardness, the ability for the material to withstand the compressive force in the Minor Strain direction is greater. The failure will occur at the closest point when plane strain conditions are met. This may not be at the centre of the bulge, hence the cracks appear elsewhere.

Chapter 4

COMPUTER ANALYSIS AND RESULTS

Chapter 4

COMPUTER ANALYSIS AND RESULTS

4.1 Introduction

In conjunction with the experimental work, computer models were developed to simulate the Erichsen and Nakazima tests. The models were implemented using the ELFEN 4.4.2 Finite Element Package. The aim is to produce a model so that future packaging steel grades can be implemented into the model to aid the prediction of the FLC, saving on expenses such as manpower, equipment costs and time.

4.2 Computer Analysis

4.2.1 Finite Element Method

The Finite Element Method (FEM) has become an important tool used in engineering problems. With the wide spread use of computer technology and Computer Aided Design (CAD) systems, engineering companies are able to model and predict how machinery, individual parts and complete products interact during manufacturing and act against various forces. Models are used to make real life processes and objects simple to predict behaviour, therefore it is important at only include areas of interest within the models. Excess detail increases both solution time and risk of errors in the programming.

At the beginning, FEM it was used only in the aerospace sector, because in the 1950-1960s only to large aircraft companies could afford the super computers of the time, for the calculations. In the early 1960s Zienkiewicz started adapting FEM to be used in the Civil Engineering applications and created an important research group at the University of Wales Swansea. This was the first major use of FEM outside the aerospace sector and led the way for FEM to be used in all areas of engineering. Since the 1970s FEM has been developed as computer technology increases, which is still happening today (Chandrupatla and Belegundu, 1991).

There are many advantages for using FEM in industry. Reduce both time and resources needed for product devolvement. This reduces final cost and increases profit margins. However experiments are still needed to validate the results produced from computer programs.

There are extensive FEM books available including Zienkiewicz and Taylor (1987), Owen and Hinton (1977), Chandrupatla and Belegundu (1991) and Belytschko et al (2000) that cover all aspects of the topic, such as, linear and nonlinear analysis, programming, various force and thermal variations.

4.2.2 Validation

Validation is the phase of model development where a model is determined to be fit for purpose, normally after comparison to a measurable quantity from experimental results. After validation the model is considered sufficiently correct to permit proper exploitation. The model can be used to extrapolative/interpolative untested situations and determination of other quantities un-retrievable by physical experimentation.

4.3 ELFEN

4.3.1 Introduction

For this project the models will be simulated using the finite element computer software ELFEN. ELFEN is a 2D and 3D numerical modelling package that was created by the Swansea based company Rockfield Software Ltd.

4.3.2 Software

The software itself consists of three main stages, the graphical pre-processing, the analysis and the post-processing. Each main stage has a series of sub-stages which makes using the software logical and easy to understand which helps reduce any error (Rockfield, 2002).

The pre-processing uses a graphical user interface (GUI) where the geometry of the model can either be manually inputted or imported from a CAD package. The GUI has been designed to speed up model preparation time and to ensure that ELFEN is an easy-to-use

package. The other information defined in the pre-processing includes the, loading forces acting on the model, boundary conditions, material selection, constraints and mesh sizes.

ELFEN comprises of two analysis parts, implicit and explicit. Implicit solution algorithms are used to solve mechanical, thermal, fluid and general field problems and explicit are used to solve dynamic mechanical problems.

The final stage is the post-processing where the results of the model can be viewed and analysed. This includes animation, contour displays and graphical plots. Animations are useful to help the user see how the model reacts under the conditions. Contour displays are used to show the variation of any variable. The graphical plots can be used to produce time history variation and variable variation long a selected line. The more useful part is that any one variable may be measured against another. This can produce forming limit diagrams, which as informed in section 2.3, are good to see the safety margin within the part (ELFEN 2.8, 1998).

4.3.3 Model

For more information or to see how the models have been constructed, the models can be found in Appendix B. EFLEN version 4.4.2 will need to be used to run either the Von-Mises yield criterion or the Hill yield criterion. EFLEN version 4.4.12 will be needed to run the Barlat yield criterion.

The strain rate hardening model, which is the change in strain within the material over a period of time, that is used in the simulations is the Zerilli-Armstrong strain rate. The reasons this hardening rate is being used over others is that it is good at high strain valves, which packaging steels achieve, and it is already currently in the computer software which makes using it simple. This hardening rate will be used with the Hill and Barlat yield criterion.

Figures 4.1 and 4.2 show the completed mode. Figure 4.1 is the top view of the model showing the blank once it has been formed against the die. Figure 4.2 shows the bottom of the model where the punch stretches the blank which is secured in place by the blankholder.

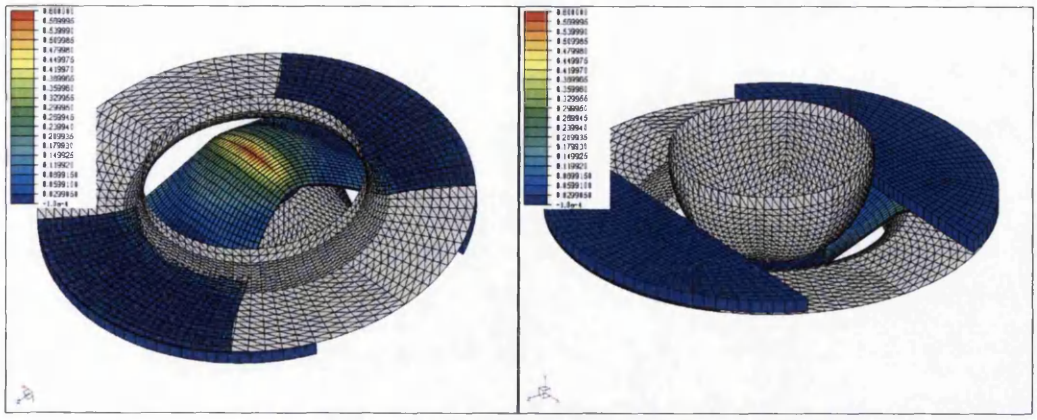

Figures 4.1 and 4.2. Completed model, top and bottom views respectively.

The model has been built to match the Nakazima test experiment. Due to the axis symmetries in the X and Z direction through the centre of the blank, the model has been created accordingly, figures 4.3 to 4.6.

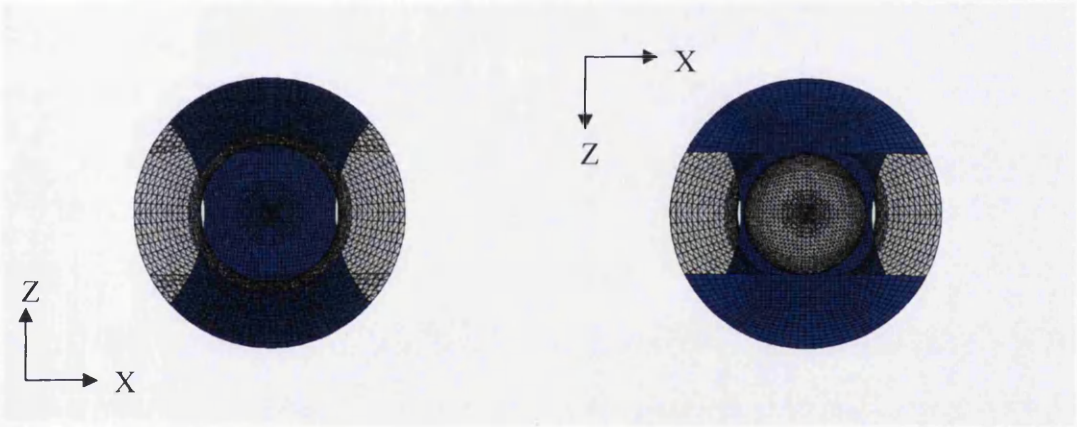

Figures 4.3 and 4.4. Top and Bottom view of the model respectively showing the axis symmetry lines.

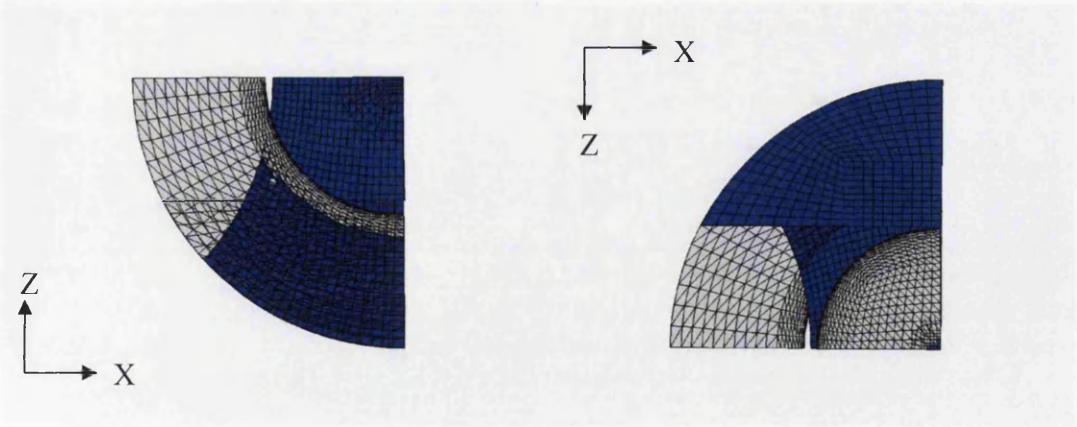

Figures 4.5 and 4.6. Model showing the axis symmetries.

This axis symmetry has been done because the experimental testing showed that the blanks are the same through these axis' hence it will increase the simulation time of the models. This increase in simulation time will allow more elements to be used increasing the final accuracy. The reader should be aware that the

The model has two stages to the simulation. The first stage is the blankholder pressure, at the beginning the model simulates the blankholder applying a 330kN force on the blank and mask which secure them in place between the blankholder and die. This is the same force used during the experimental testing. This force stops them from being drawn into the die when the punch movement is applied, figure 4.7

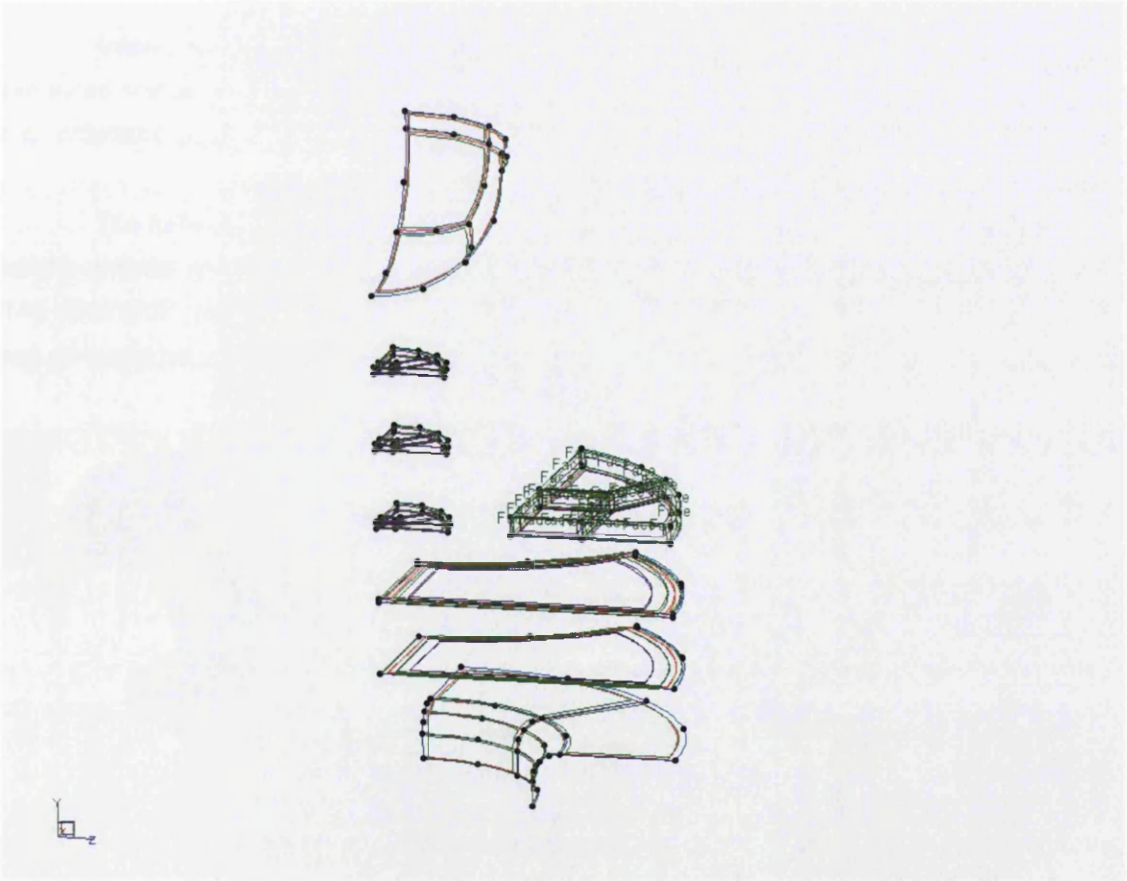

Figure 4.7. Model indicating the force which is applied by the blankholder.

The second stage is where the punch moves and forms the bulge. Figures 4.8 and 4.9 show the punch at the beginning and end of its movement.

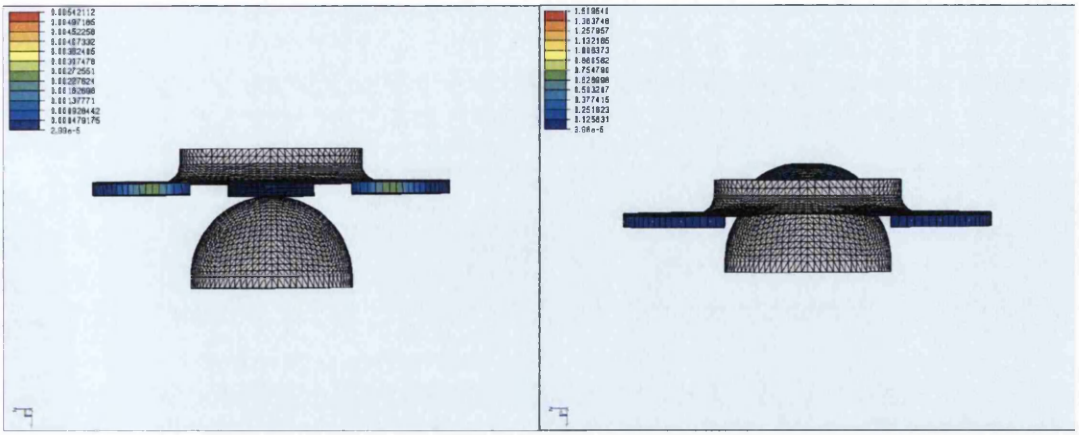

Figure 4.8 and 4.9. Model showing punch movement from start to finish respectively.

Initially three halterwidths were chosen to model to see if the results that were being produced mirrored the experimental results. Areas that were being examined were points of highest strain, general strain pattern throughout the blank and strain valves obtained.

The halterwidths chosen were 50, 90 and 125. 50 and 90 were chosen because this gave us the uniaxial and plane strain. The 125 was chosen because the results of the experimental 140 halterwidth were under question. The material used for this initial modelling was T52BA. The results would be compared to the T52BA Argus results.

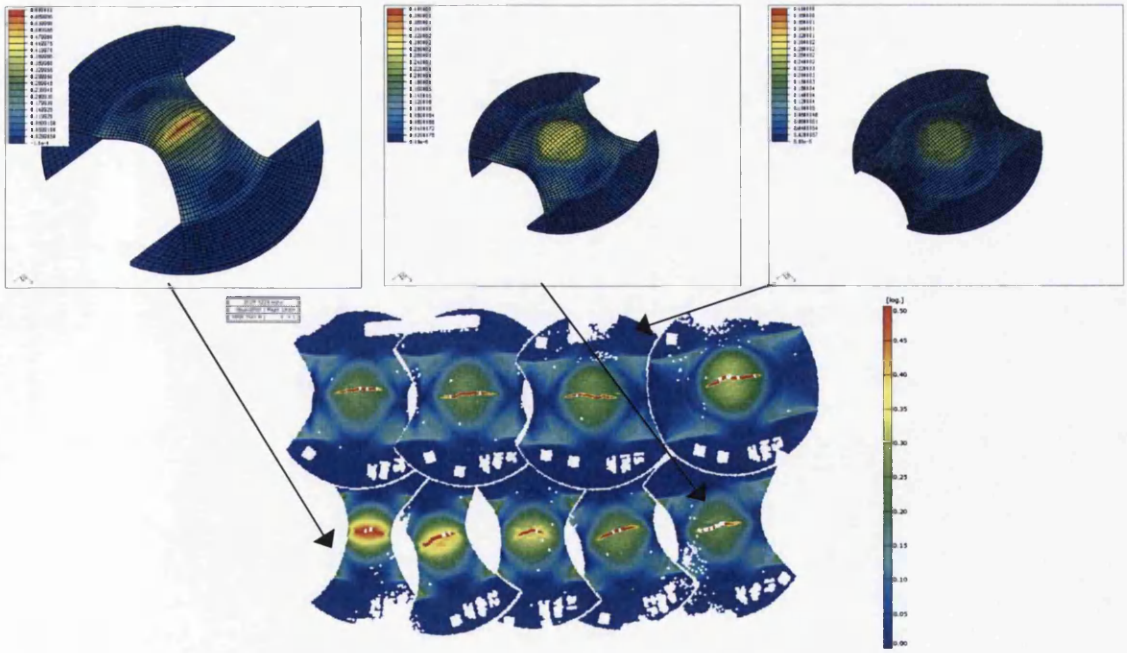

Figure 4.10. Three models left to right, of 50, 90 and 125 halterwidth respectively with a set of T52BA Argus results below.

Figure 4.10 shows the three halterwidths results. The point of highest strain can be seen best on the 50 halterwidth. It occurs on the top of the bulge. This is where the crack is formed during the experimental testing which is the point of highest strain. Looking at the whole models compared to the Argus results the general strain pattern throughout both sets of results are similar. The strain valves obtained were also of a similar valve both ranging between 0 – 0.5. These similarities give confidence in the model to continue further on and model the full set of material results. The materials that were chosen for the Isotropic modelling were, T52BA, T57BA, T57CA and T61CA.

The measurement of the strain within the model has a similar method to that of the Argus method. The model is used and a Nodal Interrogation is preformed. A centre node is selected where the highest stain occurs, area shown in figure 4.11.

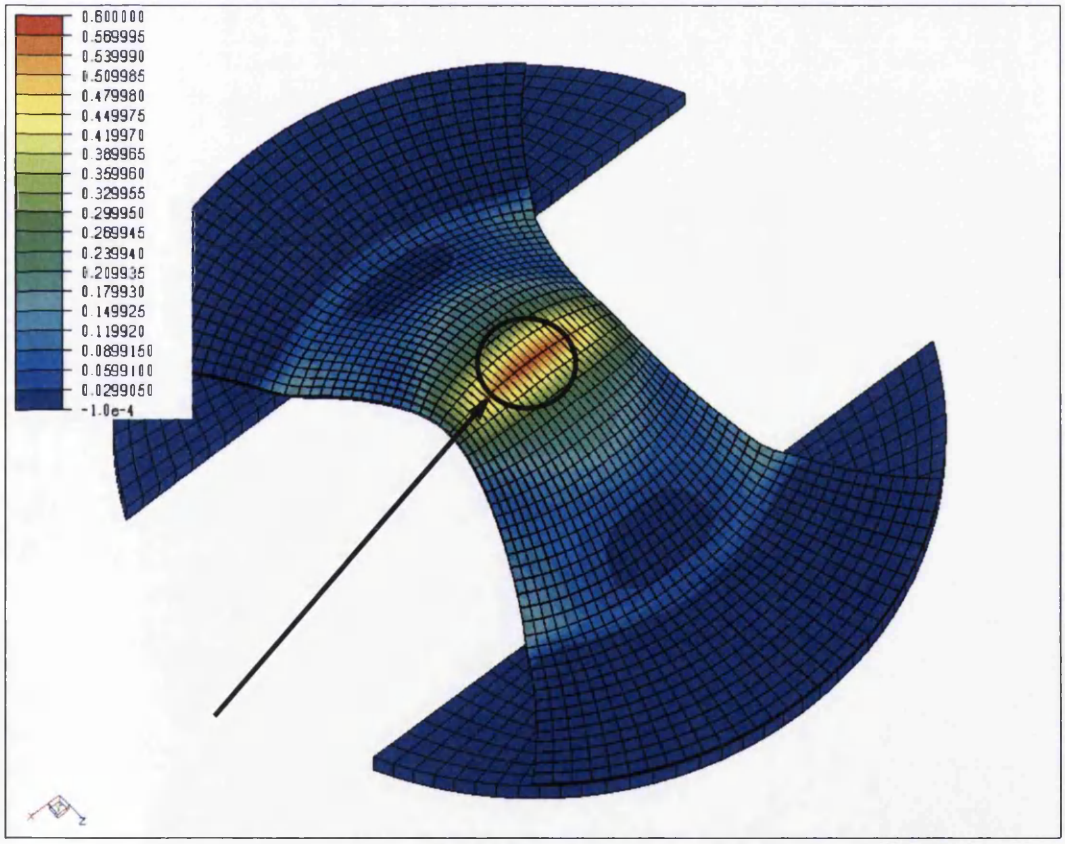

Figure 4.11. Area where node is selected for nodal interrogation.

The strain is recorded at each time step as the blank is formed. The Argus method measures the strain at the end when the crack is formed. By measuring the strain as the blank is being formed a strain path can be being produced showing how the strain evolves until the point

of failure. A graph of the strain against time can be formed. This is done for both the major and minor strains. Therefore the major and minor strain can be compared producing a FLD, figure 4.12.

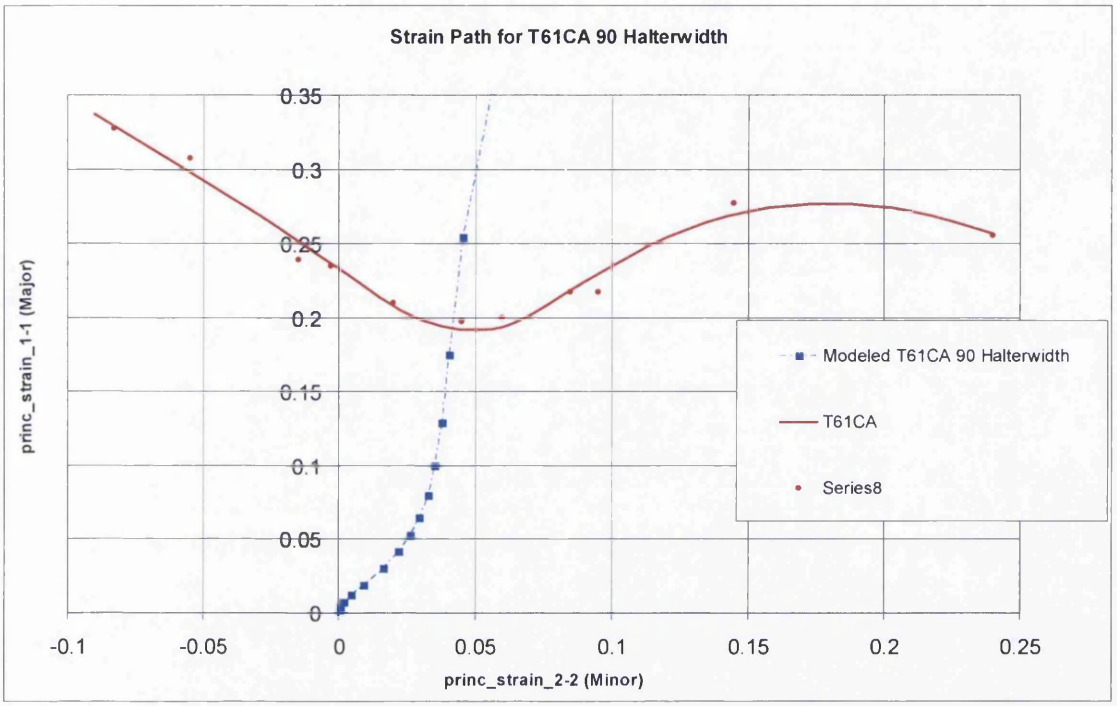

Figure 4.12 Blank size of 90 halterwidth showing its strain path.

The model will continue to simulate after the strain rate excess the failure point in reality. The use of strain rate gradient to calculate the moment of thinning of the material is used. The strain rate is potted against time. To produce this, the nodes that are at the edge of the blank, shown in figure 13, are selected. The edge is perpendicular to the crack direction. This is a similar method used in the Argus system.

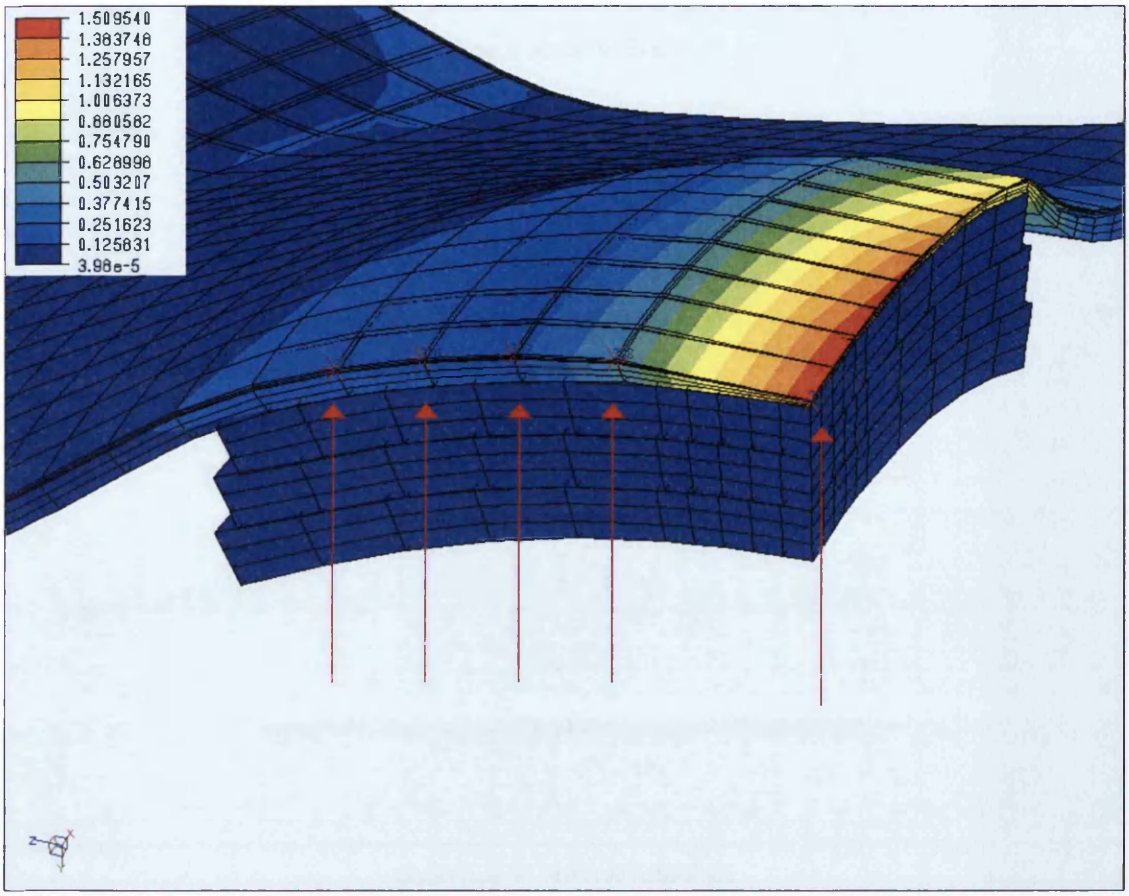

Figure 4.13. Node along the edge perpendicular to the crack direction are select for there strain rate valves.

Each of the select point has its strain rate mapped against time to produce the strain rate against time graph, figure 4.14. The nodes are examined until one node, which will be the centre node, starts to diverge away from the node it is next to. This would indicate that the material is at the point of thinning.

Once this failure point has been chosen the time at which this occurs in compared to the Strain Path of the simulated material. All the points that are above the time are ignored. The result is a graph like figure 4.15. This shows the strain path of the material and the point at which the strain rate beings to increase substantially which is the initiation of thinning.

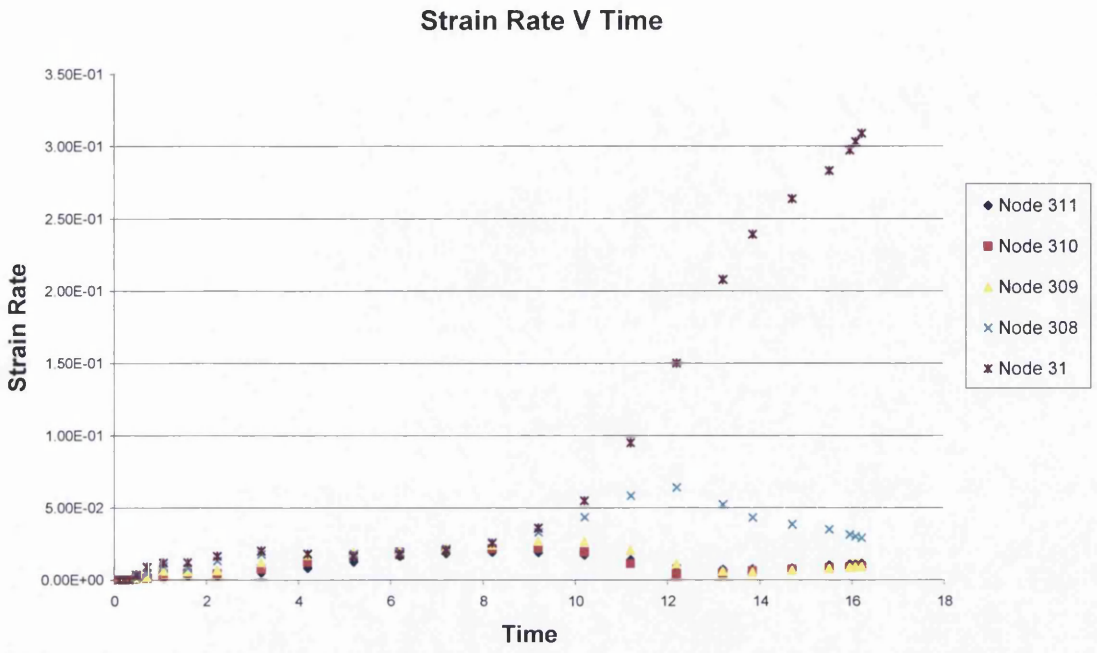

Figure 4.14. Strain rate valves of the nodes as the blank is formed.

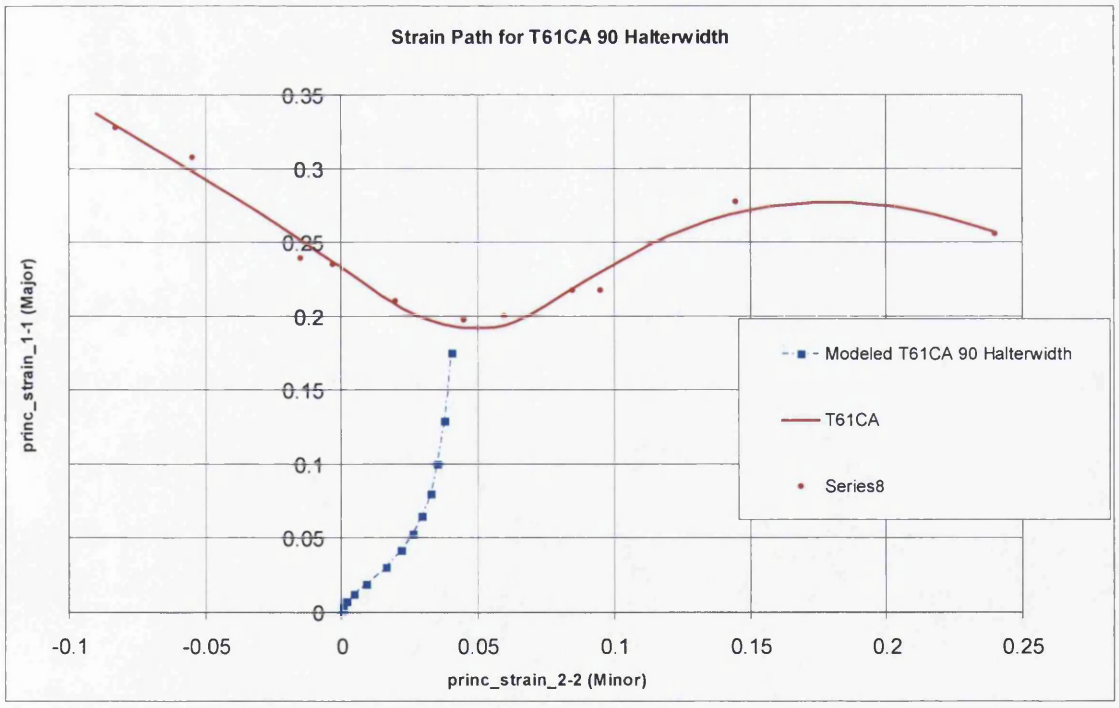

Figure 4.15 Strain path which shows then thinning of the material has initiated.

4.4.4 Discussion

There are some factors of the model that may influence the results. The model had areas of penetration around the die radius, this can be seen by the circled area in figure 4.16. This is where the blank has passed through a part of the die which will result in an incorrect radius on the blank.

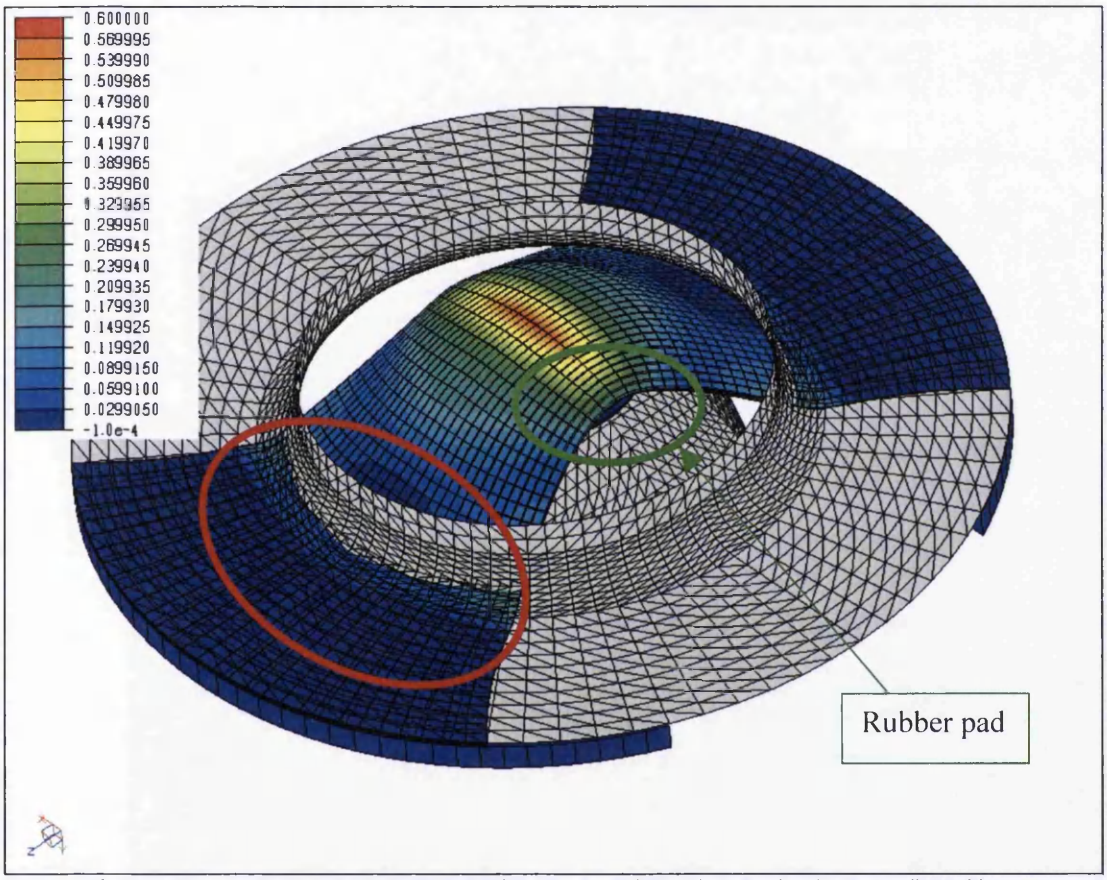

Figure 4.16. Area circled red indicating where penetration was occurring and green showing protruding rubber.

Figure 4.16 shows that the rubber pads are just protruding from under a 50 halterwidth mask and blank. During the experimental testing the rubber pads were clearly out, more so then the model suggests.

The model is unable to model the wrinkling that takes place as the halterwidth increases in size. Figures 4.17 and 4.18 show experimental results of 166 partial and 125 for T52-BA respectively. As can be seen, as the halterwidth increases, wrinkling occurs where the

blankholder does not constrain the blank. Figure 4.19 to 4.22 shows that the model bents the blank to form one arc.

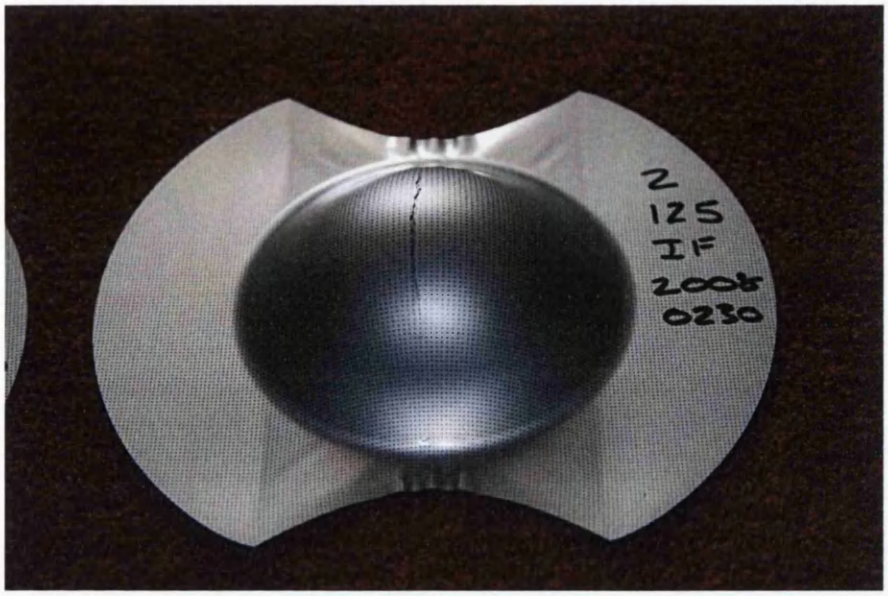

Figure 4.17. Experimental results showing wrinkling in halterwidth blank 125

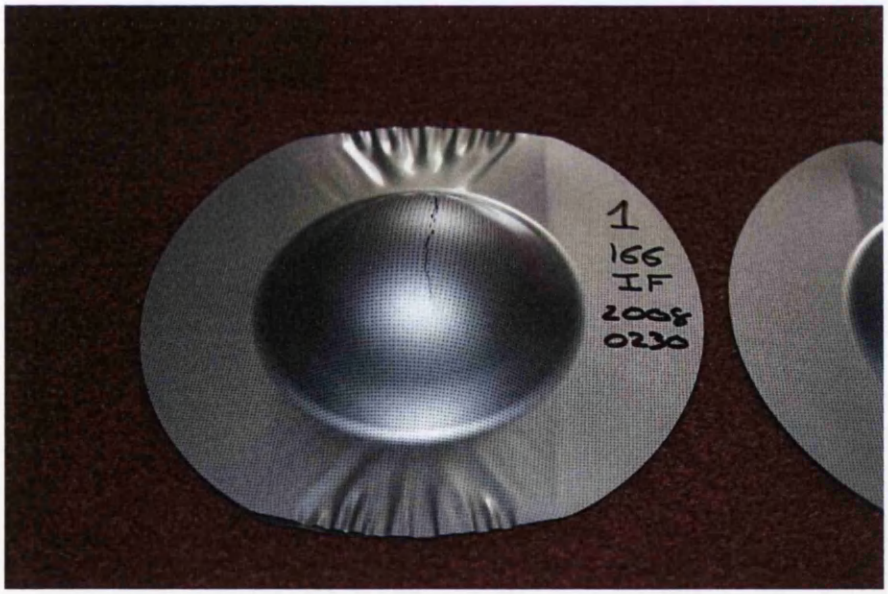

Figure 4.18 Experimental results showing wrinkling in halterwidth blank 166 partial

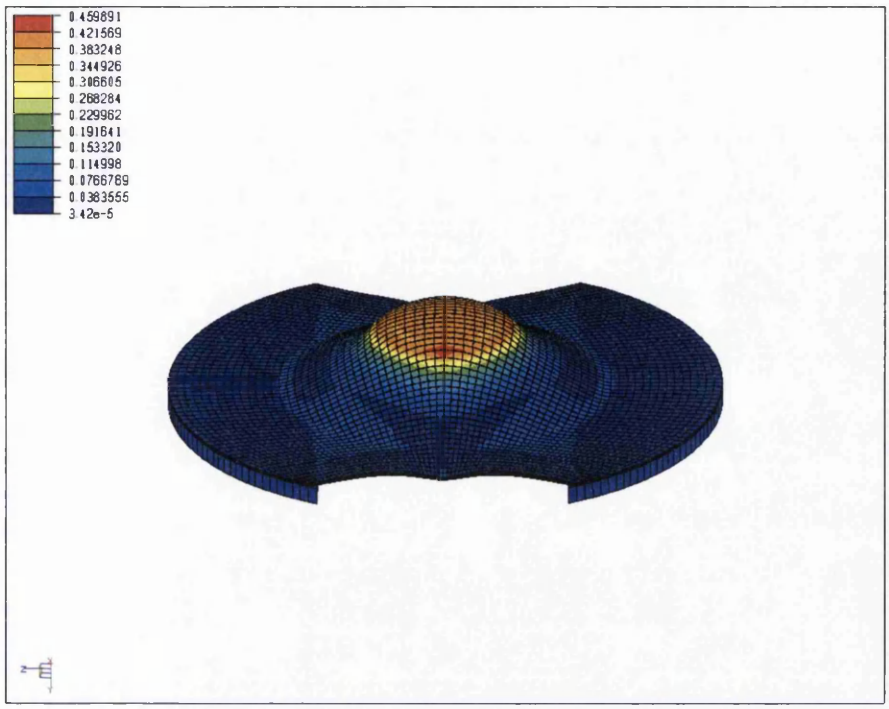

Figure 4.19. Computer model showing arc instead of wrinkling that occurs during experiments.

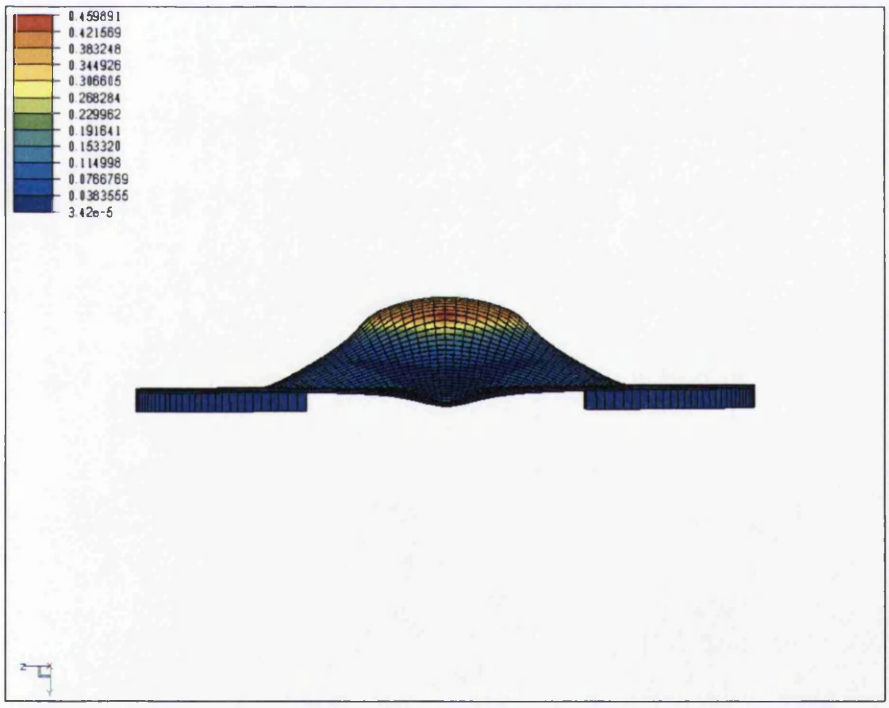

Figure 4.20. Computer model showing arc instead of wrinkling that occurs during experiments.

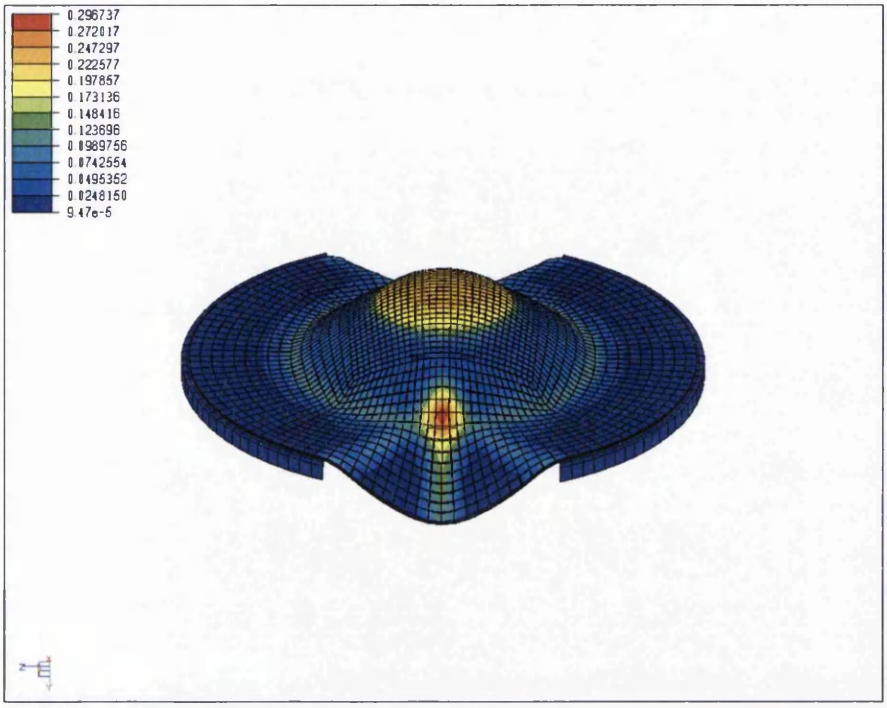

Figure 4.21. Computer model showing arc instead of wrinkling that occurs during experiments.

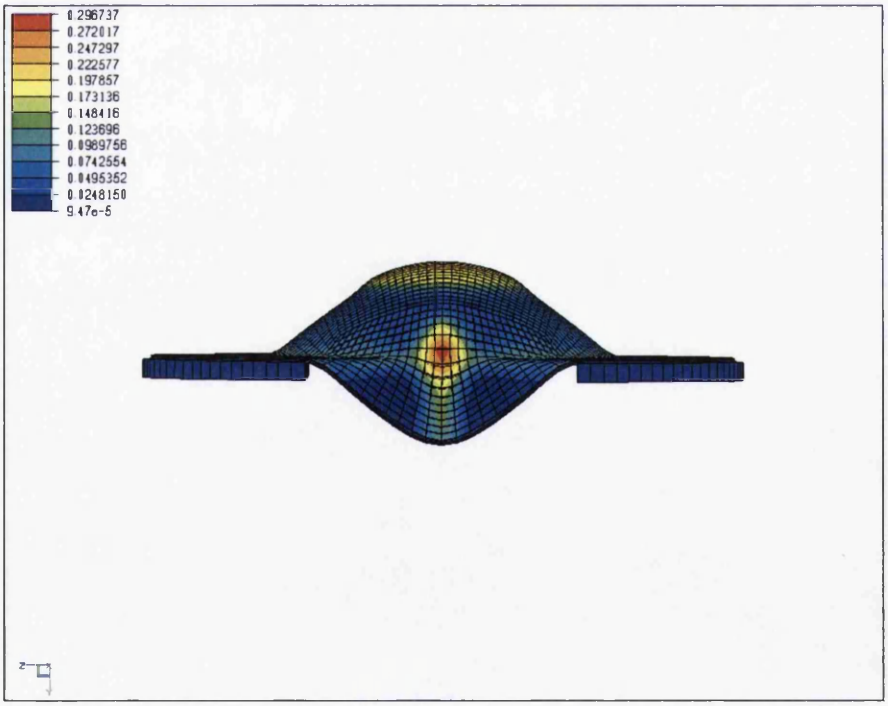

Figure 4.22. Computer model showing arc instead of wrinkling that occurs during experiments.

To increase the accuracy of the results, the model can be changed in increase the amount of output results. This increase in results will give a greater number of points along the strain path, this changes the accuracy with regards to time when thinning occurs hence altering the point on the graph that represents thinning, figure 4.23.

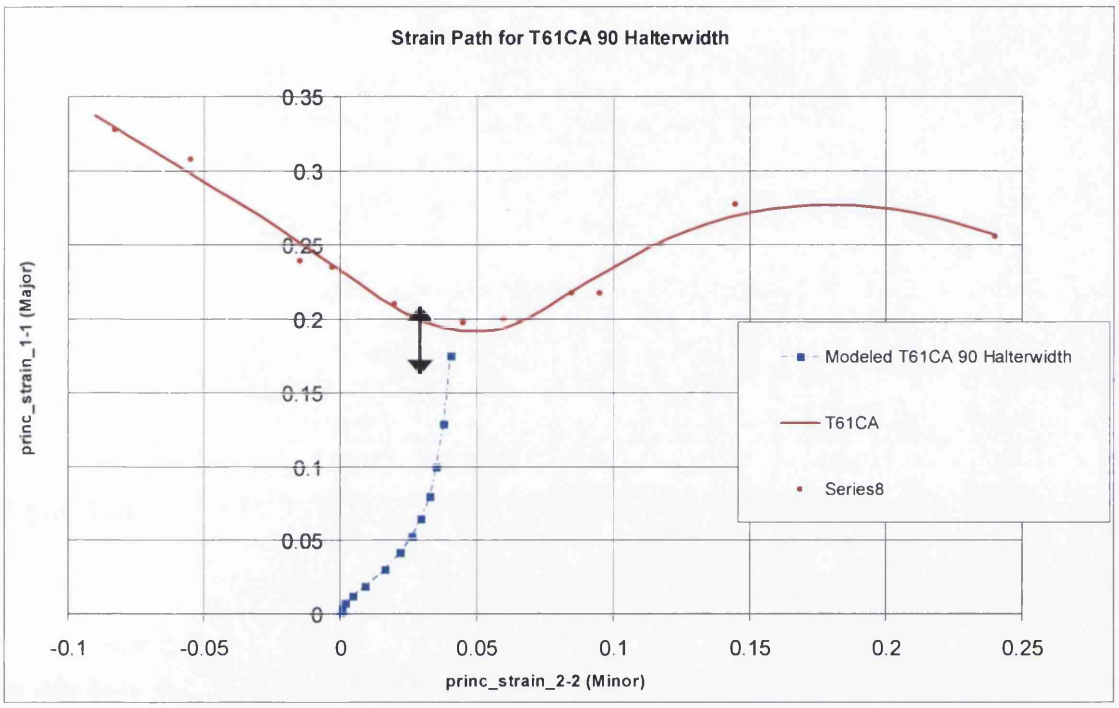

Figure 4.23. Increasing output results can alter the point on the strain path that thinning has said to be started.

Figure 4.24 shows the results of blank size of 80 halterwidth with varying mesh densities. This graph shows what happens to the strain path as the mesh density of the blank is increased. The denser the mesh the longer the simulation time, however as the density increase the strain path changes. The mesh densities affect on the strain path is decreased as the density is increased until a point is reached that increasing the density does not affect the strain paths. To start to achieve this each halterwidth simulation needs to be simulated for 2 weeks. Therefore it is possible to alter the strain path depending on the mesh density.

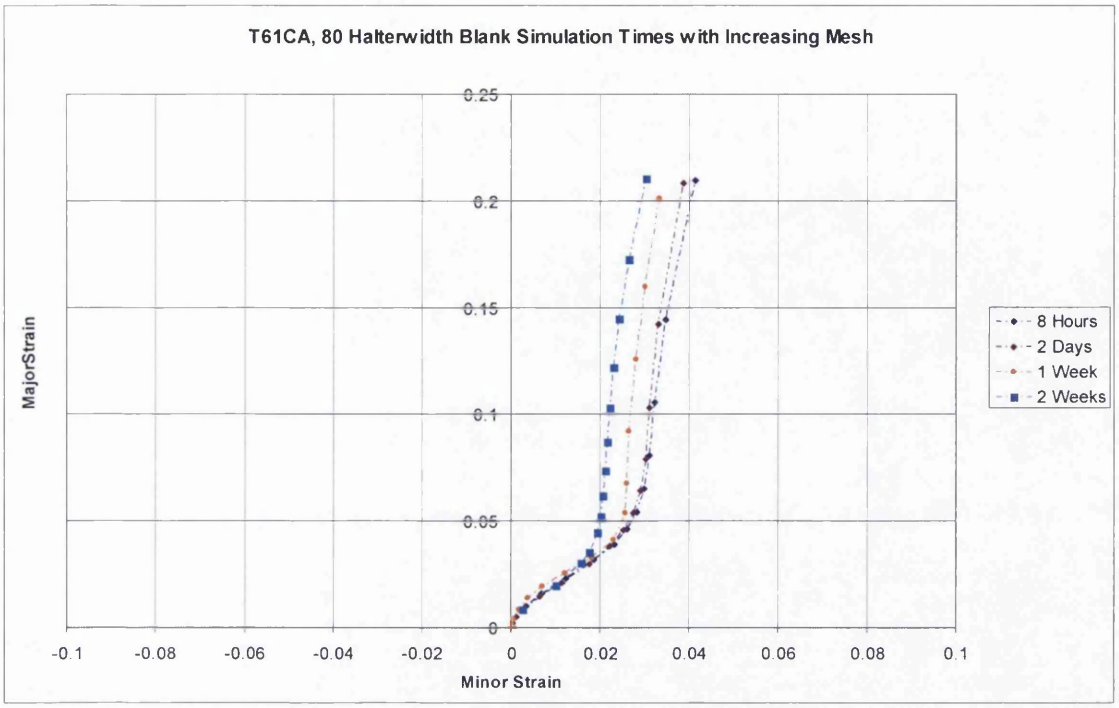

Figure 4.24

After discussions with RSL about the extent of the simulation time it was concluded that to decrease the simulation time the model need to be simplified. Currently there are several different contact surfaces, for example between the blank and the blankholder and the punch and the lubrication system, and there are a few different forces, for example the blankholder force and the punch force. All these increase the simulation time and to reduce this, the model needed to be simplified.

A few different areas were look at, the blankholder was one area. Instead of the blankholder applying a force to the blank throughout the simulation, the blankholder would be a rigid body constrained in the X, Y and Z planes and the edge of the blank would be constrained at the outer edge if the die. This was implemented and simulated. The result was that the material stretched between the blankholder and the die when the punch's force is applied. This does not happen in reality and resulted in high stress areas around the die radius. These were greater that were being achieved at the centre of the punch. So the blank geometry was change so that the area under the blankholder was constrained, not allowing it to stretch. However at the point were the blank contacted the die, severe penetration then occurred and caused the model to repeatedly crash. This was one example of how the model was tried to be simplified.

4.4 Isotropic 3D Nakazima Model

4.4.1 Introduction

The first Nakazima model will use Isotropic material properties using the Von-Mises yield criterion. The model can be found in Appendix B and will need ELFEN version 4.42. Due to the simulation time and the results obtained from the experimental work, not all of the seven materials were simulated. The materials chosen were T52 BA, T57 BA, T57 CA and T61 CA. The two DR grades were dropped because of there inability to produce results in the uniaxial to plane strain conditions and packaging material T65 CA was not used because its results were similar to the T61 CA material.

All the results simulated for the three different yield criterion were using an IF steel mask. Even though the IF mask has shown that it influences the strain path, the results obtained from the experiment work gave a good spread of strain paths from uniaxial to biaxial.

4.4.3 Isotropic Results

Figures 4.25 to 4.28 shows the simulated results using T52 BA, T57 BA, T57 CA and T61 CA material properties using the Von-Mises yield criterion.

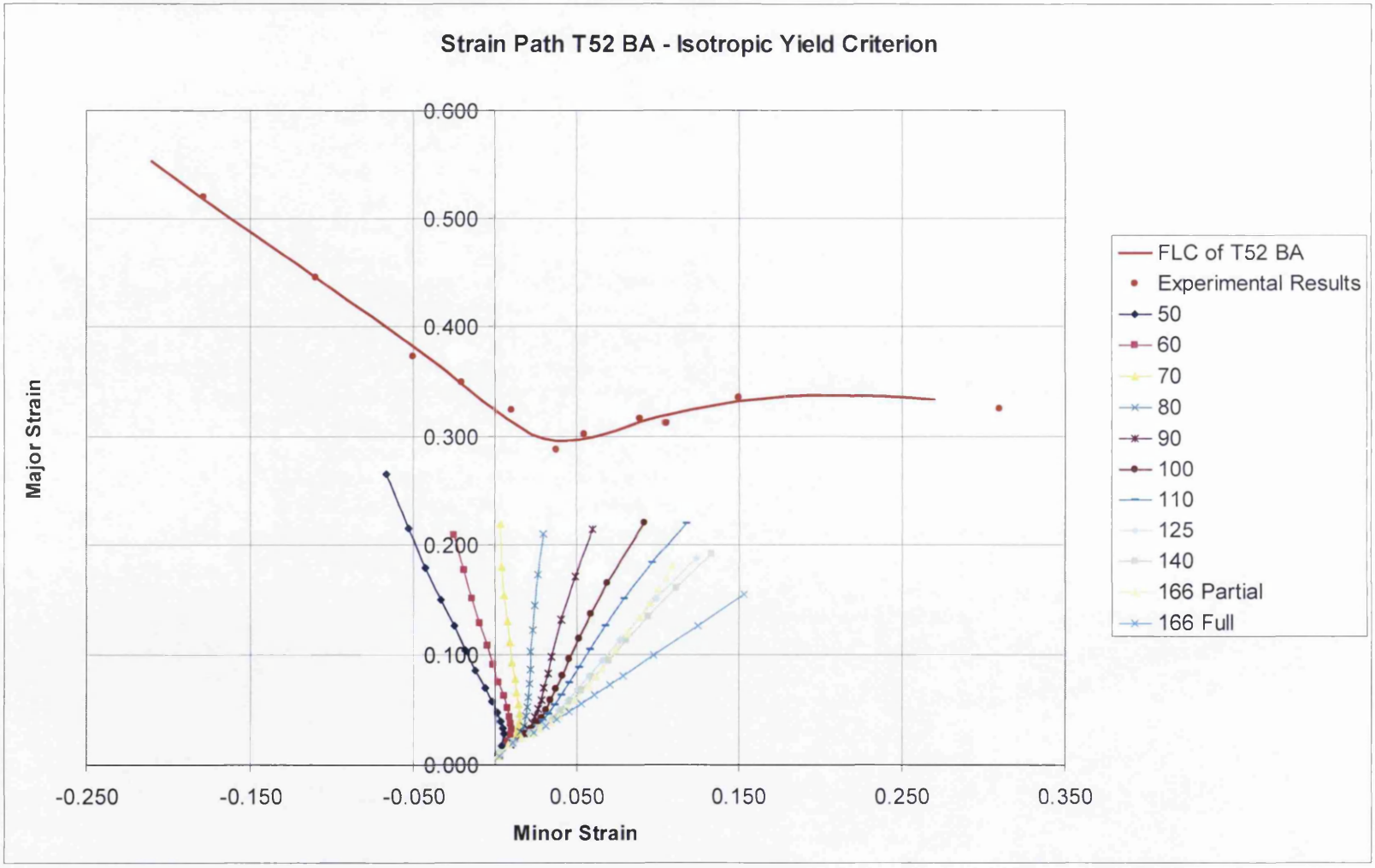

Figure 4.25. Set of simulated results for T52 BA compared to the experimental results.

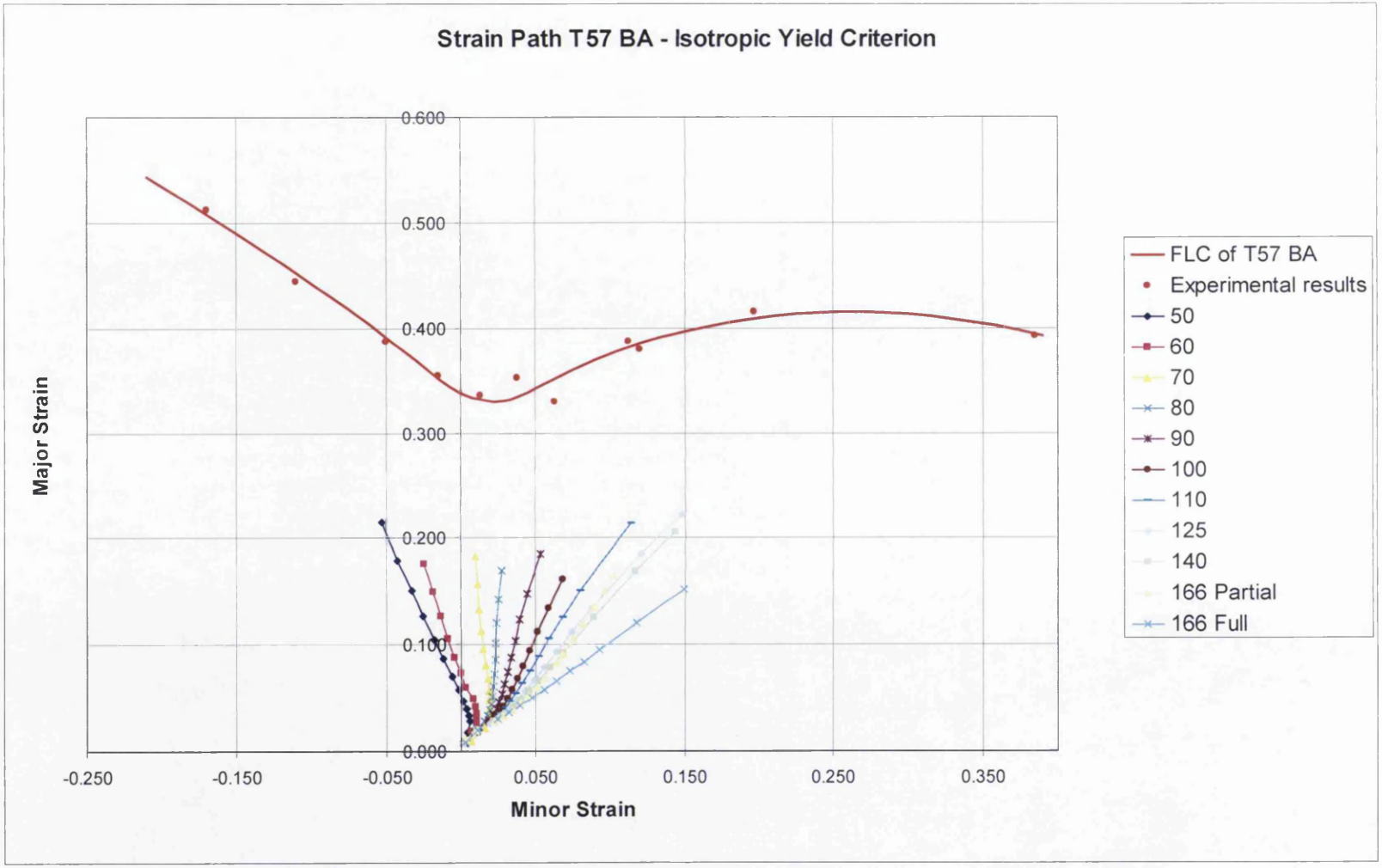

Figure 4.26. Set of simulated results for T57 BA compared to the experimental results.

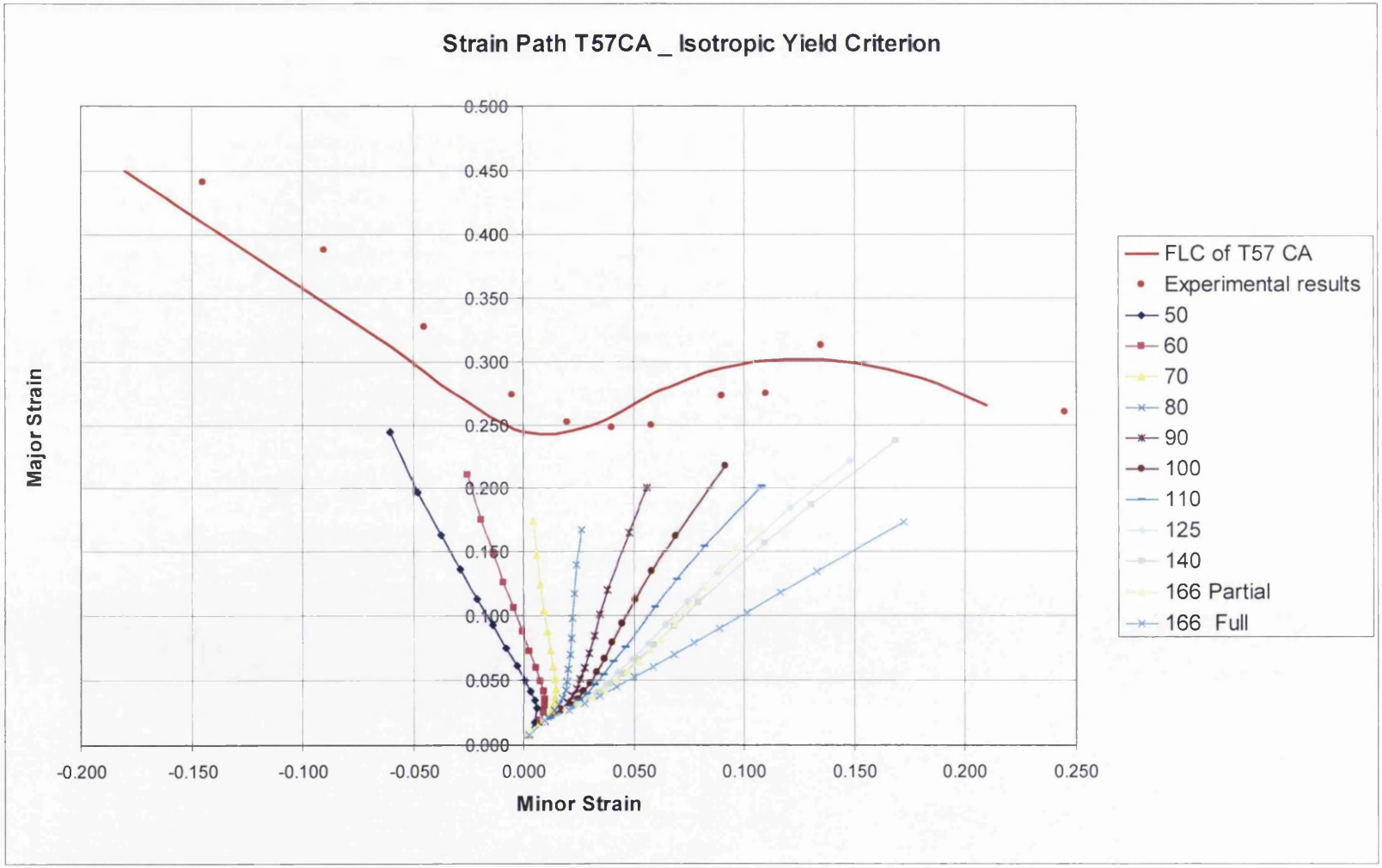

Figure 4.27. Set of simulated results for T57 CA compared to the experimental results.

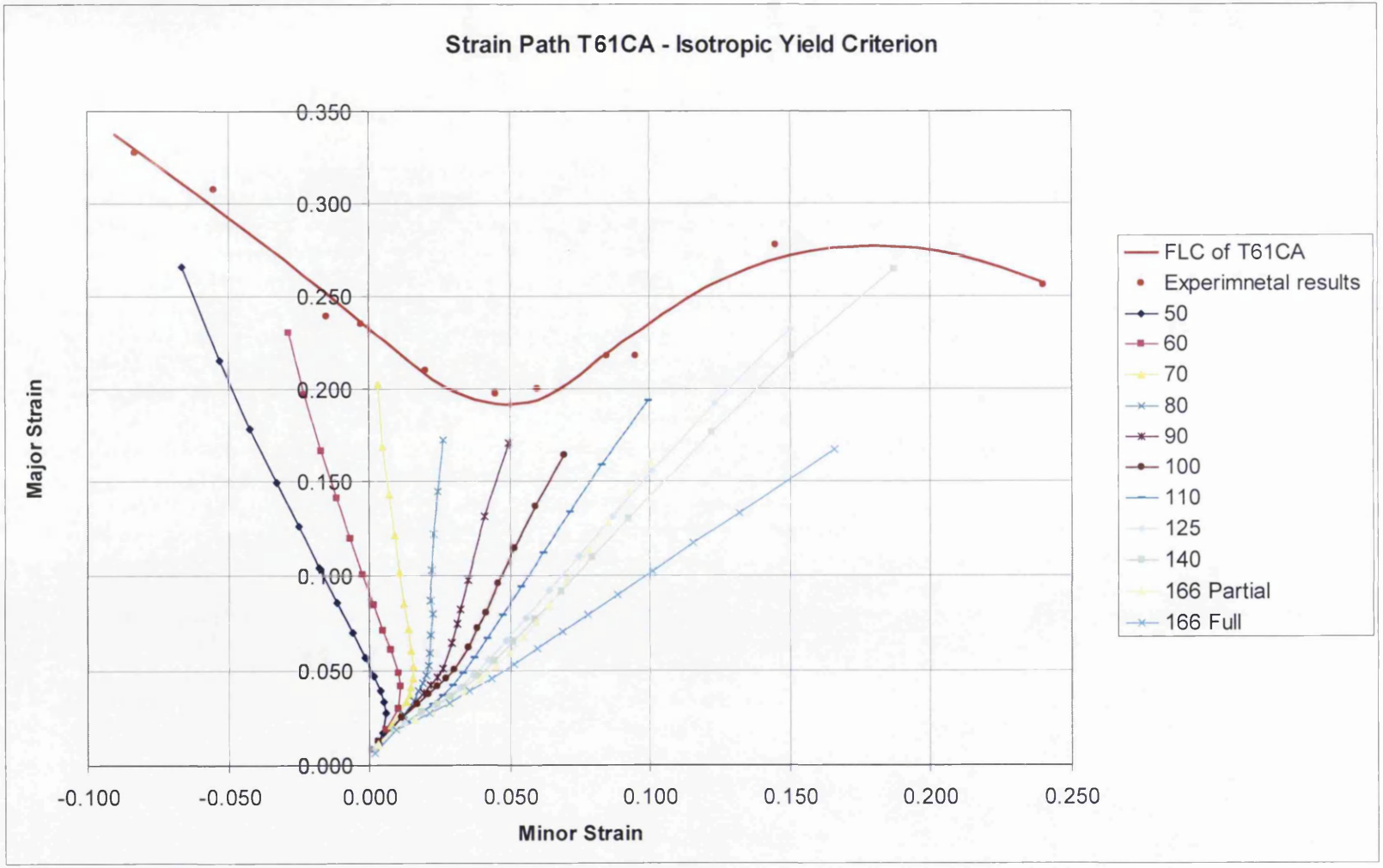

Figure 4.28. Set of simulated results for T61 CA compared to the experimental results.

4.4.4 Discussion

The results show a spread of strain paths across the halterwidth range. There seems to be a problem with the 166 partial halterwidth as the result does not fall between the 140 and 166 full results. The strain path show that initially the path is between the 140 and 166 full, but as the path continues it crosses over the 140 and 125 paths.

The isotropic model does not use any strain rate hardening laws hence why the point of thinning is near the experimental FLCs. The r-valve of the material is also not taken into affect within the yield criterion. The r-valve affect the deep drawability of the material, the strain conditions between uniaxial to plane strain (the left hand side of the graph, hence why the strain paths do not appear to be going towards the corresponding experiment point.

The combination of not using a strain rate hardening law and the fact that the yield criterion does not take into affect the r-valve, the results in the corresponding halterwidths having almost identical strain paths.

4.5 Hill 3D Nakazima Model

4.5.2 Hill Results

Figure 4.29 to 4.32 shows the simulated results using T52BA, T57 BA, T57 CA and T61 CA material properties using the Hill yield criterion.

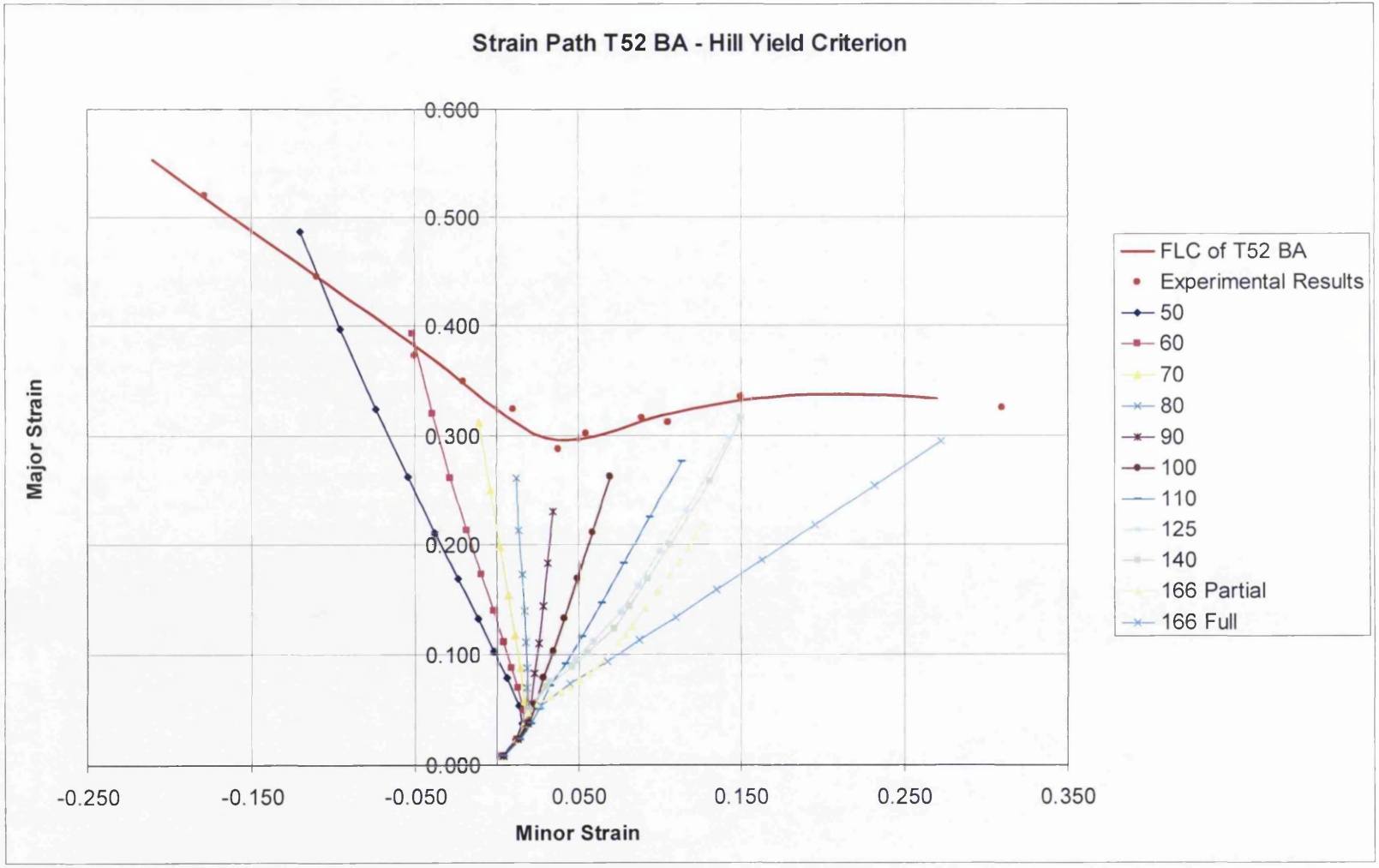

Figure 4.29. Set of simulated results for T52 BA compared to the experimental results.

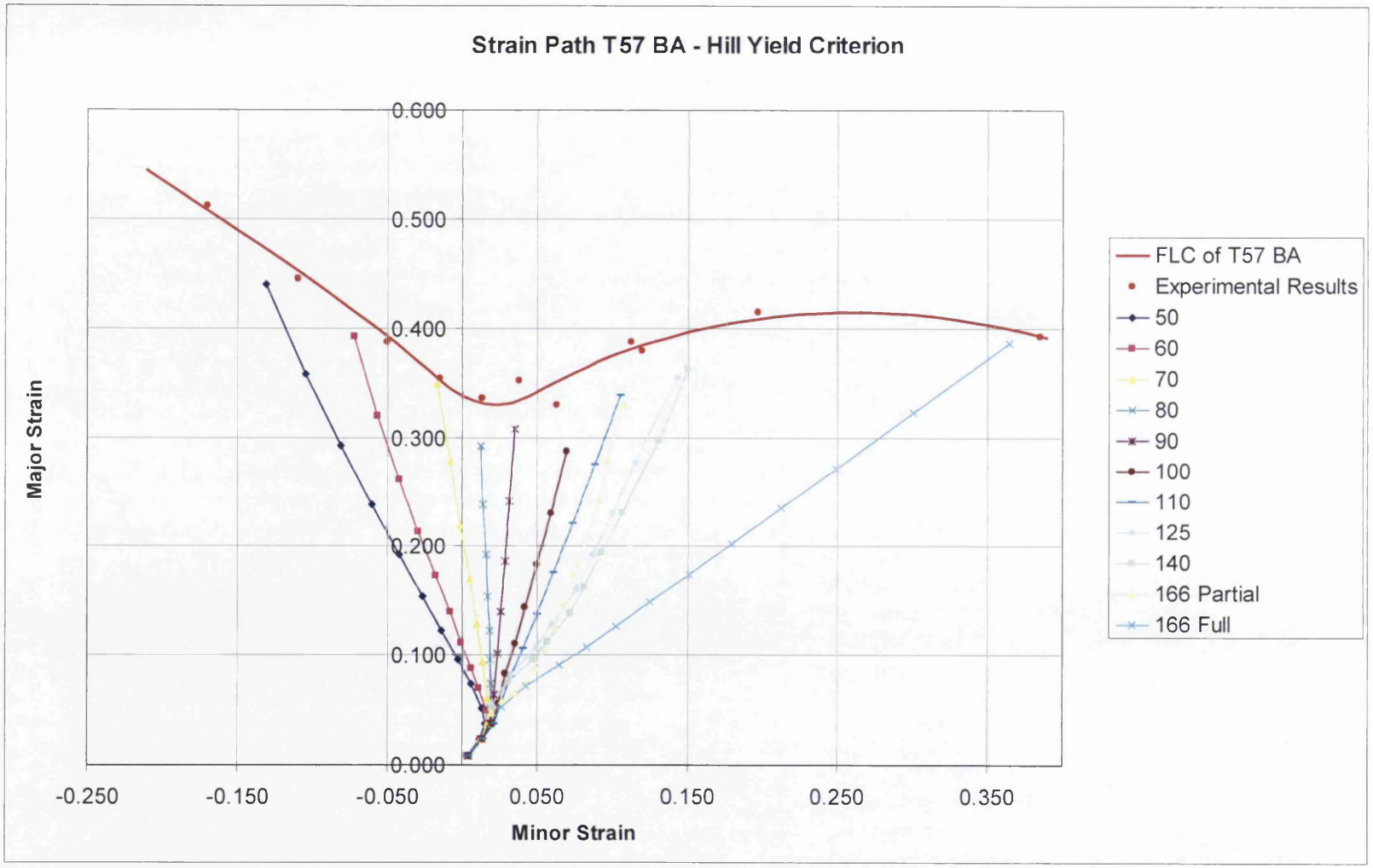

Figure 4.30. Set of simulated results for T57 BA compared to the experimental results.

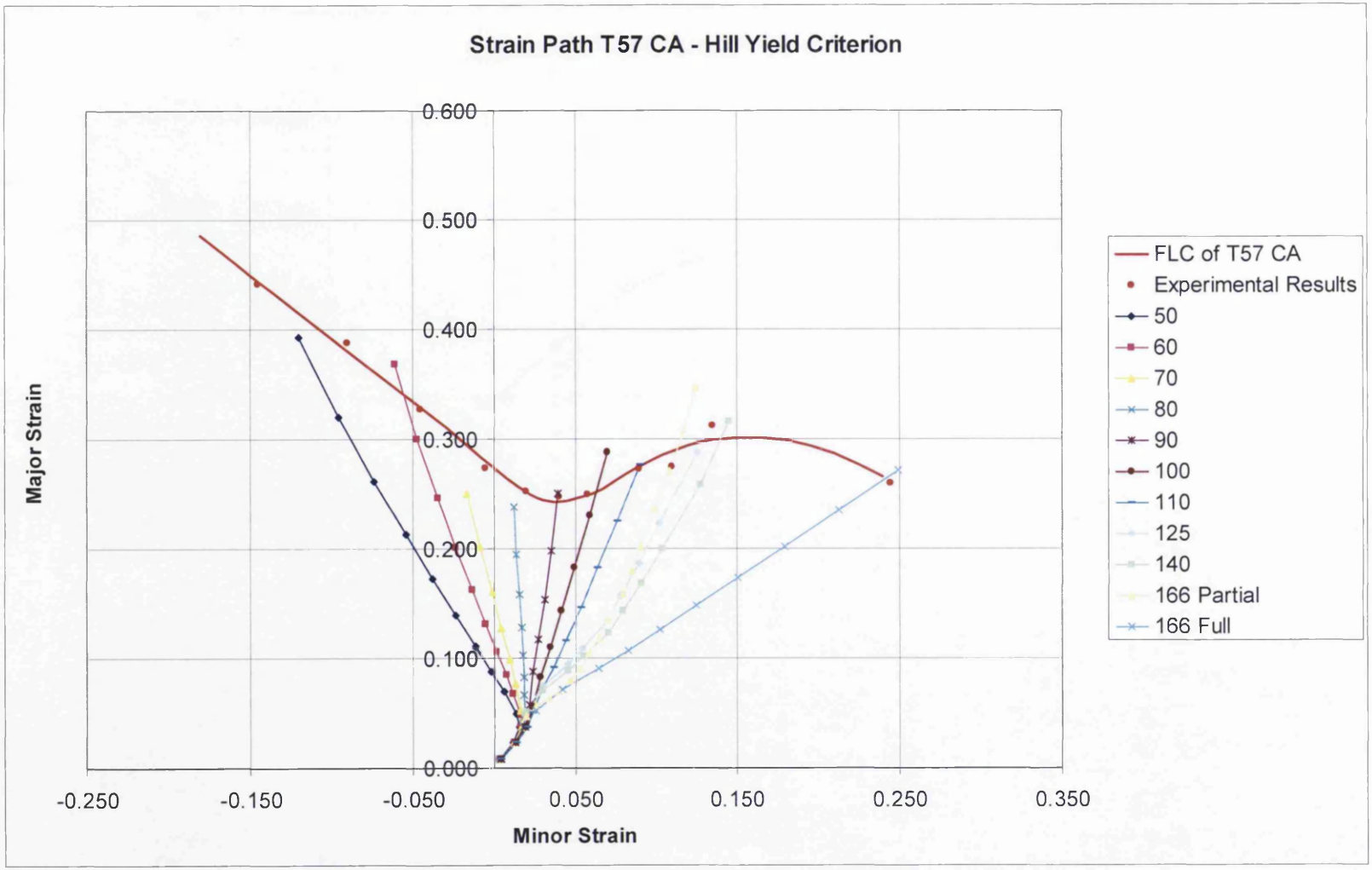

Figure 4.31. Set of simulated results for T57 CA compared to the experimental results

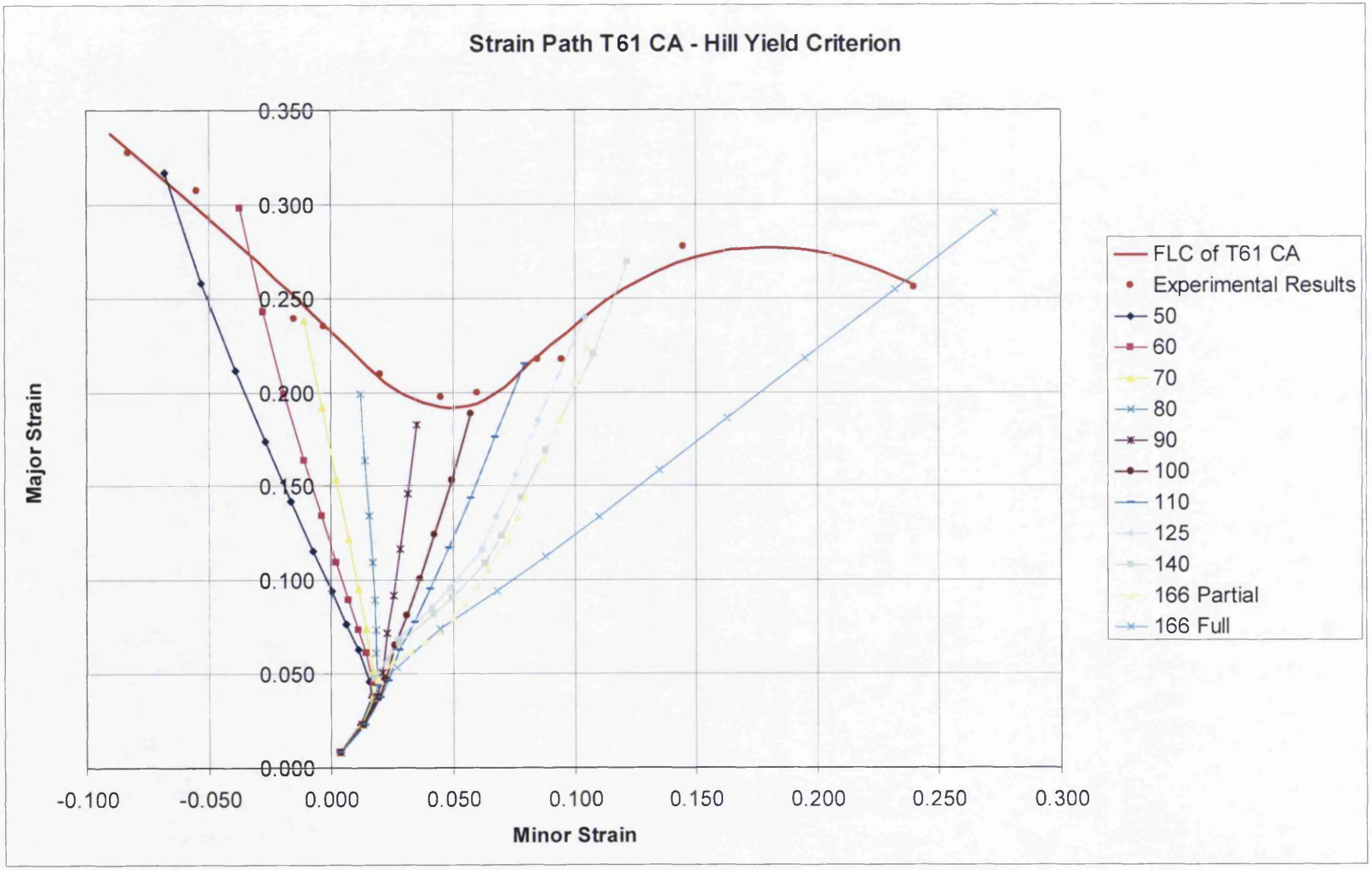

Figure 4.32. Set of simulated results for T61 CA compared to the experimental results.

4.5.3 Hill Discussion

As a general trend, all of the results, apart from the 166 full blank, seem to underestimate the Minor Strain valve with respect to the strain path.

The models results as the strain condition changes from plane strain to biaxial strain yielded poor results compared to the uniaxial to plane strain conditions. Halterwidths 125, 140 and 166 partial had strain paths that differ from the others. They are curved and not straight, after the initial yielding. 125 and 140 had similar results to each other, but the 166 partial was unreliable.

The 166 partial results, across the four materials, were quite erratic. For T57 BA the results were no better then the 110 halterwidth and for the T52 BA material, the strain path ends between the 140 and 166 full results. These results are possibly because of the inability to formed wrinkles. As showed earlier, figure 4.33, the model is incapable of forming wrinkles that occur in the circled red area. Instead an arc of material is formed which produces a high stressed area. This occurs on both sides of the blank and will influence the minor strain across the material and hence ultimately the stain path of the material being formed at the centre of the bulge.

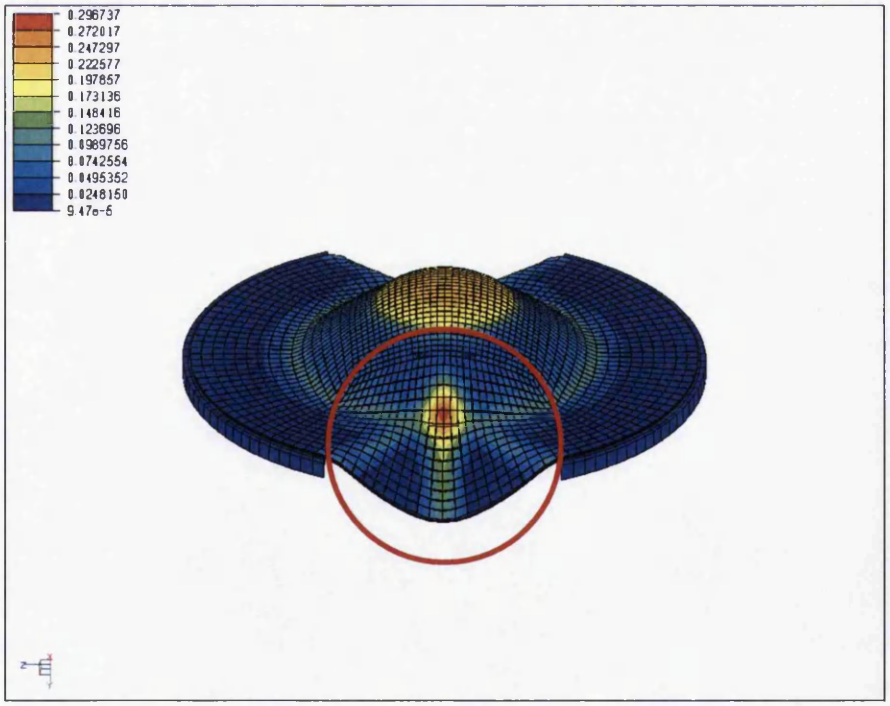

Figure 4.33. Model showing the are, indicated in red, where wrinkling should be occurring.

The 125 and 140 halterwidths had similar results however not as severe, as there is less material for form an arc and influence the strain path. This indicates that the results for the 125, 140 and 166 partial will be unfortunately wrong.

With the introduction of the Zerilli-Armstong strain rate hardening the strain path are around the FLCs produced by the experimental work.

4.6 Barlat 3D Nakazima Model

The next set of simulated results has been done using the Barlat Yield Criterion, again using the Zerilli-Armstong strain rate hardening. The processes used to obtain the results are the same as the Hill results.

4.6.2 Barlat Results

Figure 4.34 to 4.37 shows the simulated results using T52BA, T57 BA, T57 CA and T61 CA material properties using the Barlat yield criterion.

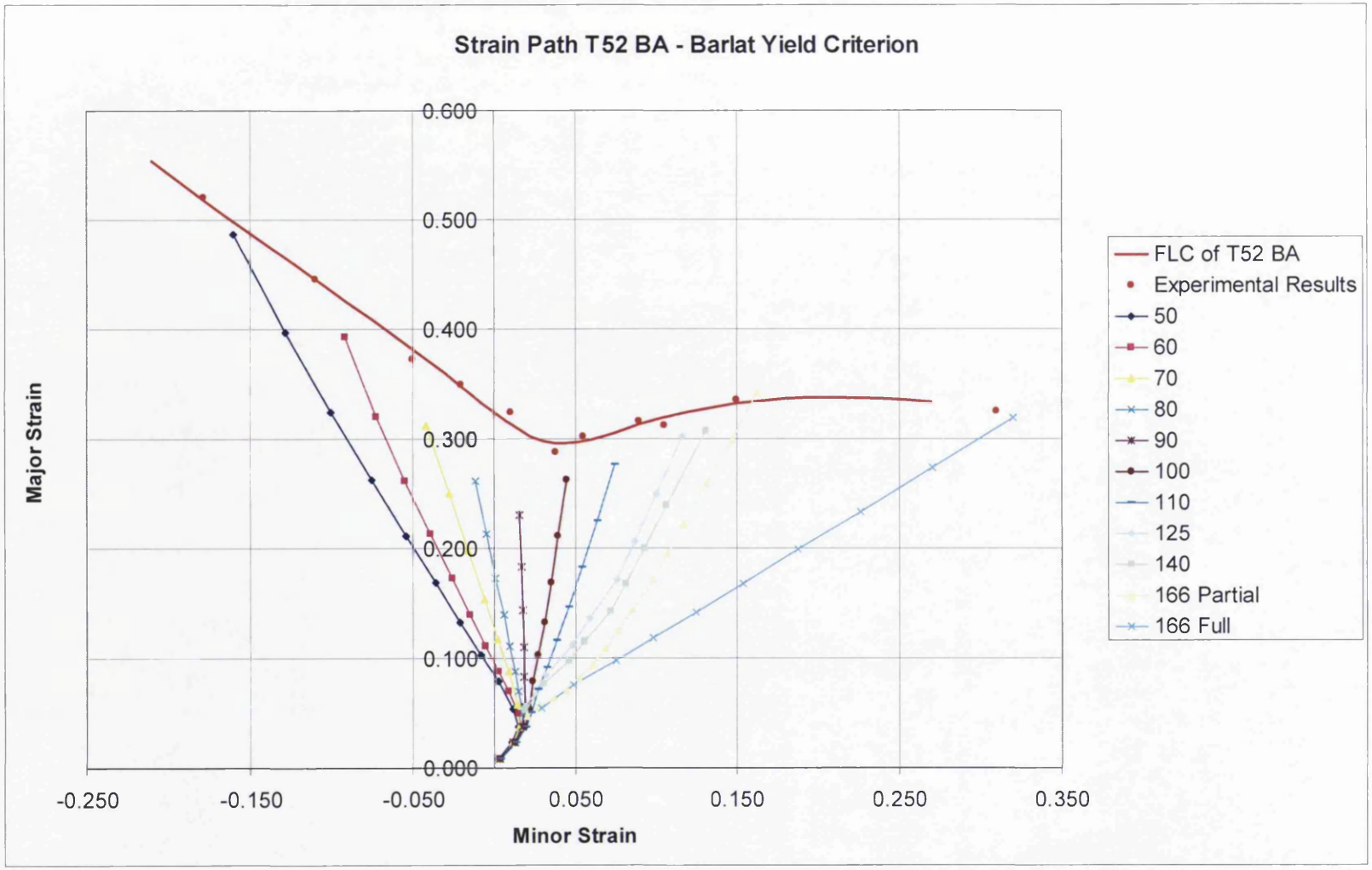

Figure 4.34. Set of simulated results for T52 BA compared to the experimental results.

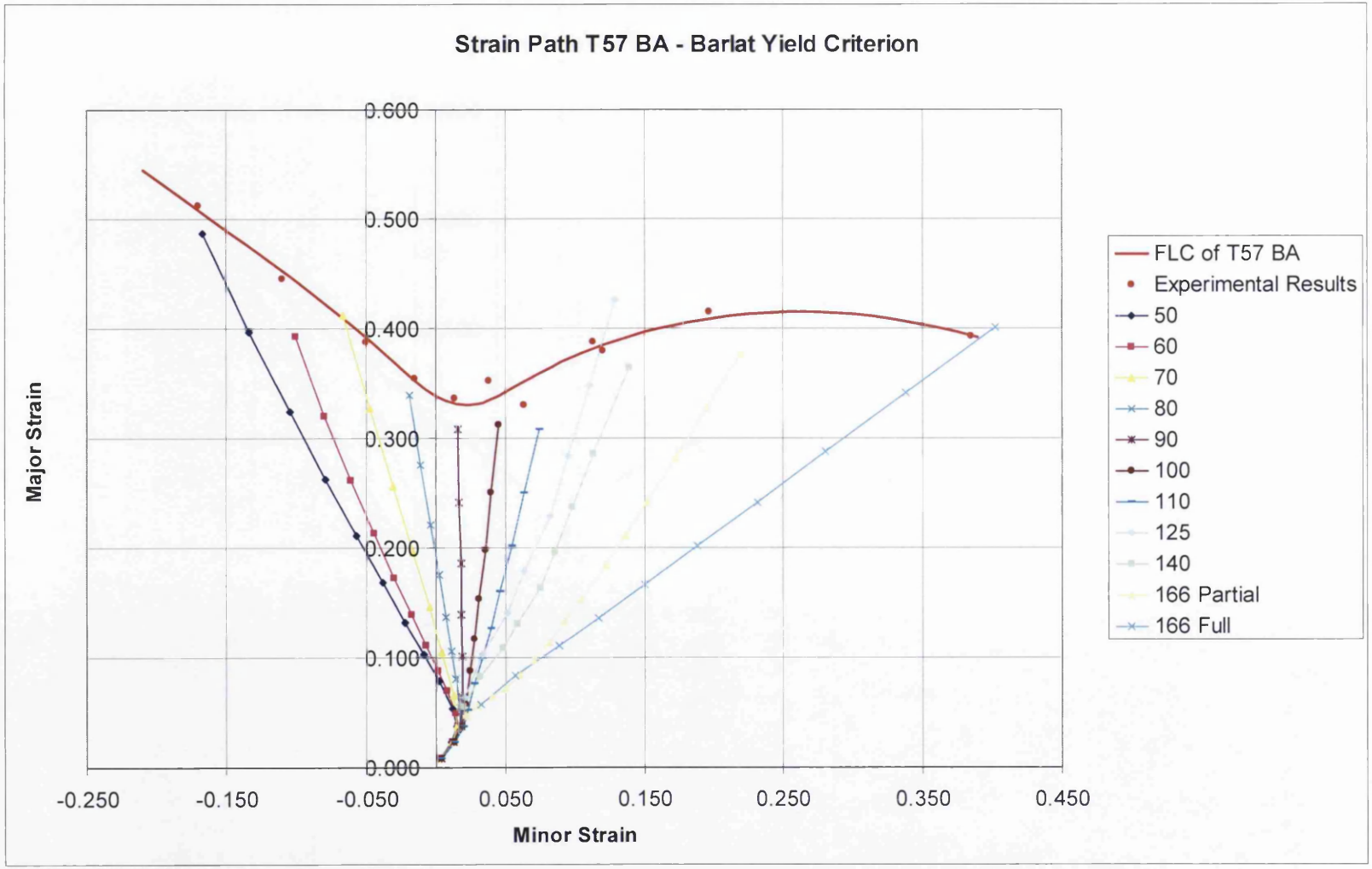

Figure 4.35. Set of simulated results for T57 BA compared to the experimental results.

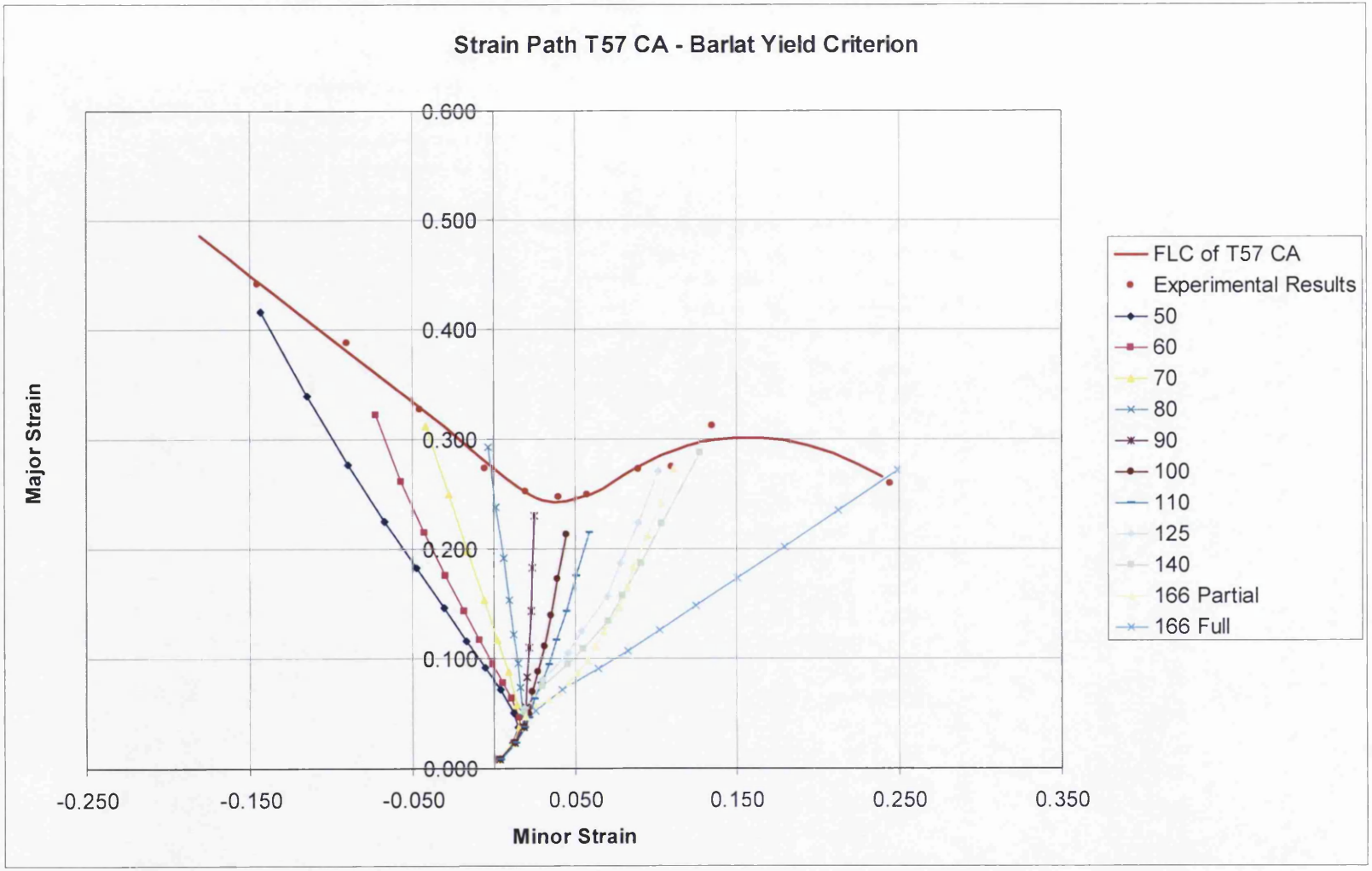

Figure 4.36. Set of simulated results for T57 CA compared to the experimental results.

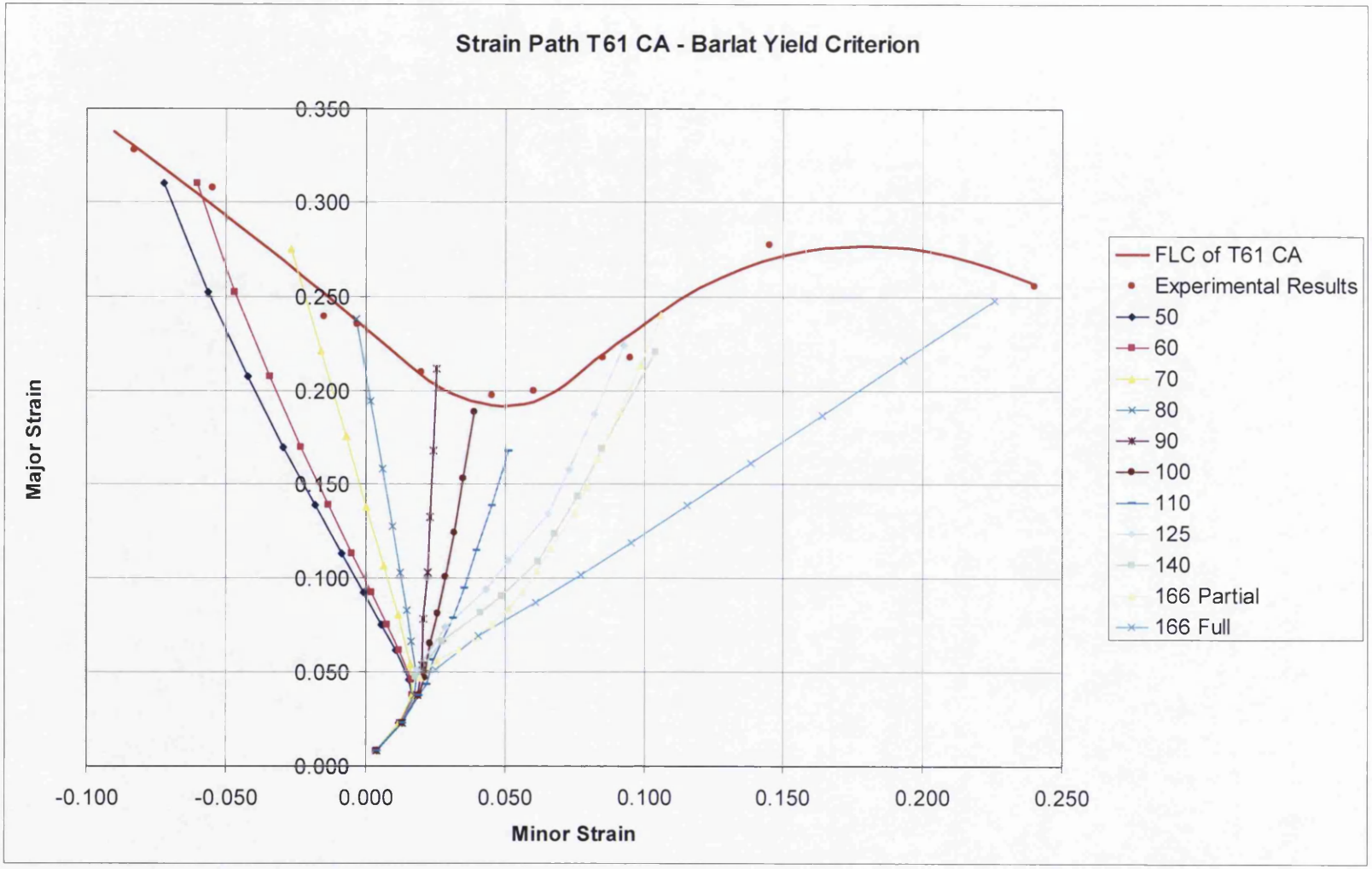

Figure 4.37. Set of simulated results for T61 CA compared to the experimental results.

4.6.3 Barlat Discussion

Like the Hill models the results for the 125, 140 and 166 partial are questionable. The results again seem erratic. This does not mean that the Hill and Barlat Yield Criterion are not capable of simulating the conditions between the plane and biaxial strain. It shows that the model needs changing to address the problem caused by the resultant material arc which is formed.

The results between uniaxial to plane strain do show an improved strain path over the Hill results. There is a trend that the strain paths are underestimating the point of failure compared to the experimental results. This has been explained earlier as follows, if the output results are increase the number of points generated along the strain path increases, when the strain rate against time is generated there will be more points, this gives a better result when determining the thinning point of the material. At present the thinning point is when a nodal point along a set of element shows an increase in rate strain, the point before the strain rate doubles compared to the node next to it. This can be argued that even though there is a higher strain the material may not yet be thinning or failed. The experimental results are when the material has failed hence the results produced through the simulations are pessimistic, which will underestimate the point of failure.

4.7 Discussion

As that has been discuss earlier, there are several point to consider when using the results obtained. The results would alter with an alteration of the mesh density, together with this and the increasing in the output results, which would alter the point where the strain path would begin to show thinning. There is scope of the resultant FLC to change based on these two areas.

The ability for the model to simulate the transition from plane to biaxial strain conditions is not ideal, the likely cause is the inability to form wrinkles. The resultant arc of material which is formed will influence the strain path at the centre of the bugle. Because of this the results for the 125, 140 and 166 partial halterwidths would be incorrect.

Between the uniaxial to plane strain the Barlat yield criterion show improved results over the Hill yield criterion. This would be explained by the Barlats yield criterion being able to fit the yield locus better.

Chapter 5

CONCLUSION

Chapter 5

CONCLUSION

CHAPTER 5 – CONCLUSION

5.1 Introduction

At the start of this project there were one main aim that was broken into two objectives. The follow section will conclude what has been achieved with regards to each of them. The aim was to develop a numerical tool which can predict the behaviour of packaging steels under strain path conditions.

3. Establish a simplified experimental test method to measure strain path dependant failure limit of packaging steels.
4. Generate a computer model in which the strain results are very closely matched to the experiment test method.

5.2 Conclusion

1. Experimental Test method

An experimental test method has been developed based on the International Standard ISO 12004-2. The alterations have happen because of the problems associated with thin steel grades. To prevent edge cracking the blank geometry has been altered, this with a combination of a smooth blankholder surface resulted in cracks being produced around the correct area at the top of the bulged. Another combination of different lubrication used with and without an IF steel mask produces good centre cracks consistently. It is still not clear how the IF steel mask affects the FLC or if the results obtained from not using the IF mask are valid.

Using the Argus measurement system the strain at the point of failure can be calculated between the uniaxial strain through plane strain to the biaxial strain using the different blank halterwidths. These can be used to produce a FLC of any material.

2. Computer Model

A computer model has been developed to obtain strain results that match the experimental results. The results were close to the experimental results however did not match. The idea behind producing the model was to obtain a FLC of any given steel material, knowing the material properties, which could be used in the packaging industry. The model could be used to give an idea if the material should be examined further or if it could be suitable for any given forming process

Although it can give a rough idea, due to the model results not matching the experimental ones the level of confidence would be low. Also to obtain the results as the model currently stands would take weeks to months, depending on the mesh size and the number of computers being used. With that long simulation time, the experimental method could achieve the results quicker. Increasing the mesh size, decreasing its density, would speed up the simulation time and obtaining the results but would have degrading affect on the resultant FLC produced from the various strain paths. Currently there is a trade off between time, accuracy of results and cost. To increase the accuracy of the results requires more simulation time. Therefore obtaining the results through experimental work would be quicker. However obtaining FLC through experimental work would increase labour and material costs. Due to this further development of the model needs to take place to increase the models simulation time and to generate improved accuracy of the results.

The model also needs changing to address the problem when the model simulates the blanks sizes between plane to biaxial strain. Due to the models inability to create wrinkles, which results in an incorrect strain path, the results for the 125, 140 and 166 partial halterwidth sizes can not be currently used with a good level of confidence.

Chapter 6

FUTURE WORK

Chapter 6

FUTURE WORK

CHAPTER 6 – FUTURE WORK

6.1 Future Work

For the experimental part, a FLC of the IF steel mask needs to be done. This result can then be compared to the results obtain during this project. This would help fully understand the affect the mask has of the blanks when they are formed.

In the same way the non-IF steel mask could also be repeated to see if the rubber pad used in the lubrication method also affects the resultant FLC. This would require a change to the lubrication method, replacing the rubber pad with another piece of Teflon for example. Again this would be compared against the results obtained to see if the rubber pad has an influence on the strain path.

With regards to the modelling side of the work, the first practical thing to do is to simplify the model to decrease the simulation time. Currently the simulation time is to long running for over a week per blank for a relatively course mesh which is not practical long term. Techniques tried to increase the simulation time have included removing contacts between the rubber pads and making the rubber pads one mass, having the blankholder a stationary object instead of a force load being applied to the surface which resulted in material movement under the blankholder. Altering the blank and mask geometry and fixing the part of the blank and mask under the blankholder in the X, Y and Z planes which end in the blank and mask geometry penetrating the die. An area not examined was the contact between the blank and the mask to see if the blank moves relative to the mask during the forming process.

From the simulation time the next area of the model to be examined would be the problem simulating the strain paths between plane to biaxial. Currently the model can produce a strain path, however the results are influenced by the inability to produce wrinkles which can produce erratic results. This means that these strain paths can not be used with a good level of confidence.

Once both the models simulation time has been decrease and it ability to simulate plane to biaxial strains have been addressed other aspects can be examined. How much does an

increase in elements increase the model to be able to predict the FLC. Investigation into how the radius of the punch affects the FLC. This can be done by altering the punch radius and repeating the simulation over and over. The resultant FLC's at different radius' will show how the strain path is affected. Simulating the results not using an IF mask in the model and compare to the experimental results produced. This would show if the model is producing results that experimental testing has proven difficult.

References

REFERENCES:

REFERENCES

- Apeal, The Association of European Producers of Steel for Packaging, 2004, 'Steel for Packaging', [Online] Available form: http://www.apeal.org/emc.asp?pageId=192 [Accessed 19th February 2007)
- APEAL1, 2010, 'Statistics, Steel packaging recycling in Europe: (recycling rates)', [Online] Available from: http://www.apeal.org/en/statistics [Accessed, 22nd June 2010]
- APEAL2, 2010, 'Statistics, Recycling of main packaging material in Europe: (2008)', [Online] Available from: http://www.apeal.org/en/statistics [Accessed, 22nd June 2010]
- Ashby, M., Bertényi, T. & Jackson, S., 2006, 'Recycling of plastics, The ImpEE project, University of Cambridge', [Powerpoint Slides] Available from: http://www-g.eng.cam.ac.uk/impee/topics/RecyclePlastics/files/Recycling%20Plastic%20v3%20PDF%20WITH%20NOTES.pdf [Accessed, 22nd June 2010]
- Barisic B, and Pepelnjak T, 2008, 'Computer-assisted engineering determination of the formability limit for thin sheet metals by a modified Marciniak method', DOI 10.1243/03093247JSA503, 459-472
- Bauschinger, J, 1881, Ueber die Veränderung der Elasticitätsgrenze und des Elasticitcitätsmoduls verschiedener Metalle. Civiling N.F, **27**, 289-348
- Beddoes, J and Bibby, M.J, 1999, Principles and Metal Manufacturing Processes, Arnold. Paris, pp 152-161
- Belytschko, T, Liu, W.K, and Moran, B, 2000, Nonlinear finite elements for continua and structures, John Wiley and Sons Ltd, New York, USA
- Blank, S.C, Chiles, V, Lissaman, A.J, and Martin, S.J, 1996, Principles of Engineering Manufacture, 3rd Edition, Arnold, Paris, pp 84-91
- Can Manufactures Institute, 2007, Can History Timeline, [Online] Available form: http://www.cancentral.com/hist_timeline.cfm [Accessed 26th March 2007]
- Cao J., Yao H., Karafillis A. and Boyce M.C. (1999), Prediction of localised thinning in sheet metal using a general anisotropic yield criterion, International Journal of Plasticity, **16**, 1105-1129
- Chandrupatla, T.R, and Belegundu, A.D, 1991, Introduction to finite element in engineering, Prentice Hall Inc, New Jersey, USA
- Chang D-F, and Wang J.E, 1997, 'Analysis of draw-redraw processes', International Journal of Mechanical Science, **40**, 793-804
- Colgan, M and Monaghan, J, 2003, Deep drawing process: analysis and experiment, Journal of Materials Processing Technology, **132**, 35-41
- Collingham, J, 2007, Product and Market Development Manager, Corus Packaging Plus, Private Communication.

- Courbon J, 2003, 'Damage evolution in a compressive forming process: ironing of beverage cans', Scripta Materialia, **48**, 1519-1524
- Danckert, J, 1994, The residual stress distribution in the wall of a deep drawn and ironed cup determined experimentally and by FEM, Annals of the CIRP, **41**, 249-252
- DEFRA, 2006, 'The producer responsibility obligations (packaging waste) regulations 2005', PB 11540, p12-13
- Doege E, Droder K, Griesbach B, 1997, 'On the development of new characteristic valves for the evaluation of sheet metal formability, Journal of material processing technology, **71**, 152-159
- Ebrahimi, R. and Najafizadeh, A., 2004, A new method for evaluation of friction in bulk metal forming, Jorunal of Materials Processing Technology, **152**, 136-143
- ELFEN 2.8, 1998,'Specification Overview [Online] Available from: http://www.rockfield.co.uk/Spec_2_8.doc [Accessed 16th April 2007]
- Europa, 2007, Environment, [Online] Available from: http://ec.europa.eu/environment /climat/eccp.htm [Accessed 14th March 2007]
- European Parliament Council, 1994, 'European Parliament and Council directive 94/62/EC of December 1994 on packaging and packaging waste', OJ L 365, p 10-23
- Fratini, L., Lo Casto, S. and Lo Valvo, E., 2006,'A technical note on an experimental device to measure friction coefficient in sheet metal forming, Journal of Materials Processing Technology, **172**, 16-21
- Gaard, A., Krakhmalev, P. V., Bergstrom, J. and Hallback, N., 2006, Galling resistance and wear mechanisms cold work tool materials sliding against carbon steel sheets, Tribology Letters, **26**, 67-72
- Gedney, R., 2006, Measuring the plastic strain ratio of sheet metals, FMA Communications Inc, Rockfield, Illinois
- Goodwin, G.M., 1968, Application of strain analysis to sheet metal forming problems in the press shop. SAE paper no. 680093
- Hassan, M.A., Takakura, N. and Yamaguchi, K., 2003, A novel technique of friction aided deep drawing using a blankholder divided into four segments, Journal of Materials Processing Technology, **139**, 408-413
- Kampus, Z, and Kuzman, K, 1993, Analysis of the Geometrical Accuracy in Ironing, Advanced Technology of Plasticity, **2**, 1005-1010
- Keller, S.P., Backofen, W.A., 1964, Plastic instability and fracture in sheets stretched over rigid punches. ASM Trans. Quart 56, 25.
- Kumar, D.R, 2002, Formability analysis of extra deep drawing steel, Journal of Materials Processing Technology, **130-131**, 31-41

- Labberton, M, G., 2009, 'Aluminium beverage can recycling in the EU 27 increases to 63%' [Online] Available from: http://www.eaa.net/en/press-room/press-releases/_doc/653 [Accessed, 23rd June 2008]
- Man, C,S., 2002, On the r-value of textured sheet metals, International Journal of Plasticity, **18**, 1683-1706
- Manabe K, Yagami T and Yamauchi Y, 2007, 'Effect of alternating blank holder motion of drawing and wrinkle elimination on deep-drawability', Journal of material processing technology, 187-191
- Maslennikov, N., A., 1957, Russian developed punchless drawing, Metalworking Production, **16**, 1417-1420
- Merchant, H.D, Hodgson, D.S, O'Reilly, I, and Embury, J.D, 1990, Structure and Property Evolution During Drawing and Wall Ironing, Materials Characterisation, **25**, 251-261
- Mielnik, E.M, 1991, Metalworking science and engineering, McGraw-Hill Inc, ISBN 0-07-041904-3
- OPSI, 1997, 'Environment Protection, The producer responsibility obligations (packaging waste) regulations 1997', Statutory Instrument 1997 No. 648
- Owen, D.R.J, and Hinton, E, 1977, Finite element programming, Academic Press, London, UK
- Panknin, W, 1977, Grundlagen des Tiefziehens zur Herstellung Zweiteiliger Dosen, Werkstatt und Betrieb, **110**, 313-319
- Ragab, M.S, and Orban, H.Z, 2000, Effect of ironing on the residual stresses in deep drawn cups, Journal of Materials Processing Technology, **99**, 54-61
- Riel, M.van, 2006, Strain path dependent material models for forming and crash, Literature Study for NIMR, P06.1.041
- Rockfield Software Ltd, 2002, Overview of ELFEN [Online] Available from: http://www.rockfield.co.uk/elfen.htm [Accessed 18th April 2007]
- Schmitt, J, Aenoudt, E, and Baudelet, B, 1985, Yield loci for polycrystalline metals without texture, Materials Science and Engineering, **75**, 13-20
- Schünemann, M, Ahmetoglu, M.A, and Altan, T, 1996, Prediction of process conditions in drawing and ironing of cans, Journal of Materials Processing Technology, **59**, 1-9
- TATA, 2011, TATA Steel, Tata steel packaging, TSY:2500:05/2011
- TATA RD&T, 2007, Friction in sheet metal forming, Automotive Applications, Ijmuiden, The Netherlands
- Thiruvarudchelvan, S. and Tan, M.J., 2005, Recent developments in friction-assisted sheet metal forming processes, Journal of Materials Processing Technology, **167**, 161-166

- Wolper, P, 2004, The Recycling of Steel: An optimised process ensuring sustainability, The Association of European Producers.
- Yagani, T., Manabe, K. and Yamauchi, Y., 2007, Effect of alternating blank holder motion of drawing and wrinkle elimination on deep drawability, Journal of Materials Processing Technology, **187-188**, 187-191
- Zienkiewicz, O.C, and Taylor, R.L, 1987, The finite element method: Basic formulation and linear problems, McGraw Hill Book Company, Maidenhead, UK

Appendix A

APPENDIX A:

Elfen Manual Addendum

Barlat Anisotropic Elasto-Plastic Material Model

AD.1 Introduction

This model describes the Barlat anisotropic elasto-plastic material model as implemented in Elfen.

AD.2 Barlat Anisotropic Model (Barlat et al, 1997)

AD.2.1 Yield Function

The isotropic plasticity equivalent (IPE) stress is given as:

$$\underset{0/}{S} = \underset{0/0/}{L}\underset{0/}{\sigma} \tag{1}$$

where, for orthotropic symmetry,

$$\underset{\%}{L} = \begin{bmatrix} (c_2+c_3)/3 & -c_3/3 & -c_2/3 & 0 & 0 & 0 \\ -c_3/3 & (c_3+c_1)/3 & -c_1/3 & 0 & 0 & 0 \\ -c_2/3 & -c_1/3 & (c_1+c_2)/3 & 0 & 0 & 0 \\ 0 & 0 & 0 & c_4 & 0 & 0 \\ 0 & 0 & 0 & 0 & c_5 & 0 \\ 0 & 0 & 0 & 0 & 0 & c_6 \end{bmatrix} \tag{2}$$

and the c_k are anisotropy coefficients. If $c_k \equiv 1$ then the above $\underset{0/}{S}$ is the standard stress deviator.

The yield function is:

$$\phi = \alpha_1 |s_2 - s_3|^a + \alpha_2 |s_3 - s_1|^a + \alpha_3 |s_1 - s_2|^a = 2\bar{\sigma}^a \tag{3}$$

or alternatively:

$$F = \phi - 2\bar{\sigma}^a = \alpha_1 |s_2 - s_3|^a + \alpha_2 |s_3 - s_1|^a + \alpha_3 |s_1 - s_2|^a - 2\bar{\sigma}^a = 0 \tag{3a}$$

where $\bar{\sigma}$ is a measure of the yield surface (strength of the material) and

$$\alpha_k = \alpha_x p_{1k}^2 + \alpha_y p_{2k}^2 + \alpha_z p_{3k}^2 \qquad (k=1,2,3) \tag{4}$$

Where s_1, s_2 and s_3 are the principal values of $\underset{0/}{S}$ and $\underset{0/}{p}$ is the transformation matrix from X, Y and Z to the principal direction; α_x, α_y and α_z are three functions given as:

$$\begin{aligned} \alpha_x &= \alpha_{x0}\cos^2\beta_1 + \alpha_{x1}\sin^2\beta_1 \\ \alpha_y &= \alpha_{y0}\cos^2\beta_2 + \alpha_{y1}\sin^2\beta_2 \\ \alpha_z &= \alpha_{z0}\cos^2\beta_3 + \alpha_{z1}\sin^2\beta_3 \end{aligned} \tag{5}$$

where $\alpha_{x0}, \alpha_{x1}, \alpha_{y0}, \alpha_{y1}, \alpha_{z0}$ and α_{z1} are positive material parameters and the angles defined as:

$$\cos^2\beta_1 = \begin{cases} Y \bullet 1 & if\ |s_1| \geq |s_3| \ \ or \\ Y \bullet 3 & if\ |s_1| < |s_3| \end{cases} \tag{6}$$

$$\cos^2\beta_2 = \begin{cases} Z \bullet 1 & if\ |s_1| \geq |s_3| \ \ or \\ Z \bullet 3 & if\ |s_1| < |s_3| \end{cases} \tag{7}$$

$$\cos^2\beta_3 = \begin{cases} X \bullet 1 & if\ |s_1| \geq |s_3| \ \ or \\ X \bullet 3 & if\ |s_1| < |s_3| \end{cases} \tag{8}$$

For the application to a rolling sheet, *X* is the rolling direction, *Y* is the transverse direction and *Z* is the normal direction.

AD.2.2 Associated Flow Rule

When the coefficients α_k are constants (to s_1, s_2 and s_3), the yield function is only a function of s_1, s_2 and s_3.

$$\phi = \phi(s_1, s_2, s_3) \qquad s_1 \geq s_2 \geq s_3 \tag{9}$$

Assuming that the principal values are ordered, the normal to the yield surface can be given in this reference frame as:

$$\frac{\dot{\varepsilon}_1}{\dot{\lambda}} = \frac{\partial \phi}{\partial S_1} = a\alpha_3 |s_1 - s_2|^{a-1} + a\alpha_2 |s_3 - s_1|^{a-1} = \frac{\dot{\varepsilon}_{11}}{\dot{\lambda}} \tag{10}$$

$$\frac{\dot{\varepsilon}_2}{\dot{\lambda}} = \frac{\partial \phi}{\partial S_2} = a\alpha_1 |s_2 - s_3|^{a-1} - a\alpha_3 |s_1 - s_2|^{a-1} = \frac{\dot{\varepsilon}_{22}}{\dot{\lambda}} \tag{11}$$

$$\frac{\dot{\varepsilon}_3}{\dot{\lambda}} = \frac{\partial \phi}{\partial S_3} = -a\alpha_2 |s_3 - s_1|^{a-1} - a\alpha_1 |s_2 - s_3|^{a-1} = \frac{\dot{\varepsilon}_{33}}{\dot{\lambda}} \tag{12}$$

where $\dot{\lambda}$ is a proportionality factor. Those can be transformed into the *X*, *Y* and *Z* axes as:

$$\dot{\varepsilon}_{ij} = p_{ik} p_{jl} \dot{\varepsilon}_{kl} \begin{cases} \dot{\varepsilon}_{11} = p_{11}^2\dot{\varepsilon}_1 + p_{12}^2\dot{\varepsilon}_2 + p_{13}^2\dot{\varepsilon}_3 \\ \dot{\varepsilon}_{22} = p_{21}^2\dot{\varepsilon}_1 + p_{22}^2\dot{\varepsilon}_2 + p_{23}^2\dot{\varepsilon}_3 \\ \dot{\varepsilon}_{33} = p_{31}^2\dot{\varepsilon}_1 + p_{32}^2\dot{\varepsilon}_2 + p_{33}^2\dot{\varepsilon}_3 \\ \dot{\varepsilon}_{23} = p_{21}p_{31}\dot{\varepsilon}_1 + p_{22}p_{32}\dot{\varepsilon}_2 + p_{23}p_{33}\dot{\varepsilon}_3 \\ \dot{\varepsilon}_{31} = p_{31}p_{11}\dot{\varepsilon}_1 + p_{32}p_{12}\dot{\varepsilon}_2 + p_{33}p_{13}\dot{\varepsilon}_3 \\ \dot{\varepsilon}_{12} = p_{11}p_{21}\dot{\varepsilon}_1 + p_{12}p_{22}\dot{\varepsilon}_2 + p_{13}p_{23}\dot{\varepsilon}_3 \end{cases} \tag{13}$$

Using the chain rule for the derivatives, the strain rates can be obtained through the linear operator $L_{0/}$:

$$\dot{\varepsilon}_{ij} = L_{klij}\dot{\varepsilon}_{kl} \tag{14}$$

AD.2.3 Principal Values and Directions for A General Traceless Stress Tensor

AD.2.3.1 Principal Values

X, *Y* and *Z* denote an orthogonal frame attached to the material (i.e. sheet rolling, transverse and normal directions). From (1) and 2, If $\underset{0}{\sigma}$ is a tensor as:

$$\underset{0}{\sigma} = \begin{bmatrix} \sigma_x & \sigma_{xy} & \sigma_{zx} \\ \sigma_{xy} & \sigma_y & \sigma_{yz} \\ \sigma_{zx} & \sigma_{yz} & \sigma_z \end{bmatrix} \tag{15}$$

Then $\underset{0}{S}$ is a tensor whose trace is zero ($H_1 = s_x + s_y + s_z = 0$):

$$\underset{0}{S} = \begin{bmatrix} s_x & s_{xy} & s_{zx} \\ s_{xy} & s_y & s_{yz} \\ s_{zx} & s_{yz} & s_z \end{bmatrix} \tag{16}$$

Following the standard procedure to obtain the principal values (solving the characteristic equation), the principal values can be written as:

$$\begin{aligned} s_1 &= 2\sqrt{H_2}\cos(\theta/3) \\ s_2 &= 2\sqrt{H_2}\cos(\theta/3 - 2\pi/3) \\ s_3 &= 2\sqrt{H_2}\cos(\theta/3 + 2\pi/3) \end{aligned} \tag{17}$$

where

$$0 \le \theta = \arccos(H_3 / H_2^{3/2}) \le \pi \tag{18}$$

and

$$H_2 = \frac{s_x^2 + s_y^2 + s_z^2 + 2(s_{yz}^2 + s_{zx}^2 + s_{xy}^2)}{6} \tag{19}$$

$$H_3 = \frac{s_x s_y s_z + 2 s_{yz} s_{zx} s_{xy} - s_x s_{yz}^2 - s_y s_{zx}^2 - s_z s_{xy}^2}{2} \tag{20}$$

AD.2.3.2 Principal Directions

The principal directions are given by:

$$(\underset{0}{s} - s_k \underset{0}{I})\underset{0}{p}_k = 0 \tag{21}$$

where $\underset{\sim}{p}_k$ is the principal direction associated with principal value s_k. This equation can be written as:

$$\begin{bmatrix} s_x - s_k & s_{xy} & s_{zx} \\ s_{xy} & s_y - s_k & s_{yz} \\ s_{zx} & s_{yz} & s_z - s_k \end{bmatrix} \begin{bmatrix} p_{1k} \\ p_{2k} \\ p_{3k} \end{bmatrix} = \begin{bmatrix} 0 \\ 0 \\ 0 \end{bmatrix} \tag{22}$$

For the general case ($s_1 > s_2 > s_3$ or $\theta \neq 0$ and $\theta \neq \pi$) we have:

$$\underset{\sim}{u}_k = \begin{bmatrix} s_x - s_k \\ s_{xy} \\ s_{zx} \end{bmatrix}, \quad \underset{\sim}{v}_k = \begin{bmatrix} s_{xy} \\ s_y - s_k \\ s_{yz} \end{bmatrix}, \quad \underset{\sim}{w}_k = \begin{bmatrix} s_{zx} \\ s_{yz} \\ s_z - s_k \end{bmatrix} \tag{23}$$

$$\underset{\sim}{p}_k = \begin{cases} \underset{\sim}{u}_k \times \underset{\sim}{v}_k / \left| \underset{\sim}{u}_k \times \underset{\sim}{v}_k \right| \\ or \\ \underset{\sim}{v}_k \times \underset{\sim}{w}_k / \left| \underset{\sim}{v}_k \times \underset{\sim}{w}_k \right| \\ or \\ \underset{\sim}{w}_k \times \underset{\sim}{u}_k / \left| \underset{\sim}{w}_k \times \underset{\sim}{u}_k \right| \end{cases} \tag{24}$$

For the singular case $\theta = 0$ or $s_2 = s_3$, the principal direction for s_1 ($\underset{\sim}{p}_1$) can be defined using the above set of equations. However, because of the rotational symmetry around $\underset{\sim}{p}_1$, it is possible to pick up $\underset{\sim}{p}_2$ and $\underset{\sim}{p}_3$ in the plane orthogonal to $\underset{\sim}{p}_1$. Three easy choices for $\underset{\sim}{p}_2$ are:

$$\underset{\sim}{p}_2 = \begin{cases} \underset{\sim}{p}_1 \times \underset{\sim}{X} / \left| \underset{\sim}{p}_1 \times \underset{\sim}{X} \right| \\ or \\ \underset{\sim}{p}_1 \times \underset{\sim}{Y} / \left| \underset{\sim}{p}_1 \times \underset{\sim}{Y} \right| \\ or \\ \underset{\sim}{p}_1 \times \underset{\sim}{Z} / \left| \underset{\sim}{p}_1 \times \underset{\sim}{Z} \right| \end{cases} \tag{25}$$

Then,

$$\underset{\sim}{p}_3 = \underset{\sim}{p}_1 \times \underset{\sim}{p}_2 \tag{26}$$

For the singular case $\theta = \pi$ or $s_1 = s_2$, the principal direction for s_3 ($\underset{\sim}{p}_3$) can be defined using the above set of equations. However, because of the rotational symmetry around $\underset{\sim}{p}_3$, it is possible to pick up $\underset{\sim}{p}_1$ and $\underset{\sim}{p}_2$ in the plane orthogonal to $\underset{\sim}{p}_3$. Three easy choices for $\underset{\sim}{p}_2$ are:

$$\underset{\%}{p_2} = \begin{cases} \underset{\%}{p_3} \times \underset{\%}{X} / \left| \underset{\%}{p_3} \times \underset{\%}{X} \right| \\ or \\ \underset{\%}{p_3} \times \underset{\%}{Y} / \left| \underset{\%}{p_3} \times \underset{\%}{Y} \right| \\ or \\ \underset{\%}{p_3} \times \underset{\%}{Z} / \left| \underset{\%}{p_3} \times \underset{\%}{Z} \right| \end{cases} \tag{27}$$

Then,

$$\underset{\sim}{p_1} = \underset{\sim}{p_2} \times \underset{\sim}{p_3} \tag{28}$$

AD.2.4 Plane Stress Case

The plane stress case is important for this kind of material and is discussed in Barlat's papers under some special assumptions. For the plane stress case, the standard assumptions are:

$$\sigma_z = \sigma_{yz} = \sigma_{zx} = 0 \tag{29}$$

and

$$\underset{\%}{s} = \begin{bmatrix} s_x & s_{xy} & 0 \\ s_{xy} & s_y & 0 \\ 0 & 0 & s_z \end{bmatrix} \tag{30}$$

Barlat et al (1997-1) gave an unsymmetrical $\underset{\sim}{L}$ as:

$$\underset{\%}{L} = \begin{bmatrix} 2/3 & -h/3 & 0 \\ -1/3 & 2h/3 & 0 \\ -1/3 & -h/3 & 0 \\ 0 & 0 & p \end{bmatrix} \tag{31}$$

As a result of the above assumptions, one of the principal directions, X_3, is always aligned with the sheet normal direction. The principal values of $\underset{\sim}{s} = \underset{\sim}{L}\underset{\sim}{\sigma}$ are:

$$\begin{aligned} s_1 &= \frac{K_1}{3} + K_2 \\ s_2 &= \frac{K_1}{3} - K_2 \\ s_3 &= -\frac{2K_1}{3} \end{aligned} \tag{32}$$

With,

$$\begin{aligned} K_1 &= \frac{\sigma_x + h\sigma_y}{2} \\ K_2 &= \sqrt{\left(\frac{\sigma_x - h\sigma_y}{2}\right)^2 + p^2\sigma_{xy}^2} \end{aligned} \tag{33}$$

Furthermore, Barlat et al (1997-1) assumed that $\alpha_x = \alpha_y = \alpha$ and $\alpha_z = (2-\alpha)$, then $\alpha_1 = \alpha_2 = \alpha, \alpha_3 = (2-\alpha)$ and the yield function becomes:

$$\phi = \alpha\left|K_1 + K_2\right|^a + \alpha\left|K_1 - K_2\right|^a + (2-\alpha)\left|2K_2\right|^a = 2\bar{\sigma}^a \qquad (34)$$

where a, α, h and p are material constants.

AD.3 Input Data Format

Material data parameters are required, plus a definition of the material directions using a local co-ordinate system in conjunction with geometric property data.

AD.3.1 Material Property Data

For 3D Solids:

```
Material_data { MATNO
 :
 :
  Plastic_material_flags { 2
    0 38
  }
  Plastic_Properties { NPRPLS
    σ̄  H  a  c1, c2, c3, c4, c5, c6, αx0, αy0, αz0, αx1  αy1, αz1
  }
}
```

For 2D Plane Stress and 3D Shells:

```
Material_data { MATNO
 :
 :
  Plastic_material_flags { 2
    0 38
  }
  Plastic_Properties { NPRPLS
    σ̄  H a  α h  p
  }
}
```

AD.3.2 Material Direction Data

Standard input data is used to relate X' (rolling direction), y' (transverse direction) and Z' (normal direction) to global X, Y and Z.

An example is shown below. More information on *Geometric_property_data* and *Local_coordinate_systems* can be found in the Elfen Explicit and Implicit manuals.

```
Geometric_property_data { IGROUP { 1 }                    Group using Barlat material
 Material_angle_flag {                    Defines reference direction for initial material angle
  1
 }
 Group_material_direction {  1
  1                                                  Refers to co-ordinate system used
 }                                  (defined under the Local_coordinate_systems tag – see below)
}
```

```
Local_coordinate_systems { 0
 System_numbers { NCSYS { 1 }
  1
 }
 System_types { NCSYS { 1 }
  1
 }
 Local_system_data { NDIMN { 3 } NDIMN { 3 } NCSYS { 1 }
  0.0   0.0   0.0
  1.0   0.0   0.0
  0     1     0.0
 }
}
```

End of Manual Addendum

Appendix B

APPENDIX B: